The Higgs Sector of the (Complex) NMSSM - Higher Order Corrections and Phenomenological Discussions

Zur Erlangung des akademischen Grades eines

DOKTORS DER NATURWISSENSCHAFTEN

von der Fakultät für Physik des
Karlsruher Instituts für Technologie (KIT)

genehmigte

DISSERTATION

von

Dipl.-Phys. Anne-Kathrin Walz
aus Hannover

Tag der mündlichen Prüfung: 29. Mai 2015

Referentin: Prof. Dr. M. Mühlleitner

Korreferent: Prof. Dr. M. Steinhauser

Abstract

We study the Higgs sector of the Next-to-Minimal Supersymmetric Extension of the Standard Model (NMSSM). With seven physical Higgs bosons the NMSSM Higgs sector offers plenty of phenomenologically interesting possibilities. Especially in light of the recent discovery of a scalar resonance at 125 GeV at the Large Hadron Collider a discussion of these is highly relevant. However, in order to draw meaningful conclusions regarding the true nature of the Higgs sector the availability of higher order corrections to parameters and observables is essential.

The first part of this thesis presents the higher order corrections to the masses of the NMSSM Higgs bosons including the full one-loop contributions and two-loop contributions of the order $\mathcal{O}(\alpha_s\alpha_t)$. The calculation is performed in the Feynman diagrammatic approach employing a renormalization scheme that mixes on-shell and $\overline{\text{DR}}$ conditions. The one-loop contributions are computed with full momentum dependence, whereas the two-loop corrections are calculated in the approximation of vanishing external momentum and in the gaugeless limit.

The second part focuses on the discussion of scenarios compatible with the experimental observations of a Higgs boson at a mass of 125 GeV and the measured signal strengths. On the one hand we analyze the properties of the 125 GeV NMSSM Higgs boson and in what subspaces of the NMSSM parameter space it can be realized. On the other hand we investigate the discovery prospects of the other NMSSM Higgs bosons. We consider standard search channels, that were already applied in the search for the discovered Higgs boson, as well as channels which rely on decay chains involving Higgs-to-Higgs decays and which can lead to very exotic final states.

Contents

CHAPTER 1

Introduction

The field of elementary particle physics entered a new era when the discovery of a Higgs-like resonance with a mass of $\sim$125 GeV at the Large Hadron Collider (LHC) was announced in July 2012 by the experiments ATLAS and CMS [1, 2]. Over the last few decades various experiments, among them also the big collider experiments LEP, Tevatron and now the LHC, have undertaken a great effort to discover all particles predicted by the Standard Model (SM) of particle physics and have striven to test its predictions at a high level of accuracy. So far all observations at the collider experiments are in very good agreement with the SM predictions, which with the Higgs boson as the last missing piece is finally complete. However, a lot of exciting questions still need to be answered. Due to experimental observations, for example from cosmology, and also because of some theoretical arguments we know that the SM is not the final answer. A wide range of models beyond the SM (BSM) has been proposed, one of the best known is certainly supersymmetry (SUSY). However, what most BSM models have in common is that they predict new particles. Therefore, one of the main objectives at the LHC is to search for new heavy resonances. Moreover, a lot of BSM models feature a Higgs sector which is more complicated than that of the SM. On the one hand an extended Higgs sector leads to several physical Higgs bosons, instead of only one as in the SM. And on the other hand the couplings of these Higgs bosons are usually modified compared to the respective couplings of a SM Higgs boson of the same mass. Thus in addition to the search for new particles a precise measurement of the couplings of the newly discovered Higgs boson to the SM particles is required to establish whether the properties of the observed Higgs boson are consistent with the SM. So far the signal strength values extracted from the data collected during the LHC runs at a center of mass (c.m.) energy of $\sqrt{s} = 7$ TeV and 8 TeV are compatible with the SM predictions [3, 4]. However, there is still room for physics beyond the SM. And maybe already the LHC run at a c.m. energy of 13 TeV, of which first results are expected soon, will reveal a hint towards physics beyond the SM.

In order to interpret the experimental results in light of BSM models, precise theoretical predictions including higher order corrections are necessary to draw meaningful conclusions. In this thesis we focus on the Next-to-Minimal Supersymmetric Extension of the SM (NMSSM). In addition to the minimal particle content required in any supersymmetric extension of the

SM the NMSSM features an extended Higgs sector. While the extension with the minimal particle content (MSSM) includes two complex Higgs doublets, which leads to five physical Higgs bosons after electroweak symmetry breaking and gauge fixing, the NMSSM contains a further complex singlet, which results in seven physical Higgs states. By the introduction of this additional singlet the so-called μ-problem of the MSSM is solved. Moreover, the NMSSM allows for scenarios with considerably less fine-tuning than scenarios within the MSSM. In this work we contribute both to the effort of increasing the accuracy of the theoretical predictions for the Higgs sector of the NMSSM, as well as to the investigation of the properties of phenomenologically valid scenarios. Part I of this thesis shortly recaps the SM and its shortcomings, offering supersymmetry as a solution to some of these problems (Ch. 2). Furthermore, the NMSSM is introduced and motivated, followed by a detailed discussion of the Higgs sector at tree level (Ch. 3). Chapter 4 gives some general remarks on regularization and renormalization, while Ch. 5 defines quantities needed in the phenomenological discussion of Higgs signals at the LHC. Apart from these introductory chapters this thesis consists of two mainly independent parts.

Part II presents the calculation of the higher order corrections to the Higgs boson masses in the NMSSM including corrections up to the order $\alpha_s\alpha_t$. We work in the complex NMSSM, i.e. including the CP-violating phases. All corrections are calculated in the Feynman diagrammatic approach. At one-loop level all possible contributions retaining the full momentum dependence are taken into account. The two-loop corrections of the order $\alpha_s\alpha_t$ are obtained in the approximation of vanishing external momentum and in the gaugeless limit. Both, at one-loop and at two-loop level a renormalization scheme that mixes on-shell and $\overline{\text{DR}}$ conditions is applied. The results presented in Part II rely on the publications [5–7]. The computed corrections to the Higgs boson masses were made publicly available by the inclusion in the program package `NMSSMCALC` [8], which interfaces the calculation of the Higgs mass spectrum with the calculation of the decays of the Higgs bosons.

Part III concentrates on the phenomenological investigation of the NMSSM. We conducted scans searching for phenomenologically valid scenarios. For scenario to be valid we required the presence of a scalar Higgs boson with a mass of 125 GeV, whose predicted signal strength values are compatible with the experimental measurements. Moreover, the signal of the other NMSSM Higgs bosons should respect the experimental exclusion bounds provided by LEP, Tevatron and LHC. We then analyzed how those valid scenarios are distributed in the NMSSM parameter space and what typical features the scenarios display. On the one hand we focused on the properties of the 125 GeV Higgs boson, i.e. its couplings to SM particles and the predicted signal strength values. While on the other hand we investigated the discovery prospects for the other NMSSM Higgs bosons during the LHC run at a c.m. energy of 13 TeV. The results presented in Part III are based on the publications [9–11].

In addition to the two projects presented here, I contributed to two other projects conducted within our group. I was involved in the computation of the full one-loop corrections to the trilinear Higgs self-coupling, where I performed the cross-check calculation for the whole process. Details on this project can be found in [12, 13]. Furthermore, I did the cross-check calculation for the electroweak corrections at one-loop level to the process $A_i \to \tilde{t}_1\tilde{t}_2$ [14, 15].

Part I

Theoretical Basics

CHAPTER 2

From the Standard Model to Supersymmetry

The Standard Model (SM) [16–26] of particle physics as we know it today was developed during the 1960s and 1970s. It very successfully describes the world of elementary particles and their interactions. With the discovery of the Higgs boson [1, 2] in summer 2012 the last missing piece of the SM has been found. The major achievement of the SM is that it not only offers a good qualitative description, but also delivers predictions with a very high precision. These predictions have been tested at the per mille level by the collider experiments and an impressive agreement has been reported. However, the SM nevertheless displays some shortcomings that hint at physics beyond the SM (BSM). Some of the best studied BSM models are supersymmetric extensions. This chapter will first review the SM in Sec. 2.1. After a discussion of the insufficiencies of the SM in Sec. 2.2, Sec. 2.3 introduces supersymmetry as a theory beyond the SM, that offers solutions to some of these insufficiencies.

2.1 The Standard Model of Particle Physics

The SM is a non-abelian renormalizable gauge theory represented by the direct product $SU(3)_C \otimes SU(2)_L \otimes U(1)_Y$. Via electroweak symmetry breaking the gauge group $SU(2)_L \otimes U(1)_Y$ is spontaneously broken to $U(1)_{\mathrm{em}}$. Each gauge group describes one of the fundamental interactions, that are mediated by the respective gauge bosons. The $SU(3)_C$ describes the strong interaction, which is mediated by the gluon. The quantum number specifying whether a particle takes part in the strong interaction is called color. There are three possible color charges: red, blue and green. The gluon carries color and anticolor, while all other elementary particles taking part in the strong interaction carry only one color (or anticolor in the case of antiparticles). In each interaction color has to be conserved. The electroweak interactions are described by the product $SU(2)_L \otimes U(1)_Y$. After electroweak symmetry breaking the photon, by coupling to electric charge, mediates the electromagnetic interaction, while the W and Z bosons mediate the weak interaction.

In addition to these spin one force carriers, there are the fermionic matter particles: the quarks and the leptons. They are classified according to their transformation properties under

name	field	$(SU(3)_C \otimes SU(2)_L \otimes U(1)_Y)$
quarks	$Q = (u_L, d_L)^T$	$(\mathbf{3}, \mathbf{2}, 1/6)$
	$u_R^\dagger$	$(\overline{\mathbf{3}}, \mathbf{1}, -2/3)$
	$d_R^\dagger$	$(\overline{\mathbf{3}}, \mathbf{1}, 1/3)$
leptons	$L = (\nu_L, e_L)^T$	$(\mathbf{1}, \mathbf{2}, -1/2)$
	$e_R^\dagger$	$(\mathbf{1}, \mathbf{1}, 1)$
Higgs	$\phi = (\phi^+, \phi^0)^T$	$(\mathbf{1}, \mathbf{2}, 1/2)$

Table 2.1: Matter particles and Higgs doublet of the SM and their transformation properties under the gauge groups. All generation and color indices are suppressed for readability. For the hypercharge Y we use the convention $Q = I_W^3 + Y$, with Q denoting the electric charge and I_W^3 the third component of the weak isospin.

the different gauge groups (see Tab. 2.1). The quarks carry both electric and color charge, hence they are involved in the strong as well as in the electromagnetic interaction. Whereas the leptons do not carry any color charge, but are only electrically charged and therefore interact electromagnetically. Both the leptons and the quarks come in three generations, where all generations share the same quantum numbers with the only exception being the mass. The second and third generation are essentially heavier copies of the first. The quarks are divided into up-type and down-type quarks. The down-type quarks carry the electric charge $Q = -1/3$ and are called down, strange and bottom. The up-type quarks carry the charge $Q = 2/3$ and are named up, charm and top. Since these are fermions they are usually split into left-handed and right-handed fields. The weak interaction couples only to the left-handed fields. Hence, due to their transformation properties the left-handed up-type and down-type quarks can be arranged in a doublet under the $SU(2)_L$ transformation, whereas the right-handed components are arranged in separate singlets. On the one hand there are charged leptons, which carry $Q = -1$ and are called electron, muon and tau, and on the other hand there are the neutral leptons, the neutrinos. The neutrinos are massless and do not carry color or electric charge and therefore only interact via the weak interaction. Furthermore, there are only left-handed neutrinos in the SM. The left-handed fields of the charged leptons and the respective neutrinos can also be combined in a doublet, while the right-handed fields of the charged leptons are arranged in singlets.

In a theory with exact gauge symmetry all gauge bosons are massless. This is the case for the gluon and photon, however the W and Z bosons are known to be massive. Therefore, gauge symmetry has to be broken. To avoid explicit breaking, it is spontaneously broken via the Higgs mechanism [22–26]. A scalar complex Higgs doublet is introduced. When the neutral component of this Higgs doublet acquires a vacuum expectation value, electroweak symmetry is broken spontaneously and masses for all particles coupling directly to the Higgs boson are generated. Of the four degrees of freedom, that are inherent in the introduced doublet, three are absorbed into the gauge bosons to create all polarization modes, and the remaining one manifests as the Higgs particle, which has finally been observed at the LHC and completes the SM.

2.2 Standing Issues of the Standard Model

Despite the success of the SM, there are some experimental observations and theoretical arguments that hint at a theory beyond the SM. Cosmological observations revealed that only about 5% percent of the mass-energy content of the universe can actually be accounted for with the known particles [27]. The rest is made up of so-called dark matter and dark energy. Although for the moment nobody really knows what exactly those two are. Furthermore, experiments observing neutralino oscillations have proven that neutrinos do have mass, although it is very small with the current upper bound being at 2 eV [28]. Another issue is the baryon-antibaryon-asymmetry we observe in today's universe, as the CP-violation inherent in the SM is not sufficient to create this asymmetry.

In addition to these experimental observations that are not explained by the SM, there are also a few theoretical issues, most of which are related to the SM probably being the low-energy limit of a more fundamental theory. If there really exists such a fundamental theory, one expects that the gauge couplings unify at some high scale, just as the weak and electromagnetic theory unify to the electroweak theory in the SM. However, within the framework of the SM the unification of all three gauge couplings cannot be accomplished. The assumption that the SM is some low-energy limit of a more fundamental theory, could also lead to a natural explanation to why the SM features so many unrelated parameters, which have to be fixed by experimental observations, but cannot be predicted. A fundamental theory would allow for a derivation of the SM parameters in terms of the parameters of the fundamental theory and maybe result in relations between the SM parameters. And ideally this fundamental theory is even a "theory of everything" that incorporates gravity, which is not included at all in the SM. In addition to those arguments there is also the so-called hierarchy problem, which we would like to elaborate on.

The hierarchy problem [29–32] is related to the radiative corrections the mass of the Higgs boson receives. If one calculates the corrections to the mass of the Higgs boson at one-loop order, they are quadratic in the cut-off scale. Assuming that the SM is valid up to the Planck scale the cut-off scale is of the order $M_{\mathrm{Pl}} \sim 10^{18}$ GeV. Hence, the Higgs boson mass receives very large corrections. This in itself does not really pose a problem, since the mass parameter appearing in the Lagrangian is not equal to the physical mass. However, in order to achieve a physical mass of ~ 125 GeV the counterterm for the Higgs boson mass has to be chosen appropriately so that it cancels the contribution of the radiative corrections. But since the radiative corrections are roughly 32 orders of magnitude larger than the physical Higgs mass, this can only be accomplished by extremely fine-tuning the counterterm[1]. On the one hand one can simply accept this, or on the other hand one can look for theories that solve this issue. Supersymmetry is such a theory. Supersymmetry is a symmetry that relates bosons and fermions. In supersymmetric theories the radiative corrections to the mass of a scalar particle, that are quadratic in the cut-off scale and originate from fermions, are canceled by the contributions of the respective bosonic partners and vice versa, because the couplings of the superpartners are related.

[1] This is only an issue for the mass of the Higgs boson, since the Higgs boson is the only scalar particle in the SM. The masses of the vector bosons and fermions are protected from quadratic divergences by gauge invariance and chirality, respectively.

2.3 Supersymmetry

Supersymmetry (SUSY) [33–45] is a spacetime symmetry described by an extended Poincaré algebra, that includes, in addition to the bosonic operators of the Poincaré algebra, also fermionic operators, which relate bosons and fermions. In their no-go theorem Coleman and Mandula stated that the maximal set of spacetime symmetry transformations compatible with a relativistic quantum field theory is represented by the Poincaré group [46]. However, they had not considered anticommuting relations for the symmetry generators. It was shown by Haag, Lopuszanski and Sohnius [47] that including both commuting and anticommuting relations for the symmetry generators, which leads to a so-called graduated Lie algebra, the only symmetry consistent with relativistic quantum field theory is supersymmetry. In addition to the generators of translations and Lorentz transformations N anticommuting spinorial generators Q_a $(a = 1...N)$ can be introduced. These fermionic operators are the generators of supersymmetry, which turn a bosonic state into a fermionic state and vice versa

$$Q\,|\text{Boson}\rangle = |\text{Fermion}\rangle\ , \quad Q\,|\text{Fermion}\rangle = |\text{Boson}\rangle\ . \tag{2.1}$$

The single particle states related to each other via this transformation are referred to as superpartners. The superpartners can be arranged in so-called supermultiplets, that are irreducible representations of the SUSY algebra. There are two types of supermultiplets. The chiral supermultiplets consist of a scalar and a fermionic particle, whereas the so-called gauge supermultiplets combine a vector boson and a fermion. The supermultiplets contain an equal number of bosonic and fermionic degrees of freedom. Since the generators of the extended Poincaré algebra commute with the generators of internal symmetries, all particles included in one supermultiplet have the same transformation properties under the respective gauge groups, i.e. they have the same quantum numbers. In fact, they also have the same mass by construction. While it is of advantage that the couplings of the superpartners to other particles are related, because this allows to circumvent the hierarchy problem as outlined in the previous section, the prediction of equal masses indicates that SUSY cannot be an exact symmetry. Otherwise the superpartners of the SM particles would already have been observed. However, how exactly this SUSY breaking takes place, is yet to be established.

In addition to solving the hierarchy problem, SUSY also offers solutions to some of the other issues of the SM mentioned earlier. In supersymmetric extensions of the SM, it is common to impose the so-called R-parity conservation. R-parity is a multiplicative quantum number, that is 1 for SM particles and -1 for their superpartners. If R-parity conservation is assumed, this implies that in collisions of SM particles only pairs of SUSY particles can be produced, and the lightest SUSY particle (LSP) cannot decay any further, as this would violate R-parity. Thus, SUSY offers a candidate for cold dark matter. Furthermore, it has been shown that within in the MSSM ("Minimal Supersymmetric Extension of the SM") the gauge couplings come way closer to actually unifying at the GUT-scale than in the SM [48, 49]. Finally, it should be mentioned that SUSY even hints at a possible solution for the incorporation of gravity[2]. Just like local gauge invariance leads to a massless spin 1 vector boson in quantum electrodynamics, namely the photon, local supersymmetry leads to a massless spin 2 boson, which could be identified with the graviton that mediates the gravitational force.

[2] Even though the resulting theories are not renormalizable.

CHAPTER 3

The Next-to-Minimal Supersymmetric Extension of the Standard Model

This chapter introduces the Next-to-Minimal Supersymmetric Extension of the Standard Model (NMSSM) [50–63] by describing its main features and explaining the phenomenological motivation. Furthermore, the notation for the remaining part of this thesis will be introduced via a thorough discussion of the Higgs sector of the NMSSM at tree level. For extensive reviews of the NMSSM see for example [64] and [65].

3.1 Particle Content and Motivation for the NMSSM

In order to introduce the Next-to-Minimal Supersymmetric Extension of the Standard Model (NMSSM) let us first consider the minimal supersymmetric extension (MSSM). The "minimal" in the name indicates that it is the supersymmetric extension with the minimal particle content. Since it is an extension of the Standard Model (SM) and features the same gauge structure, i.e. $SU(3)_C \otimes SU(2)_L \otimes U(1)_Y$, it is apparent that the particle content is at least doubled compared to the SM. In fact, the particle content is even slightly larger due to the fact that one complex Higgs doublet as in the SM is not sufficient to generate all fermion masses. Because the superpotential must be analytic in the superfields any supersymmetric extension of the SM needs at least two complex Higgs doublets to generate masses for both up- and down-type quarks. The NMSSM features an extended Higgs sector compared to the MSSM. In addition to the two complex Higgs doublets a complex singlet is introduced.

The particle content of the NMSSM is given in Tab. 3.1. The matter particles of the SM and their respective superpartners can be arranged in chiral supermultiplets (upper part of the table), while the force carriers, i.e. the vector bosons, and their superpartners are arranged in gauge supermultiplets (lower part of the table). The first column lists the names of the superfields (denoted as hatted fields), the second and third column give the bosonic and fermionic partners forming the supermultiplets (tilde denotes the superpartners) and the last column gives the quantum numbers of the supermultiplets with respect to the gauge groups. To accommodate the quarks and their superpartners, the scalar squarks, three chiral supermultiplets are required. The left-handed up- and down-type quarks can be arranged

chiral supermultiplets		spin-0	spin-1/2	$SU(3)_C \otimes SU(2)_L \otimes U(1)_Y$
squark/quark	$\hat{Q}$	$\tilde{Q} = (\tilde{u}_L,\, \tilde{d}_L)^T$	$Q = (u_L,\, d_L)^T$	(**3**,**2**,1/6)
	$\hat{u}$	$\tilde{u}_R^*$	$u_R^\dagger$	($\overline{\mathbf{3}}$,**1**,–2/3)
	$\hat{d}$	$\tilde{d}_R^*$	$d_R^\dagger$	($\overline{\mathbf{3}}$,**1**,1/3)
slepton/lepton	$\hat{L}$	$\tilde{L} = (\tilde{\nu}_L,\, \tilde{e}_L)^T$	$L = (\nu_L,\, e_L)^T$	(**1**,**2**,–1/2)
	$\hat{e}$	$\tilde{e}_R^*$	$e_R^\dagger$	(**1**,**1**,1)
Higgs/Higgsino	$\hat{H}_u$	$H_u = (H_u^+,\, H_u^0)^T$	$\tilde{H}_u = (\tilde{H}_u^+,\, \tilde{H}_u^0)^T$	(**1**,**2**,1/2)
	$\hat{H}_d$	$H_d = (H_d^0,\, H_d^-)^T$	$\tilde{H}_d = (\tilde{H}_d^0,\, \tilde{H}_d^-)^T$	(**1**,**2**,–1/2)
	$\hat{S}$	S	$\tilde{S}$	(**1**,**1**,0)

gauge supermultiplets	spin-1	spin-1/2	$SU(3)_C \otimes SU(2)_L \otimes U(1)_Y$
gluon/gluino	g	$\tilde{g}$	(**8**,**1**,0)
W boson/wino	$W^\pm, W^0$	$\tilde{W}^\pm, \tilde{W}^0$	(**1**,**3**,0)
B boson/bino	B^0	$\tilde{B}^0$	(**1**,**1**,0)

Table 3.1: Particle content of the NMSSM. The names of the supermultiplets and the bosonic and fermionic partners forming the multiplets are listed, both for the chiral supermultiplets (upper part) and the gauge supermultiplets (lower part). The last column gives the quantum numbers with respect to the gauge groups. The hypercharge Y is given in the convention such that for the electric charge $Q = I_W^3 + Y$ holds, with I_W^3 being the third component of the weak isospin.

in the $SU(2)_L$-doublet Q, which together with the doublet $\tilde{Q}$ that includes the left-handed scalar squarks[1] forms the superfield $\hat{Q}$. To represent the right-handed fields two singlets are introduced. The up-type quarks and squarks are grouped in $\hat{u}$ and the down-type ones in $\hat{d}$. Note that both $\hat{u}$ and $\hat{d}$ are defined to include the conjugate right-handed fields. This is commonly done so that they transform as left-handed fields. Altogether there is one left- and one right-handed up-type quark for each of the three generations. The same holds for the down-type quarks. For the squarks there are two up-type and two down-type squarks for each generation, which mix to form the respective mass eigenstates. Similarly the left-handed charged leptons and the neutrinos are combined in a doublet L, which together with their superpartners, the scalar sleptons, forms the superfield $\hat{L}$. The right-handed charged leptons and sleptons are arranged in a singlet denoted by $\hat{e}$. Hence, there are six charged sleptons (two for each generation) and three sneutrinos. As already mentioned there are two complex Higgs doublets comprising each a scalar and a charged component plus one complex singlet. Together with their superpartners, the Higgsinos, they form the superfields $\hat{H}_u$, $\hat{H}_d$ and $\hat{S}$. After electroweak symmetry breaking and gauge fixing there are seven physical Higgs bosons. The gauge supermultiplets contain the vector bosons and their superpartners. The fermionic superpartner of the gluon is the gluino. The superpartners of the W and B bosons are the winos, respectively the bino. As the neutral wino, the bino and the neutral Higgsinos feature the same quantum numbers, they mix to the so-called neutralinos. There are five neutralinos, one more than in the MSSM due to the additional singlet. The charged winos and the charged Higgsinos mix to the mass eigenstates referred to as charginos.

[1] Please note, that for the scalar particles the term "left-handed" does not refer to chirality, but simply indicates that it is the superpartner to a fermion of left-handed chirality.

Once the particle content of a supersymmetric theory is defined, the only missing piece is the superpotential, as from the superpotential the complete Lagrangian, i.e. all interactions, mass terms, etc. can be derived. The superpotential of the NMSSM reads in terms of the superfields defined above

$$W = \hat{u}\, Y_u \left(\hat{Q}^T \epsilon \hat{H}_u\right) - \hat{d}\, Y_d \left(\hat{Q}^T \epsilon \hat{H}_d\right) - \hat{e}\, Y_e \left(\hat{L}^T \epsilon \hat{H}_d\right) + \lambda \hat{S} \left(\hat{H}_u^T \epsilon \hat{H}_d\right) + \frac{1}{3}\kappa \hat{S}^3 \,, \tag{3.1}$$

where all generation and color indices have been suppressed for readability. The dimensionless Yukawa couplings Y_u, Y_d and Y_e are assumed to be diagonal, i.e. generation mixing is not included. Written with all indices the first term of the superpotential is $\hat{u}^i Y_u^{ij} (\hat{Q}^{j,a} \epsilon_{ab} \hat{H}_u^b)$ with the generation indices $i, j \in \{1, 2, 3\}$, the indices of $SU(2)$ $a, b \in \{1, 2\}$ and the totally antisymmetric tensor $\epsilon_{12} = -\epsilon_{21} = 1$. The first three terms of the superpotential are responsible for the generation of the fermion masses. When H_u acquires a vacuum expectation value the masses for the up-type quarks are generated, while H_d acquiring a vacuum expectation value generates masses for the down-type fermions[2]. The last two terms depend only on the Higgs fields. The term which goes with the dimensionless coupling λ couples all three Higgs fields, while the term that goes with the dimensionless coupling κ is cubic in the singlet field. In general the couplings λ and κ are complex and therefore sources of CP-violation.

The superpotential given in Eq. (3.1) is not the most general one. In fact, we work with a scale invariant superpotential here, omitting terms of the form

$$W^{\text{scale}} = \mu' \left(\hat{H}_u^T \epsilon \hat{H}_d\right) + \xi_F \hat{S} + \frac{1}{2}\mu'' \hat{S}^2 \,, \tag{3.2}$$

which include the dimensionful parameters μ', μ'' (mass dimension) and ξ_F (mass^2 dimension). Recalling one of the main motivations of going from the MSSM to the NMSSM, it becomes obvious why those terms with dimensionful couplings are discarded. The MSSM suffers of the so-called μ-problem [66]. In the MSSM the most general superpotential reads

$$W^{\text{MSSM}} = \hat{u}\, Y_u \left(\hat{Q}^T \epsilon \hat{H}_u\right) - \hat{d}\, Y_d \left(\hat{Q}^T \epsilon \hat{H}_d\right) - \hat{e}\, Y_e \left(\hat{L}^T \epsilon \hat{H}_d\right) + \mu \left(\hat{H}_u^T \epsilon \hat{H}_d\right) . \tag{3.3}$$

Phenomenology requires the dimensionful parameter μ to be of the order of the electroweak scale. However, this term is already present before electroweak symmetry breaking (EWSB) takes place. Hence, there is no evident reason why μ should be of this order and it has to be put in by hand. More natural scales for μ would be zero or the Planck scale. The NMSSM circumvents this problem by generating a term similar to the μ term in the MSSM dynamically when the singlet acquires a vacuum expectation value according to

$$\lambda S \left(H_u^T \epsilon H_d\right) \xrightarrow{\text{EWSB}} \lambda \langle S \rangle \left(H_u^T \epsilon H_d\right) \longleftrightarrow \mu_{\text{eff}} = \lambda \langle S \rangle \,. \tag{3.4}$$

On the one hand these considerations motivate the next-to-last term of Eq. (3.1), while at the same time they explain why the terms including dimensionful parameters should not be introduced in the NMSSM superpotential, as this would reintroduce the μ-problem.

In addition to solving the μ-problem of the MSSM the next-to-last term of Eq. (3.1) also has the nice effect of raising the tree-level bound on the mass of the lightest non-singlet-like Higgs boson. In the MSSM the tree-level mass of the lightest Higgs boson cannot be larger than the mass of the Z boson, the explicit bound being

$$M_{H_1}^2 \lesssim M_Z^2 \cos^2 2\beta \,, \tag{3.5}$$

[2] Down-type fermions means both down-type quarks and charged leptons.

with the mass of the Z boson M_Z and the angle β, which is defined via the ratio of the vacuum expectation values of the Higgs doublets as $\tan\beta = \langle H_u^0 \rangle / \langle H_d^0 \rangle$. Hence, in order to obtain a Higgs mass in the observed region of ~ 125 GeV large radiative corrections are necessary in the MSSM, i.e. the model is fine-tuned. In the NMSSM the bound receives a further contribution from the quartic coupling which raises the bound to

$$M_{H_1}^2 \lesssim M_Z^2 \cos^2 2\beta + \tfrac{\lambda^2 v^2}{2} \sin^2 2\beta \,. \tag{3.6}$$

Where $v \approx 246$ GeV is the vacuum expectation value. Therefore, in the NMSSM phenomenologically valid scenarios are often less fine-tuned.

The term cubic in the singlet field is important, because it breaks an accidental Peccei-Quinn (PQ) symmetry explicitly. If this term was not present, the symmetry would be broken spontaneously when the singlet acquires a vacuum expectation value. Due to this spontaneous breaking a massless axion would appear [67]. The non-observation of such an PQ axion, would severely constrain λ to be extremely small and to generate an effective μ term of the right order the vacuum expectation value of the singlet would have to be unacceptably large [68].

To summarize: the NMSSM features an enlarged Higgs sector compared to the MSSM, which will be discussed in detail in the following section. Altogether there are seven physical Higgs bosons. It is phenomenologically interesting to discuss such an extended Higgs sector, because it solves the μ-problem of the MSSM and is generally less fine-tuned. Furthermore, the introduction of the singlet offers the possibility to construct scenarios with light Higgs bosons, even below the LEP exclusion limits, that feature reduced couplings to the SM particles due to a large singlet admixture. In this sense the Higgs sector of the NMSSM is less restricted by the experimental results. In contrast to the MSSM, the complex NMSSM allows for CP-violation already at tree level. This plethora of phenomenological possibilities is reason enough to accept the NMSSM, although it is more complicated with a larger particle content (two more Higgs bosons and one additional neutralino) and lengthy expressions for the couplings.

3.2 NMSSM Lagrangian and Higgs Sector at Tree Level

3.2.1 The NMSSM Lagrangian

Starting from the superpotential given in Eq. (3.1) almost the whole Lagrangian can be constructed. Let us denote this part, which includes all kinetic terms and interactions of the unbroken supersymmetric theory as $\mathcal{L}_{\text{SUSY}}$. The missing pieces are $\mathcal{L}_{\text{soft}}$, which contains the soft SUSY breaking terms, the gauge-fixing part, denoted by $\mathcal{L}_{\text{fix}}$, and the part including the ghost fields $\mathcal{L}_{\text{ghost}}$. Hence, the complete Lagrangian is given by

$$\mathcal{L}_{\text{NMSSM}} = \mathcal{L}_{\text{SUSY}} + \mathcal{L}_{\text{soft}} + \mathcal{L}_{\text{fix}} + \mathcal{L}_{\text{ghost}} \,. \tag{3.7}$$

In the light of the non-observation of any superpartners, it is obvious that supersymmetry cannot be exact and has to be broken. Since the mechanism of supersymmetry breaking is not known, it is common to introduce the respective terms by hand. However, only terms that break SUSY softly are allowed. Soft breaking here means that the terms induce the mass splitting between the SM particles and their superpartners, while taking care not to spoil the relations of the couplings, that led to the cancellation of the quadratic loop divergences in the

loop corrections to the Higgs boson mass. In the NMSSM those soft SUSY breaking terms read

$$\begin{aligned}-\mathcal{L}_{\text{soft}} =& m_{\tilde{Q}}^2 \tilde{Q}^\dagger \tilde{Q} + m_{\tilde{u}_R}^2 |\tilde{u}_R|^2 + m_{\tilde{d}_R}^2 |\tilde{d}_R|^2 + \Big(A_u Y_u \tilde{u}_R^* (\tilde{Q}^T \epsilon H_u) - A_d Y_d \tilde{d}_R^* (\tilde{Q}^T \epsilon H_d) + h.c. \Big) + \\ &+ m_{\tilde{L}}^2 \tilde{L}^\dagger \tilde{L} + m_{\tilde{e}_R}^2 |\tilde{e}_R|^2 - \Big(A_e Y_e \tilde{e}_R^* (\tilde{L}^T \epsilon H_d) + h.c. \Big) + \\ &+ m_{H_u}^2 H_u^\dagger H_u + m_{H_d}^2 H_d^\dagger H_d + m_S^2 |S|^2 + \left(A_\lambda \lambda (H_u^T \epsilon H_d) S + \frac{1}{3} A_\kappa \kappa S^3 + h.c. \right) + \\ &+ \frac{1}{2} \Big(M_1 \tilde{B}^0 \tilde{B}^0 + M_2 \tilde{W}^i \tilde{W}^i + M_3 \tilde{g} \tilde{g} + h.c. \Big) . \end{aligned} \tag{3.8}$$

The first line of Eq. (3.8) specifies the soft SUSY breaking terms for the squark sector, the second line those of the slepton sector, the third line those of the Higgs sector and the fourth line those of the gauginos. Soft SUSY breaking masses and trilinear couplings are introduced for the different sectors; i.e. $m_{\tilde{Q}}$, $m_{\tilde{u}_R}$, $m_{\tilde{d}_R}$ and A_u, A_d for the squark sector, $m_{\tilde{L}}$, $m_{\tilde{e}_R}$ and A_e for the slepton sector, m_{H_u}, m_{H_d}, m_S and A_λ, A_κ for the Higgs sector and finally for the gauginos the soft SUSY breaking masses M_1, M_2 and M_3. The trilinear couplings of the sfermions are in general complex 3×3 matrices, but just as the Yukawa matrices we take them to be diagonal, however still complex. Furthermore, the trilinear soft SUSY breaking couplings of the Higgs sector and the soft SUSY breaking masses of the gauginos are complex. All other soft SUSY breaking parameters, i.e. the soft SUSY breaking masses of the bosonic states, are real.

3.2.2 The Higgs Potential

The Higgs potential as derived from the superpotential reads

$$\begin{aligned} V =& |\lambda|^2 |S|^2 \left(H_u^\dagger H_u + H_d^\dagger H_d \right) + \left| \lambda (H_u^T \epsilon H_d) + \kappa S^2 \right|^2 + \\ &+ \frac{1}{2} g_2^2 |H_u^\dagger H_d|^2 + \frac{1}{8} (g_1^2 + g_2^2) (H_u^\dagger H_u - H_d^\dagger H_d)^2 + \\ &+ m_{H_u}^2 H_u^\dagger H_u + m_{H_d}^2 H_d^\dagger H_d + m_S^2 |S|^2 + \left(A_\lambda \lambda (H_u^T \epsilon H_d) S + \frac{1}{3} A_\kappa \kappa S^3 + h.c. \right) , \end{aligned} \tag{3.9}$$

where the first line lists the F-terms, the second line consists of the D-terms and the third line originates from the soft SUSY breaking Lagrangian. Here g_1 and g_2 denote the electroweak gauge couplings.

The neutral components of the Higgs fields can be expanded around their respective vacuum expectation values. Furthermore, the remaining shifted complex fields can be written in terms of two real fields, the scalar fields are denoted as h_X and the pseudoscalar fields are denoted as a_X, with the index X indicating whether the field is part of one of the doublets ($X = u, d$) or the singlet ($X = s$). Inserting this into the doublets yields

$$H_d = \begin{pmatrix} \frac{1}{\sqrt{2}} (v_d + h_d + \mathrm{i} a_d) \\ H_d^- \end{pmatrix} \qquad \text{and} \qquad H_u = \mathrm{e}^{\mathrm{i}\varphi_u} \begin{pmatrix} H_u^+ \\ \frac{1}{\sqrt{2}} (v_u + h_u + \mathrm{i} a_u) \end{pmatrix} , \tag{3.10}$$

while the singlet can be decomposed as

$$S = \frac{1}{\sqrt{2}} \mathrm{e}^{\mathrm{i}\varphi_s} (v_s + h_s + \mathrm{i} a_s) . \tag{3.11}$$

In the above parametrization the phases φ_u and φ_s were introduced. Due to these phases the vacuum expectation values v_u, v_d and v_s can always be chosen to be real and non-negative. Note that the introduction of only two phases is sufficient, because only the relative phases between the Higgs fields have a physical meaning, as one phase can always be rotated away.

Not all of the parameters appearing in the Higgs potential are independent. Exploiting the minimization conditions of the Higgs potential relations between the parameters can be derived.

3.2.3 The Tadpole Conditions

When the Higgs fields acquire their vacuum expectation values given by

$$\langle H_d \rangle = \begin{pmatrix} \frac{v_d}{\sqrt{2}} \\ 0 \end{pmatrix}, \qquad \langle H_u \rangle = \mathrm{e}^{\mathrm{i}\varphi_u} \begin{pmatrix} 0 \\ \frac{v_u}{\sqrt{2}} \end{pmatrix} \qquad \text{and} \quad \langle S \rangle = \mathrm{e}^{\mathrm{i}\varphi_s} \frac{v_s}{\sqrt{2}}, \tag{3.12}$$

the Higgs potential has to display a minimum. Hence, the first derivatives of the Higgs potential with respect to the Higgs fields have to vanish at the minimum,

$$\text{i.e. } \left\langle \frac{\partial V}{\partial h_d} \right\rangle = \left\langle \frac{\partial V}{\partial h_u} \right\rangle = \left\langle \frac{\partial V}{\partial h_s} \right\rangle = \left\langle \frac{\partial V}{\partial a_d} \right\rangle = \left\langle \frac{\partial V}{\partial a_u} \right\rangle = \left\langle \frac{\partial V}{\partial a_s} \right\rangle = 0\,. \tag{3.13}$$

This is equivalent to the statement that the Higgs potential cannot feature terms linear in the Higgs fields. When going to higher orders the tadpole relations gain corrections as well which ensure that the Higgs potential is still minimized correctly. Therefore, it is useful to define the so-called tadpole parameters

$$t_X := \left\langle \frac{\partial V}{\partial X} \right\rangle \text{ with } X = \{h_d, h_u, h_s, a_d, a_u, a_s\} \text{ and } t_X = 0 \text{ at tree level.} \tag{3.14}$$

The tadpole parameters are obtained as

$$\begin{aligned}
t_{h_d} =& \frac{1}{2}|\lambda| \left(-\sqrt{2} v_s v_u \, |A_\lambda| \cos\varphi_x + |\lambda| v_d \left(v_s^2 + v_u^2 \right) - |\kappa| v_s^2 v_u \cos\varphi_y \right) + \\
& + \frac{1}{8} \left(g_1^2 + g_2^2 \right) v_d \left(v_d^2 - v_u^2 \right) + m_{H_d}^2 v_d \,, && \text{(3.15a)} \\
t_{h_u} =& \frac{1}{2}|\lambda| \left(-\sqrt{2} v_s v_d \, |A_\lambda| \cos\varphi_x + |\lambda| v_u \left(v_s^2 + v_d^2 \right) - |\kappa| v_s^2 v_d \cos\varphi_y \right) + \\
& + \frac{1}{8} \left(g_1^2 + g_2^2 \right) v_u \left(v_u^2 - v_d^2 \right) + m_{H_u}^2 v_u \,, && \text{(3.15b)} \\
t_{h_s} =& \frac{1}{2} v_s \left(\sqrt{2} v_s |\kappa| \, |A_\kappa| \cos\varphi_z + |\lambda|^2 \left(v_d^2 + v_u^2 \right) - 2 v_d v_u |\kappa| |\lambda| \cos\varphi_y + 2|\kappa|^2 v_s^2 \right) + \\
& - \frac{1}{\sqrt{2}} v_d v_u |\lambda| \, |A_\lambda| \cos\varphi_x + m_S^2 v_s \,, && \text{(3.15c)} \\
t_{a_d} =& \frac{1}{\sqrt{2}} v_s v_u |\lambda| \, |A_\lambda| \sin\varphi_x + \frac{1}{2} v_s^2 v_u |\kappa| |\lambda| \sin\varphi_y \,, && \text{(3.15d)} \\
t_{a_u} =& \frac{1}{\sqrt{2}} v_s v_d |\lambda| \, |A_\lambda| \sin\varphi_x + \frac{1}{2} v_s^2 v_d |\kappa| |\lambda| \sin\varphi_y \,, && \text{(3.15e)} \\
t_{a_s} =& \frac{1}{\sqrt{2}} v_d v_u |\lambda| \, |A_\lambda| \sin\varphi_x - \frac{1}{\sqrt{2}} v_s^2 |\kappa| \, |A_\kappa| \sin\varphi_z - v_d v_s v_u |\kappa| |\lambda| \sin\varphi_y \,, && \text{(3.15f)}
\end{aligned}$$

where we introduced abbreviations for the three phase combinations that appear, which are

$$\begin{aligned}\varphi_x &= \varphi_u + \varphi_s + \varphi_\lambda + \varphi_{A_\lambda}\,,\\ \varphi_y &= \varphi_u - 2\varphi_s + \varphi_\lambda - \varphi_\kappa\,,\\ \varphi_z &= 3\varphi_s + \varphi_\kappa + \varphi_{A_\kappa}\,.\end{aligned} \tag{3.16}$$

The tadpole relations can be used to replace some of the parameters appearing originally in the Higgs potential in favor of the tadpole parameters. The tadpole relations for the scalar fields are typically used to eliminate the soft SUSY breaking masses m_{H_d}, m_{H_u} and m_S. The tadpole relations for the pseudoscalar fields are trivially satisfied for the CP-conserving NMSSM, since then all phases are multiples of π. For the CP-violating case, i.e. for arbitrary phases, the pseudoscalar tadpole relations can be used to eliminate two parameters[3]. One possible choice is to eliminate two of the three appearing phase combinations. This reveals that the Higgs sector at tree level only features one physical phase. However, it might also be useful to substitute the imaginary parts of A_λ and A_κ to comply with certain conventions as will be elaborated later on.

3.2.4 The Mass Matrices of the Neutral Higgs Fields

The Higgs potential given in Eq. (3.9) can be cast into the general form

$$V = \frac{1}{2}\Phi^T \mathcal{M}_{\text{Higgs}}\Phi + V_{\Phi\Phi\Phi} + V_{\Phi\Phi\Phi\Phi} + \Phi_i t_{\Phi_i} \text{ with } \Phi = (a_d, a_u, a_s, h_d.h_u, h_s)^T\,. \tag{3.17}$$

Here the terms $V_{\Phi\Phi\Phi}$ and $V_{\Phi\Phi\Phi\Phi}$ are the parts of the potential including the trilinear and quartic Higgs self-interactions. The last term stands for the tadpole part as defined in the previous section. From the terms bilinear in the Higgs fields the mass matrix $\mathcal{M}_{\text{Higgs}}$ in the interaction basis Φ can be read off. It is common to split this 6×6 mass matrix into three submatrices according to

$$\mathcal{M}^{6\times6}_{\text{Higgs}} = \begin{pmatrix} \mathcal{M}^{3\times3}_{\mathbf{a}} & \mathcal{M}^{3\times3}_{\mathbf{ah}} \\ \left(\mathcal{M}^{3\times3}_{\mathbf{ah}}\right)^T & \mathcal{M}^{3\times3}_{\mathbf{h}} \end{pmatrix}\,. \tag{3.18}$$

The usefulness of this division becomes obvious when looking at the explicit entries of

$$\mathcal{M}_{\mathbf{ah}} = \frac{1}{2}|\kappa||\lambda|\sin\varphi_y \begin{pmatrix} 0 & 0 & v_s v_u \\ 0 & 0 & v_d v_s \\ -3v_s v_u & -3v_d v_s & 4v_d v_u \end{pmatrix} \tag{3.19}$$

where the tadpole relations were applied to eliminate φ_x and φ_z so that only φ_y as defined in Eq. (3.16) remains. As can be easily seen, in the real NMSSM all entries of $\mathcal{M}_{\mathbf{ah}}$ vanish and the scalar and pseudoscalar interaction eigenstates do not mix at all. Hence, the real NMSSM is CP-conserving and the scalar and pseudoscalar sectors can be considered separately. On the other hand in the complex NMSSM CP-violation is already induced at tree level in contrast to the MSSM, where it enters only at loop level. Note, however, that the CP-violation at tree level induces only scalar-pseudoscalar-mixing between doublet and singlet but no doublet-doublet mixing.

[3] They cannot be used to replace three parameters because t_{a_d} and t_{a_u} are linearly dependent.

The submatrix for the scalar Higgs fields in the basis (h_d, h_u, h_s) reads

$$\mathcal{M}_{\mathbf{h}}|_{11} = \frac{1}{4}\left(2|\lambda|v_s \tan\beta\left(\sqrt{2}\,|A_\lambda|\cos\varphi_x + v_s|\kappa|\cos\varphi_y\right) + v^2\cos^2\beta\left(g_1^2+g_2^2\right)\right), \tag{3.20a}$$

$$\mathcal{M}_{\mathbf{h}}|_{12} = \mathcal{M}_{\mathbf{h}}|_{21} = \frac{1}{4}\Big(-2\sqrt{2}v_s|\lambda|\,|A_\lambda|\cos\varphi_x + v^2\sin\beta\cos\beta\left(4|\lambda|^2 - g_1^2 - g_2^2\right) + -2v_s^2|\kappa||\lambda|\cos\varphi_y\Big), \tag{3.20b}$$

$$\mathcal{M}_{\mathbf{h}}|_{13} = \mathcal{M}_{\mathbf{h}}|_{31} = \frac{1}{2}v|\lambda|\left(2v_s\cos\beta|\lambda| - \sin\beta\left(\sqrt{2}\,|A_\lambda|\cos\varphi_x + 2v_s|\kappa|\cos\varphi_y\right)\right), \tag{3.20c}$$

$$\mathcal{M}_{\mathbf{h}}|_{22} = \frac{1}{4}\left(2\sqrt{2}v_s\cot\beta|\lambda|\,|A_\lambda|\cos\varphi_x + 2v_s^2\cot\beta|\kappa||\lambda|\cos\varphi_y + v^2\sin^2\beta\left(g_1^2+g_2^2\right)\right), \tag{3.20d}$$

$$\mathcal{M}_{\mathbf{h}}|_{23} = \mathcal{M}_{\mathbf{h}}|_{32} = \frac{1}{2}v|\lambda|\left(-\sqrt{2}\cos\beta\,|A_\lambda|\cos\varphi_x + 2v_s\sin\beta|\lambda| - 2v_s\cos\beta|\kappa|\cos\varphi_y\right), \tag{3.20e}$$

$$\mathcal{M}_{\mathbf{h}}|_{33} = \frac{1}{\sqrt{2}v_s}\Big(v^2\sin\beta\cos\beta|\lambda|\,|A_\lambda|\cos\varphi_x + v_s^2|\kappa|\,|A_\kappa|\cos\varphi_z\Big) + 2|\kappa|^2v_s^2\,. \tag{3.20f}$$

Here we exchanged the two vacuum expectation values v_u and v_d by $\tan\beta$ and v, which are defined as

$$\tan\beta = \frac{v_u}{v_d} \quad \text{and} \quad v^2 = v_d^2 + v_u^2\,, \tag{3.21}$$

where v takes on the same value as in the Standard Model, i.e. $v \approx 246$ GeV.

The submatrix for the pseudoscalar Higgs fields in the basis (a_d, a_u, a_s) reads

$$\mathcal{M}_{\mathbf{a}}|_{11} = \frac{1}{2}|\lambda|\tan\beta v_s\left(\sqrt{2}\,|A_\lambda|\cos\varphi_x + |\kappa|v_s\cos\varphi_y\right), \tag{3.22a}$$

$$\mathcal{M}_{\mathbf{a}}|_{12} = \mathcal{M}_{\mathbf{a}}|_{21} = \frac{1}{2}|\lambda|v_s\left(\sqrt{2}\,|A_\lambda|\cos\varphi_x + |\kappa|v_s\cos\varphi_y\right), \tag{3.22b}$$

$$\mathcal{M}_{\mathbf{a}}|_{13} = \mathcal{M}_{\mathbf{a}}|_{31} = \frac{1}{\sqrt{2}}v\sin\beta|\lambda|\,|A_\lambda|\cos\varphi_x - v_sv\sin\beta|\kappa||\lambda|\cos\varphi_y\,, \tag{3.22c}$$

$$\mathcal{M}_{\mathbf{a}}|_{22} = \frac{1}{2}|\lambda|\cot\beta v_s\left(\sqrt{2}\,|A_\lambda|\cos\varphi_x + |\kappa|v_s\cos\varphi_y\right), \tag{3.22d}$$

$$\mathcal{M}_{\mathbf{a}}|_{23} = \mathcal{M}_{\mathbf{a}}|_{32} = \frac{1}{\sqrt{2}}v\cos\beta|\lambda|\,|A_\lambda|\cos\varphi_x - v_sv\cos\beta|\kappa||\lambda|\cos\varphi_y\,, \tag{3.22e}$$

$$\mathcal{M}_{\mathbf{a}}|_{33} = \frac{1}{\sqrt{2}v_s}\Big(v^2\sin\beta\cos\beta|\lambda|\,|A_\lambda|\cos\varphi_x - 3v_s^2|\kappa|\,|A_\kappa|\cos\varphi_z\Big) + + 2v^2\sin\beta\cos\beta|\kappa||\lambda|\cos\varphi_y\,. \tag{3.22f}$$

It is convenient to go to a basis in which the Goldstone boson is already separated. This is achieved by the following transformation

$$\begin{pmatrix} G \\ a \end{pmatrix} = \begin{pmatrix} -\cos\beta_n & \sin\beta_n \\ \sin\beta_n & \cos\beta_n \end{pmatrix}\begin{pmatrix} a_d \\ a_u \end{pmatrix}. \tag{3.23}$$

At tree level the rotation angle β_n coincides with the angle $\beta = \arctan v_u/v_d$. The distinction is only important when higher orders are considered as will be elaborated in Ch. 7. For the following tree-level discussion we set $\beta_n = \beta$. In this new basis (G, a, a_s) the elements of the

submatrix for the pseudoscalar Higgs bosons, now denoted by $\mathcal{M}'_{\mathbf{a}}$, are

$$\mathcal{M}'_{\mathbf{a}}\big|_{11} = \mathcal{M}'_{\mathbf{a}}\big|_{12} = \mathcal{M}'_{\mathbf{a}}\big|_{13} = \mathcal{M}'_{\mathbf{a}}\big|_{21} = \mathcal{M}'_{\mathbf{a}}\big|_{31} = 0 \tag{3.24a}$$

$$\mathcal{M}'_{\mathbf{a}}\big|_{22} = \frac{1}{2}\frac{|\lambda| v_s}{\sin\beta\cos\beta}\left(\sqrt{2}\,|A_\lambda|\cos\varphi_x + |\kappa| v_s \cos\varphi_y\right) \tag{3.24b}$$

$$\begin{aligned}\mathcal{M}'_{\mathbf{a}}\big|_{33} =& \frac{v^2|\lambda|\cos\beta\sin\beta}{2v_s}\left(\sqrt{2}\,|A_\lambda|\cos\varphi_x + 4|\kappa| v_s\cos\varphi_y\right) + \\ & - \frac{3}{\sqrt{2}}|\kappa|\,|A_\kappa|\, v_s \cos\varphi_z\end{aligned} \tag{3.24c}$$

$$\mathcal{M}'_{\mathbf{a}}\big|_{23} = \mathcal{M}'_{\mathbf{a}}\big|_{32} = \frac{v|\lambda|\,|A_\lambda|\cos\varphi_x}{\sqrt{2}} - v v_s |\kappa||\lambda|\cos\varphi_y \tag{3.24d}$$

The submatrix

$$\mathcal{M}'_{\mathbf{ah}} = \frac{1}{2}|\kappa||\lambda|\sin\varphi_y v \begin{pmatrix} 0 & 0 & 0 \\ 0 & 0 & v_s \\ -3\sin\beta v_s & -3\cos\beta v_s & 2v\sin 2\beta \end{pmatrix} \tag{3.25}$$

describes the pseudoscalar-scalar-mixing in the new basis. A look at $\mathcal{M}'_{\mathbf{a}}$ and $\mathcal{M}'_{\mathbf{ah}}$ reveals that the massless[4] Goldstone mode decouples completely. Hence, it is sufficient to consider either a 5×5 mass matrix in the CP-violating case, or the submatrices for the pseudoscalar (2×2) and scalar (3×3) Higgs fields separately in the CP-conserving case.

The Higgs masses at tree level are given by the square roots of the eigenvalues of the Higgs mass matrix. The rotation matrix that diagonalizes the mass matrix relates the mass eigenstates to the interaction eigenstates. Even for the complex NMSSM the mass matrix is always real and symmetric, hence it can be diagonalized by means of an orthogonal matrix, denoted by $\mathcal{R}$ for the complex case, according to

$$\begin{aligned}&\mathcal{R}\,\mathcal{M}^{5\times5}_{\text{Higgs}}\,\mathcal{R}^T = \text{diag}\left(m^2_{h_1}, m^2_{h_2}, m^2_{h_3}, m^2_{h_4}, m^2_{h_5}\right) && \Rightarrow \quad h_i = \mathcal{R}_{ij}\,\boldsymbol{\phi}_j \\ &\text{with} \quad m^2_{h_1} \le m^2_{h_2} \le m^2_{h_3} \le m^2_{h_4} \le m^2_{h_5} && \text{and} \quad \boldsymbol{\phi} = (a, a_s, h_d, h_u, h_s)^T .\end{aligned} \tag{3.26}$$

Here the tree-level mass eigenstates are denoted by h_i $(i = 1...5)$ and we order them by ascending mass, hence h_1 is the lightest state.

In the case of the real NMSSM the 5×5 matrix can be decomposed into the two submatrices $\mathcal{R}^P$ (2×2) and $\mathcal{R}^S$ (3×3) that diagonalize the pseudoscalar and scalar mass matrix, respectively.

$$\mathcal{R}^P\,\mathcal{M}_{\mathbf{a}}\,(\mathcal{R}^P)^T = \text{diag}\big(m^2_{a_1}, m^2_{a_2}\big) \quad \Rightarrow \quad a_i = \mathcal{R}^P_{ij}\,(\boldsymbol{\phi}_a)_j \quad \text{with} \quad \boldsymbol{\phi}_a = (a, a_s)^T \tag{3.27a}$$

$$\mathcal{R}^S\,\mathcal{M}_{\mathbf{h}}\,(\mathcal{R}^S)^T = \text{diag}\big(m^2_{h_1}, m^2_{h_2}, m^2_{h_3}\big) \quad \Rightarrow \quad h_i = \mathcal{R}^S_{ij}\,(\boldsymbol{\phi}_h)_j \quad \text{with} \quad \boldsymbol{\phi}_h = (h_d, h_u, h_s)^T \tag{3.27b}$$

Here a_i $(i = 1, 2)$ are the CP-odd mass eigenstates states, while h_i $(i = 1, 2, 3)$ are the CP-even mass eigenstates. Once again they are ordered by ascending mass.

[4]The Goldstone boson acquires the same mass as the Z boson when the gauge fixing terms are added.

3.2.5 The Charged Higgs Boson

Analogously to the way the neutral Goldstone was separated, the charged Goldstone boson can be decoupled via the transformation

$$\begin{pmatrix} G^+ \\ H^+ \end{pmatrix} = \begin{pmatrix} -\cos\beta_c & \sin\beta_c \\ \sin\beta_c & \cos\beta_c \end{pmatrix} \begin{pmatrix} \left(H_d^-\right)^* \\ H_u^+ \end{pmatrix} . \tag{3.28}$$

At tree level $\beta_c = \beta_n = \beta$ holds[5]. Applying this transformation to the mass matrix of the charged Higgs sector yields the massless Goldstone boson and the tree-level mass of the charged Higgs boson

$$M_{H^\pm}^2 = \frac{1}{2}\frac{|\lambda| v_s}{\sin\beta\cos\beta}\left(\sqrt{2}\,|A_\lambda|\cos\varphi_x + |\kappa| v_s \cos\varphi_y\right) - \frac{1}{4}v^2\left(2|\lambda|^2 - g_2^2\right) . \tag{3.29}$$

3.2.6 Independent Parameters of the Higgs Sector

When calculating higher order corrections one needs to renormalize (see Ch. 4). To perform the renormalization correctly it is essential to chose an adequate set of independent parameters. So let us look at the parameters that appear in the Higgs sector at first sight, which are

$$g_1,\, g_2,\, v_u,\, v_d,\, v_s,\, \kappa,\, \lambda,\, A_\kappa,\, A_\lambda,\, m_{H_d}^2,\, m_{H_u}^2,\, m_S^2,\, \varphi_u \text{ and } \varphi_s\,, \tag{3.30}$$

the electroweak gauge couplings, the vacuum expectation values of the Higgs fields, the dimensionless complex couplings λ and κ introduced in the superpotential, the complex trilinear soft SUSY breaking couplings, the soft SUSY breaking masses of the Higgs fields and the phases of the Higgs fields. However, not all of these parameters are independent and for some it is advantageous to exchange them by other quantities. The electroweak gauge couplings and the vacuum expectation values of the doublet fields can be traded for the masses of the W and Z bosons, the electric charge and the ratio of the vacuum expectation values of the doublet fields :

$$g_1,\, g_2,\, v_u,\, v_d \quad \longrightarrow \quad M_W^2,\, M_Z^2,\, e,\, \tan\beta\,. \tag{3.31a}$$

The required relations are

$$\tan\beta = \frac{v_u}{v_d}, \quad M_W = \frac{1}{2}v g_2, \quad M_Z = \frac{1}{2}v\sqrt{g_1^2+g_2^2}, \quad e = \frac{g_1 g_2}{\sqrt{g_1^2+g_2^2}}, \quad v^2 = v_u^2 + v_d^2\,. \tag{3.31b}$$

As already pointed out earlier, the tadpole conditions for the scalar interaction eigenstates can be used to eliminate the soft SUSY breaking masses, i.e.

$$m_{H_d}^2,\, m_{H_u}^2,\, m_S^2 \quad \longrightarrow \quad t_{h_d},\, t_{h_u},\, t_{h_s}\,. \tag{3.32}$$

The remaining parameters provide at first sight eleven degrees of freedom[6]. However, as was shown earlier only the three phase combinations defined in Eq. (3.16) appear and the tadpole equations can be used to replace two of them. Hence, the following replacements are made

$$\kappa,\, \lambda,\, A_\kappa,\, A_\lambda,\, \varphi_u,\, \varphi_s \quad \longrightarrow \quad |\kappa|,\, |\lambda|,\, |A_\kappa|,\, |A_\lambda|,\, \varphi_y,\, t_{a_d},\, t_{a_s}\,. \tag{3.33}$$

[5] The rotation angles β_c and β_n are defined to be the angles at tree level, i.e. the relation $\beta_c = \beta_n$ always holds.
[6] Two degrees of freedom for each of the 4 complex parameters, two for the phases of the Higgs fields and one for the vacuum expectation value of the singlet.

Finally, replacing $|A_\lambda|$ with the mass of the charged Higgs boson, leads to the following set of independent parameters

$$M_W^2,\, M_Z^2,\, e,\, M_{H^\pm}^2, \tan\beta,\, v_s,\, |\kappa|,\, |\lambda|,\, |A_\kappa|,\, \varphi_y,\, t_{h_d},\, t_{h_u},\, t_{h_s},\, t_{a_d},\, t_{a_s}\,. \tag{3.34}$$

This is the set we used in our publications that deal with the one-loop corrections to the Higgs masses in the real [5] and complex [6] NMSSM. In later publications covering the two-loop corrections of the order $\alpha_s\alpha_t$ [7] and the program package `NMSSMCALC` [8] we switched to a slightly modified set given by

$$M_W^2,\, M_Z^2,\, e,\, M_{H^\pm}^2, \tan\beta,\, v_s,\, |\kappa|,\, |\lambda|,\, \mathrm{Re}A_\kappa,\, \varphi_y,\, \varphi_z',\, t_{h_d},\, t_{h_u},\, t_{h_s},\, t_{a_d},\, t_{a_s}, \tag{3.35}$$

to comply with the conventions of the SUSY Les Houches Accord (SLHA) [69,70]. A detailed explanation on this will be given in Sec. 7.1.2. Essentially we traded $|A_\kappa|$ for the real part of A_κ and the phase φ_z', which is defined as

$$\varphi_z' = 3\varphi_s + \varphi_\kappa\,. \tag{3.36}$$

When performing the replacement

$$\kappa,\, \lambda,\, A_\kappa,\, A_\lambda,\, \varphi_u,\, \varphi_s \quad \longrightarrow \quad |\kappa|,\, |\lambda|,\, \mathrm{Re}A_\kappa,\, M_{H^\pm}^2,\, \varphi_y,\, \varphi_z', t_{a_d}\,, t_{a_s} \tag{3.37}$$

the phases φ_{A_κ} and φ_{A_λ} are eliminated completely as before. However the remaining phases φ_u, φ_s, φ_λ and φ_κ appear in two combinations, φ_y and φ_z'.

CHAPTER 4

Regularization and Renormalization

In this chapter we shortly introduce the main features of regularization and renormalization, which are indispensable techniques if one wants to carry out a higher order calculation. Higher order corrections require the evaluation of loop integrals. These loop integrals involve the integration over the loop momentum and can be divergent. If an integral diverges due to the upper integration limit of infinity, it is called ultraviolet (UV) divergent, whereas integrals that diverge due to the lower integration limit of zero are called infrared (IR) divergent. Since we encounter only UV-divergences in our calculation, we will focus on these for now. Of course we know that physical observables are UV-finite. Hence, we have to find some way to deal with these divergences that appear at intermediate steps of the calculation. At Born level the parameters appearing in the Lagrangian, which we will refer to as bare parameters, can be directly linked to measurable quantities, such as masses or coupling constants. The inclusion of potentially divergent loop corrections destroys this relation. One can, however, calculate several observables in terms of the bare parameters. If the resulting system of equations is not too complicated, one can solve for the bare parameters and eliminate them from the equations by reinsertion. In such a way it is possible to obtain relations between the observables, i.e. one gains a prediction for one observable in terms of other measurable quantities. In these relations the UV-divergences have to cancel. Otherwise the theory is not renormalizable. But in order to check whether the divergences really do cancel, we need to parametrize them. This is called regularization.

4.1 Regularization

To regularize a UV-divergent integral one or several regularization parameters are introduced. This regularization parameter has of course no physical meaning. When taking the proper limit the original UV-divergent integral is recovered. However, if in the end the calculated observable does not depend on the regularization parameter anymore, this implies that all the UV-divergent contributions canceled against each other. For calculations within the SM the method of dimensional regularization is very common, since it preserves Lorentz and

gauge invariance. In dimensional regularization the four dimensional spacetime is extended to $D = 4 - 2\epsilon$ dimensions. To ensure the correct dimensionality of the momentum integrals the introduction of an arbitrary scale μ_R, the so-called renormalization scale, is necessary

$$\int \frac{\mathrm{d}^4 q}{(2\pi)^4} \to \mu_R^{4-D} \int \frac{\mathrm{d}^D q}{(2\pi)^D} \,. \tag{4.1}$$

The UV-divergences can now be expressed as $1/\epsilon$ poles. Hence, ϵ is the regularization parameter and taking the limit $\epsilon \to 0$ restores the original integral. However, dimensional regularization has a flaw when it is applied to supersymmetric theories. Extending the spacetime dimension introduces new bosonic degrees of freedom and thereby breaks SUSY. There are ways to cure this, for example the introduction of SUSY restoring counterterms, but mostly a different technique is used in SUSY calculations. The so-called method of dimensional reduction is similar to dimensional regularization, but in order to preserve SUSY only the momenta are treated in D dimensions, while the fields are kept four dimensional.

4.2 Renormalization: The Counterterm Formalism

These regularization procedures offer a neat and standardized way to parametrize the divergences. It would be nice to have such a formalized procedure also for the renormalization itself, since it is not always straightforward to eliminate the bare parameters in favor of physical observables, because the equations involved tend to become quite complicated. The so-called counterterm formalism offers such a standardized way for performing the renormalization procedure. The bare parameters (denoted as p^0) are split into a renormalized parameter (denoted as p^{ren}) and a counterterm, δp

$$p^0 = p^{\mathrm{ren}} + \delta p \,. \tag{4.2}$$

All the divergences are shifted to the counterterm, which automatically leads to p^{ren} being UV-finite. It is common to introduce one counterterm for each order of corrections, i.e. $\delta p = \delta^{(1)} p + \delta^{(2)} p + \cdots$, where $\delta^{(n)} p$ includes contributions of the n-th order. But there is still a freedom of choice, whether finite contributions are included in the counterterm. The conditions that fix what exactly is absorbed into the counterterm are referred to as renormalization conditions. By choosing a renormalization condition the relation between the renormalized parameter and physical observables is fixed. There are two main types of renormalization conditions: on-shell conditions and MS/$\overline{\mathrm{MS}}$ or DR/$\overline{\mathrm{DR}}$ conditions.

- **on-shell:** If on-shell renormalization conditions are applied the counterterms of the respective parameters are chosen in such a way that the renormalized quantity is equivalent to the corresponding physical observable and remains unchanged up to all orders of perturbation theory. The name indicates that this is commonly done for masses, i.e. the counterterm δm is defined to include not only the divergent but also some finite contributions such that the renormalized mass is equal to the physical mass. The particle mass is renormalized on-shell.
- **MS/$\overline{\mathrm{MS}}$ or DR/$\overline{\mathrm{DR}}$:** In MS and DR renormalization only the divergent parts are absorbed into the counterterm, whereas in $\overline{\mathrm{MS}}$ and $\overline{\mathrm{DR}}$ also a finite part is included in the counterterm. To be more precise all terms proportional to $\Delta = 1/\epsilon - \gamma_E + \ln 4\pi$ are absorbed into the counterterm, where γ_E is the Euler-Mascheroni constant. However, due to the fact, that we know that the $1/\epsilon$ terms have to drop out in the physical

results, this implies that also the terms proportional to $(-\gamma_E + \ln 4\pi)$ will cancel in the physical results. Therefore, it does not matter whether they are included in the counterterm or in the renormalized parameter. The difference between MS/$\overline{\text{MS}}$ and DR/$\overline{\text{DR}}$ renormalization is that in the latter dimensional reduction is applied, whereas the former uses dimensional regularization.

In our calculation we use on-shell and $\overline{\text{DR}}$ renormalization. The choice of a set of independent parameters and the renormalization conditions for those is referred to as a renormalization scheme.

At this point let us remark that if all orders of perturbation were included, the result would not depend on the choice of the renormalization scheme anymore. If a calculation is only performed up to a fixed order this is not the case. Hence, the difference between two results, which were obtained in different renormalization schemes provides a hint at the missing higher order corrections. Another commonly applied method to determine the error of the theory prediction, is the variation of the renormalization scale. This procedure is applicable if $\overline{\text{DR}}$ (or $\overline{\text{MS}}$) renormalization is used. In this case the higher order corrections display a dependence on the renormalization scale μ_R. This is of course only introduced as a reference scale and does not have any physical meaning. The dependence on this scale would vanish, if the higher order corrections up to all orders were included. Hence, the dependence of the predictions on this scale is a measure for the missing higher order corrections.

Introducing counterterms for all the independent parameters of the model is sufficient to render the S-matrix elements finite. In order to also obtain finite Green's functions one needs to renormalize the fields as well. The fields originally appearing in the Lagrangian, denoted as ϕ^0 and referred to as bare fields, are replaced by the wavefunction renormalization constants, Z_ϕ and the renormalized fields, denoted as ϕ^{ren}. Commonly the wavefunction renormalization constants are introduced as multiplicative constants according to

$$\phi^0 = \sqrt{Z_\phi}\,\phi^{\text{ren}}\,, \tag{4.3}$$

and are then rewritten in terms of the deviations caused by the corrections of the respective order. This leads to a notation similar to that used for the counterterms of the parameters

$$\begin{aligned}
\phi^0 =& \sqrt{Z_\phi}\,\phi^{\text{ren}} && (4.4)\\
=& \sqrt{1 + \delta^{(1)}Z_\phi + \delta^{(2)}Z_\phi + \cdots}\,\phi^{\text{ren}} && (4.5)\\
=& \Big(1 + \frac{1}{2}\delta^{(1)}Z_\phi - \frac{1}{8}\big(\delta^{(1)}Z_\phi\big)^2 + \frac{1}{2}\delta^{(2)}Z_\phi + \cdots\Big)\phi^{\text{ren}}\,. && (4.6)
\end{aligned}$$

In the very last step we expanded the expression assuming that the counterterms are small.

Inserting these replacement rules for the bare parameters and bare fields into the Lagrangian, it is apparent that the bare Lagrangian can be split into a part that has exactly the same form as the bare Lagrangian, but depends on the renormalized parameters instead of the bare ones, and a part that contains the counterterms of the parameters and fields. These parts are usually referred to as the renormalized Lagrangian and the counterterm Lagrangian,

$$\mathcal{L}_0 = \mathcal{L}_{\text{ren}} + \delta\mathcal{L}\,. \tag{4.7}$$

From the counterterm Lagrangian a new set of Feynman rules can be derived. In the calculation of higher order corrections these new Feynman rules lead to new contributions. If the renormalization procedure is performed correctly the UV-divergences of these new contributions will cancel those of the loop integrals in the physical observables.

To illustrate the renormalization procedure via the counterterm formalism, we consider the simple example of the renormalization of the mass of a scalar particle. The physical mass of the scalar particle is given by the real part of the pole of the propagator. The renormalized one-particle irreducible two-point function $\hat{\Gamma}_S$ at one-loop order, which is basically the inverse propagator is given by

$$\hat{\Gamma}_S = \mathrm{i}(p^2 - m^2_{\mathrm{ren}}) + \mathrm{i}\hat{\Sigma}_S(p^2)\,, \tag{4.8}$$

where the first part is the Born contribution, which can be read off the renormalized Lagrangian, while $\hat{\Sigma}_S(p^2)$ is the renormalized one-loop self-energy. On the one hand this includes the unrenormalized self-energy $\Sigma_S(p^2)$, i.e. all one-loop contributions that can be constructed with the Feynman rules derived from the renormalized Lagrangian. These contributions are UV-divergent. On the other hand there are also contributions originating from the counterterm Lagrangian, i.e. contributions that depend on the wavefunction renormalization constant δZ_S and the counterterm for the mass δm^2_S. Hence, the renormalized self-energy can be decomposed as

$$\hat{\Sigma}_S(p^2) = \Sigma_S(p^2) + (p^2 - m^2_{\mathrm{ren}})\,\delta Z_S - \delta m^2_S\,. \tag{4.9}$$

Now, the proper condition to renormalize the scalar mass on-shell is obviously $\mathrm{Re}\hat{\Sigma}_S(m^2_S) = 0$, because this yields m^2_{ren} as the real part of the pole of the propagator and therefore as the physical mass, i.e. $m^2_{\mathrm{ren}} = m^2_S$. Evaluating this condition and solving for the counterterm δm^2_S yields

$$\delta m^2_S = \mathrm{Re}\Sigma_S(m^2_S)\,. \tag{4.10}$$

To fix the wavefunction renormalization constant the condition

$$\lim_{p^2\to m^2_S} \frac{1}{p^2 - m^2_S}\widetilde{\mathrm{Re}}\hat{\Gamma}_S(p^2) = \mathrm{i} \qquad \Leftrightarrow \qquad \widetilde{\mathrm{Re}}\left.\frac{\partial\hat{\Sigma}_S(p^2)}{\partial p^2}\right|_{p^2=m^2_S} = 0 \tag{4.11}$$

sets the residue of the renormalized propagator to one, thereby ensuring that the renormalized field is normalized correctly. Here $\widetilde{\mathrm{Re}}$ indicates that the Re only acts on the loop functions, i.e. the real part of the loop functions is taken, while the complex structure of the parameters is kept.

The expressions we will encounter later on during the renormalization of the Higgs sector of the NMSSM, will be a bit more complicated, because in the complex NMSSM all five interaction eigenstates mix to form the mass eigenstates. Hence, the one-particle irreducible two-point function we have to consider is a 5×5 matrix. However, the basic idea remains the same as in the simple example presented above.

CHAPTER 5

Higgs Signals at the LHC

For the Standard Model Higgs boson there are several production mechanisms at a proton-proton collider such as the LHC. The most important production mode is certainly gluon fusion since it has by far the largest cross section – at least if only Higgs masses lighter than 1 TeV are considered. Above 1 TeV the production via vector boson fusion delivers a similar cross section. Other relevant production modes are Higgs-strahlung and associated production with a quark-antiquark pair. The schematic diagrams for these production modes are given in Fig. 5.1.

In principle an NMSSM Higgs boson is produced via the same mechanisms. However, the couplings of the Higgs boson are modified compared to the SM and there can be additional particles in the loops. Let us consider gluon fusion as an example. Both, in the SM and in the NMSSM, this is a loop mediated process. In the SM the most important contributions originate from the top loops, but also bottom loops and other quarks contribute. Within the NMSSM the coupling to the up-type and down-type quarks is modified. If the coupling to bottom quarks is enhanced, while the one to top quarks is suppressed, the bottom quark loops gain importance. Furthermore, there can also be contributions from diagrams with stops and sbottoms in the loop. Hence, if one is interested in the production of an NMSSM Higgs boson via gluon fusion one has to add the additional loops and modify the top and bottom coupling. This has been done within our group by adapting the program `HIGLU` [71,72] for the NMSSM. However, for the scans we performed for our phenomenological investigations invoking `HIGLU` for every single point is not practicable. We applied the approximation of rescaling the gluon fusion cross section for a SM Higgs boson of the same mass as the NMSSM Higgs boson we are interested in by the square of the reduced gluon coupling of the NMSSM Higgs boson

$$\begin{aligned} \sigma(ggH_i) &= C_g^2(H_i)\,\sigma(ggH^{\rm SM}) \\ \text{with} \quad M_{H_i} = M_{H^{\rm SM}} \quad &\text{and} \quad C_g^2(H_i) = \frac{\Gamma^{\rm NMSSM}(H_i \to gg)}{\Gamma^{\rm SM}(H^{\rm SM} \to gg)}\,. \end{aligned} \tag{5.1}$$

We obtain the reduced gluon coupling C_g by taking the ratio of the Higgs decay widths into

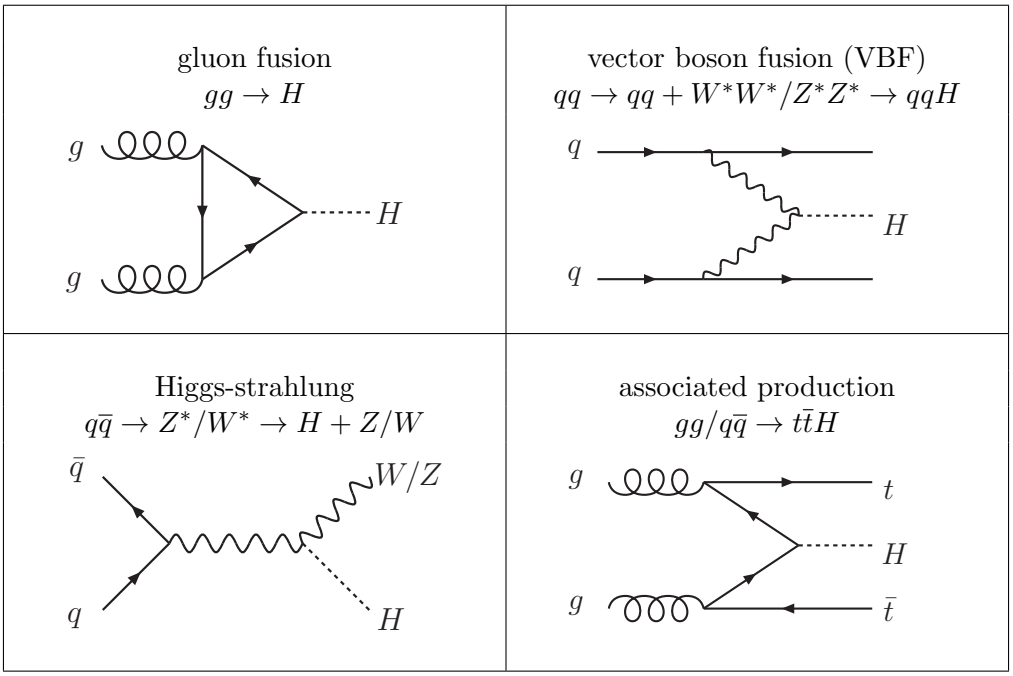

Figure 5.1: Schematic diagrams for Higgs production in the SM at the LHC.

gluons in the NMSSM and SM[1]. The reduced gluon coupling can be both suppressed and enhanced compared to the SM.

The reduced coupling to the massive vector bosons is given by

$$C_V(H_i) = \cos\beta\, \mathcal{R}_{i3} + \sin\beta\, \mathcal{R}_{i4}\,, \tag{5.2}$$

where $\mathcal{R}$ is the rotation matrix defined in Eq. (3.26). The coupling to vector bosons is always smaller than in the SM, therefore also the production cross sections of vector boson fusion and Higgs-strahlung are suppressed. Furthermore, these production modes do of course not apply to the pseudoscalar Higgs bosons, since they do not couple to the vector boson pairs due to parity.

The reduced couplings to the quarks can also be enhanced or suppressed and are used to rescale the cross sections for associated production. The experimental analyses sometimes restrict themselves to just a single production mode, but often the results are given including all production modes. The inclusive production cross section is given by the sum of the cross sections for gluon fusion (denoted by $\sigma(ggH_i)$), vector boson fusion (denoted by $\sigma(\text{VBF})$), Higgs-strahlung (denoted by $\sigma(WH_i)$ and $\sigma(ZH_i)$) and associated production with top quarks (denoted by $\sigma(t\bar{t}H_i)$),

$$\sigma_{\text{incl}}(H_i) = \sigma(ggH_i) + \sigma(\text{VBF}) + \sigma(WH_i) + \sigma(ZH_i) + \sigma(t\bar{t}H_i)\,. \tag{5.3}$$

Of course, the Higgs boson is not directly observed at the LHC, but its decay products – or better the particles at the very end of the decay chain – are observed. Usually, the Higgs

[1] This approximation for the gluon fusion cross section works very well for a Higgs boson with SM-like couplings. The deviation here is less than 1% as we found by comparing with the `HIGLU` result. For a heavy MSSM-like Higgs boson the deviations are $\mathcal{O}(10\%)$. The largest difference of $\mathcal{O}(20\%)$ occurs for light Higgs bosons with a large singlet admixture.

search channels are classified according to the particles the Higgs decays into, although these decay further. In the search for the SM Higgs boson five major channels have been used: ZZ, $\gamma\gamma$, WW, bb and $\tau\tau$. Further channels that are under investigation are for example $\mu\mu$ and γZ. To predict the measured signal rates, the branching ratio of the Higgs boson into the respective final state is required in addition to the production cross section. The signal rate into the final state XX is then given by the product of production and decay, it is commonly normalized to the SM prediction for a Higgs boson of the same mass and is called the signal strength or μ-value,

$$\mu_{XX}^{\text{single}}(H_i) = \frac{\sigma_{\text{prod}}(H_i)\,\text{BR}(H_i \to XX)}{\sigma_{\text{prod}}(H^{\text{SM}})\,\text{BR}(H^{\text{SM}} \to XX)} \quad \text{with} \quad M_{H^{\text{SM}}} = M_{H_i}\,. \tag{5.4}$$

Here σ_{prod} can be either the inclusive cross section or a specific production mode. The branching ratio is obtained as the ratio of the partial width of the Higgs boson decaying into the final state and the total width (i.e. the sum of the partial widths of all possible decays),

$$\text{BR}(H_i \to XX) = \frac{\Gamma_{XX}(H_i)}{\Gamma_{\text{tot}}(H_i)}\,. \tag{5.5}$$

A deviation from the SM prediction of $\mu = 1$ can occur either due to changes in the production cross section or due to modifications in the decay or both. Since, we want to trace such deviations later, we define the two useful quantities

$$R_{\sigma_{\text{prod}}}(H_i) = \frac{\sigma_{\text{prod}}(H_i)}{\sigma_{\text{prod}}(H^{\text{SM}})} \qquad \text{and} \qquad R_{XX}^{\text{BR}}(H_i) = \frac{\text{BR}(H_i \to XX)}{\text{BR}(H^{\text{SM}} \to XX)}\,. \tag{5.6}$$

We already discussed that both modified couplings and additional particles in the loop lead to a modified production cross section, i.e. $R_{\sigma_{\text{prod}}} \neq 1$. The ratio of the branching ratios R_{XX}^{BR}, can be decomposed further into the ratio of the total widths and the ratio of the partial width,

$$R_{XX}^{\text{BR}}(H_i) = \frac{\Gamma_{XX}(H_i)}{\Gamma_{XX}(H^{\text{SM}})}\,\frac{\Gamma_{\text{tot}}(H^{\text{SM}})}{\Gamma_{\text{tot}}(H_i)}\,. \tag{5.7}$$

A suppressed (enhanced) branching ratio can on the one hand be caused by a suppressed (enhanced) partial width or on the other hand by an enhanced (suppressed) total width. The ratio of the partial widths is basically controlled by the respective Higgs coupling. For example a suppressed coupling to b quarks leads to a suppressed partial decay width into b quarks. The total width can either be modified due to coupling deviations, but there can also be additional contributions from decays into non-SM particles.

In addition to the modifications that apply to the cross sections and branching ratios of the individual NMSSM Higgs bosons, there is the possibility of overlapping signals that has to be taken into account. If two Higgs bosons are relatively close in mass, the experiments might not be able to resolve the actual double peak structure, but just see one peak, which is a combination of the two single peaks. Since the mass resolution varies from search channel to search channel also the viewpoint on what "relatively close in mass" means changes. The poorer the mass resolution the further away two Higgs bosons can be in mass and still lead to an overlapping signal. To deal with this superposition we adopted the method as implemented in the public computer code `NMSSMTools` [73–75]. To calculate the signal predicted at the mass of the i-th Higgs boson the signals of all individual Higgs bosons multiplied with a weighting function F_X are added,

$$\mu_{XX}(H_i) = \sum_k F_X(M_{H_i}, M_{H_k})\;\mu_{XX}^{\text{single}}(H_k)\,. \tag{5.8}$$

The weighting function depends on the mass at which we want to determine the signal, on the mass of the Higgs boson, whose signal is added and on the resolution in the search channel

$$F_X(M_{H_i}, M_{H_k}) = \exp\left(\frac{-(M_{H_k} - M_{H_i})^2}{2\big(d_X \cdot M_{H_k}\big)^2}\right) . \tag{5.9}$$

The resolution is reflected by the newly introduced parameter d_X, which for the standard channels takes on the following values[2]:

X	$\tau\tau$	WW	bb	ZZ	$\gamma\gamma$
d_X	0.2	0.2	0.1	0.02	0.02

Hence, the channels ZZ and $\gamma\gamma$ feature the best mass resolution, followed by that of the bb channel, while the channels WW and $\tau\tau$ are worse.

[2]These are the values as implemented in `NMSSMTools`

Part II

Higher Order Corrections to the Higgs Boson Masses up to $\mathcal{O}(\alpha_{\rm s}\alpha_{\rm t})$

CHAPTER 6

Introduction to Part II

In this part of the thesis we present the calculation of higher order corrections up to the order $\mathcal{O}(\alpha_s\alpha_t)$ to the masses of the Higgs bosons in the NMSSM. In light of the discovery of a Higgs boson at the LHC and of ongoing searches for further resonances the availability of precise predictions for the Higgs sectors of models beyond the SM (BSM) is indispensable if one wants to interpret the experimental results in terms of the respective models. The measured Higgs mass of ~ 125 GeV and the signal strength measurements reported by the ATLAS and CMS collaborations are so far in good agreement with a SM Higgs boson [3, 4]. However, this does not exclude the possibility, that the observed Higgs boson is actually part of an extended Higgs sector. In fact, the experiments are already searching for further scalar resonances and first model independent exclusion bounds are available, see e.g. [76]. In order to apply those exclusion bounds to specific models, precise predictions within these models are necessary. The Higgs mass is special in the sense, that it is not only an important observable in itself, but also enters in the calculation of other observables such as the production cross sections and branching ratios. Furthermore, the calculation of the higher order Higgs masses goes hand in hand with the computation of higher order corrections to the Higgs mixing matrix, which can be used to obtain effective higher order couplings, that in turn enter the observables.

Supersymmetric extensions of the SM are among the most popular BSM models and especially the MSSM has been studied extensively. However, as explained in Sec. 3.1 the MSSM displays some weaknesses, like the μ-problem or the naturalness problem, that are solved by the NMSSM. Within the MSSM the available precision for the Higgs masses is impressive and includes already corrections at the three-loop level [77] and some of the two-loop corrections are available with full momentum dependence [78].

Next, let us review the current status in the NMSSM. In the CP-conserving NMSSM the radiative one-loop corrections due to (s)top and (s)bottom contributions were computed using the effective potential approach in [79–82]. Calculations in the same approach including also the one-loop contributions of neutralinos, charginos and scalar particles followed in [83, 84]. Reference [85] presented the first full one-loop result, as well as the two-loop corrections of the order $\mathcal{O}(\alpha_s\alpha_t + \alpha_s\alpha_b)$ computed via the effective potential approach. Furthermore, the

full one-loop corrections were also presented in [86] and by us in [5]. In contrast to the other calculations that all employ pure $\overline{\text{DR}}$ renormalization, we use a scheme that mixes on-shell and $\overline{\text{DR}}$ conditions. The details of this calculation will be presented in the following chapters. In addition we provide the two-loop corrections of the order $\mathcal{O}(\alpha_s\alpha_t)$ computed in the diagrammatic approach with vanishing external momentum applying the same mixed renormalization scheme we utilized in our one-loop calculation [7]. Finally, recently the first corrections beyond $\mathcal{O}(\alpha_s\alpha_t + \alpha_s\alpha_b)$ have been given in [87].

Some one-loop corrections to the masses of the Higgs bosons of the CP-violating NMSSM including the most important contributions, obtained via the effective potential approach, have been presented in [88–92]. The full one-loop corrections and the logarithmically enhanced two-loop effects obtained via the renormalization group improved method are given in [93]. Our calculation at one- and two-loop level is not limited to the CP-conserving NMSSM but also includes the CP-violating phases [6, 7].

Some of these corrections have been made available within public programs. The program `NMSSMTools` [73–75] calculates the NMSSM mass spectrum in the CP-conserving and $\mathbb{Z}^3$ invariant NMSSM. The program `SOFTSUSY` [94,95] can also generate the spectrum if $\mathbb{Z}^3$ violating terms are included in the superpotential. With the help of `SARAH` [96–99] an NMSSM version of `SPheno` [100,101] can be generated. Similarly `FlexibleSUSY` [102], which is based on `SOFTSUSY` and `SARAH`, allows to automatically generate a program, which calculates the spectrum for the NMSSM. All of these programs include the corrections of the order $\mathcal{O}(\alpha_s\alpha_t + \alpha_s\alpha_b)$. `SOFTSUSY` also includes the MSSM-like $\mathcal{O}(\alpha_t^2 + \alpha_b^2 + \alpha_t\alpha_b)$ corrections, whereas `SARAH` can even generate two-loop contributions stemming from all superpotential parameters. Finally, the only program specifically developed for the CP-violating NMSSM is our program `NMSSMCALC` [8][1]. It includes the corrections up to the order $\mathcal{O}(\alpha_s\alpha_t)$ and uses a renormalization scheme that mixes on-shell and $\overline{\text{DR}}$ conditions[2]. Furthermore, it also supplies the branching ratios of the Higgs bosons including the state-of-the-art higher order corrections to the decays widths as well as off-shell decays.

The outline of this part is as follows. In Ch. 7 the general procedure of the calculation of the higher order corrections to the Higgs boson masses is described. Chapter 8 and Ch. 9 detail the computation of the corrections at one-loop and two-loop level. The main features of the program package `NMSSMCALC` are shortly summarized in Ch. 10. To conclude Ch. 11 illustrates the relevance of the computed higher order corrections by presenting a numerical analysis for a benchmark point.

[1] Although it has been announced recently that `NMSSMTools` will be extended to include CP-violating phases [103].

[2] All other programs apply solely $\overline{\text{DR}}$ conditions.

CHAPTER 7

Calculation of the Higgs Masses and Higgs Mixing Matrix Elements at Higher Orders

We present the calculation of the masses of the neutral NMSSM Higgs bosons up to the order $\mathcal{O}(\alpha_s\alpha_t)$. We employ the Feynman diagrammatic approach to calculate all possible one-loop corrections with full momentum dependence plus the leading two-loop corrections, which are those of the order $\mathcal{O}(\alpha_s\alpha_t)$, in the approximation of vanishing external momentum in the gaugeless limit. We apply a renormalization scheme that mixes on-shell and $\overline{\text{DR}}$ conditions. The details of the one- and two-loop part of the calculation will be addressed in Ch. 8 and Ch. 9.

7.1 Calculation of the Higgs Masses

The Higgs masses are defined as the real parts of the poles of the propagators, which at higher order is equivalent to determining the zeroes of the determinant of the renormalized[1] two-point function $\hat{\Gamma}(p^2)$,

$$\text{Det}\Big(\hat{\Gamma}(p^2)\Big) = 0\,, \quad \text{with} \quad \Big(\hat{\Gamma}(p^2)\Big)_{ij} = \mathrm{i}\delta_{ij}\big(p^2 - m_{h_i}^2\big) + \mathrm{i}\hat{\Sigma}_{h_ih_j}(p^2)\,, \quad i,j = 1...5\,, \tag{7.1}$$

where m_{h_i} is the tree-level mass and $\hat{\Sigma}_{h_ih_j}$ is the renormalized self-energy of the $h_i \to h_j$ transition with h_i denoting the tree-level mass eigenstates. In the complex NMSSM all five tree-level mass eigenstates mix to form the higher order eigenstates, i.e. the renormalized two-point function is a 5×5 matrix. In the special case of the real NMSSM transitions between CP-odd and CP-even eigenstates and vice versa are forbidden by CP-conservation and hence it is sufficient to consider the submatrices for the CP-even and CP-odd fields individually. In the following the formulas for the general complex case will be given. Please note, that we neglect the mixing with the Goldstone boson which can occur at higher orders. We verified numerically that it is negligible.

[1] A hat on top indicates the renormalized quantities.

To solve Eq. (7.1) an iterative procedure is applied. This is necessary because the dependence on p^2 appears not only in a polynomial way as it originates from the entries on the diagonal of $\hat{\Gamma}(p^2)$, but also in the loop functions included in the renormalized self-energy. As a first step the p^2 appearing in the renormalized self-energy is set to a starting value, which we choose to be one of the tree-level masses. One can then solve the resulting polynomial for p^2, reinsert the thus obtained solution[2] into the renormalized self-energy and once again solve for p^2. This procedure is repeated until an adequate precision is reached[3]. The resulting solutions for p^2 are in general complex, let us denote them by $\mathcal{M}^2_{H_k}$. The physical Higgs masses at the respective order are then given by the real part of this complex solution, i.e. $M^2_{H_k} = \mathrm{Re}\mathcal{M}^2_{H_k}$. During the iteration steps, however, we always reinsert the full complex solution. Since the loop functions cannot be evaluated at complex momenta we use the following expansion

$$\hat{\Sigma}_{h_i h_j}(\mathcal{M}^2_{H_k}) \approx \hat{\Sigma}_{h_i h_j}(M^2_{H_k}) + \mathrm{iIm}\big[\mathcal{M}^2_{H_k}\big] \left.\frac{\partial \hat{\Sigma}_{h_i h_j}}{\partial p^2}\right|_{p^2 = M^2_{H_k}} . \tag{7.2}$$

This is just a first order Taylor expansion in the imaginary part of the complex $\mathcal{M}^2_{H_k}$ around zero.

7.1.1 The Renormalized Self-Energy

The renormalized self-energy of the Higgs bosons $\hat{\Sigma}_{h_i h_j}$ contains one-loop and two-loop contributions, denoted by the superscripts (1) and (2),

$$\hat{\Sigma}_{h_i h_j}(p^2) = \hat{\Sigma}^{(1)}_{h_i h_j}(p^2) + \hat{\Sigma}^{(2)}_{h_i h_j}(0)\,. \tag{7.3}$$

To derive the explicit form of the renormalized self-energy, one has to introduce one-loop and two-loop counterterms for the independent parameters of the Higgs sector as given in Eq. (3.35). To fix these counterterms we employ a renormalization scheme that applies on-shell conditions to parameters that are easily linked to physical observables, while the remaining counterterms are fixed via $\overline{\mathrm{DR}}$ conditions. The explicit conditions will be given later on. The counterterms are listed in Tab. 7.1. The on-shell parameters are the tadpole parameters[4], the masses of the W and Z bosons, the electric charge and the mass of the charged Higgs boson. The remaining $\overline{\mathrm{DR}}$ parameters are $\tan\beta$, the vacuum expectation value of the singlet v_s, the absolute values of the dimensionless couplings $|\lambda|$ and $|\kappa|$, the real part of A_κ and finally the two phase combination, φ_y and φ'_z as defined in Eq. (3.16) and Eq. (3.36). Furthermore, the Higgs fields have to be renormalized. Therefore, global wavefunction renormalization constant for each of the doublets and the singlet are introduced

$$H_d \to \left(1 + \frac{1}{2}\delta^{(1)} Z_{H_d} + \frac{1}{2}\delta^{(2)} Z_{H_d}\right) H_d\,, \tag{7.4a}$$

$$H_u \to \left(1 + \frac{1}{2}\delta^{(1)} Z_{H_u} + \frac{1}{2}\delta^{(2)} Z_{H_u}\right) H_u\,, \tag{7.4b}$$

[2] Of course, there are five possible solutions. If one is interested in the loop corrected mass of the lightest Higgs boson one takes the lightest solution. If one is interested in the loop corrected mass of the next-to-lightest Higgs boson one takes the next-to-lightest solution and so on.

[3] For most of the scenarios we considered an absolute precision of 10^{-6} was usually achieved in less than 15 iterations. The Higgs bosons are typically not much heavier than 1 TeV in these scenarios.

[4] Calling the tadpole parameters "on-shell" is of course a slight abuse of the term. We mean by this that the counterterms contain finite contributions in addition to the divergences.

on-shell parameters	$\overline{\text{DR}}$ parameters
$t_{h_d} \to t_{h_d} + \delta^{(1)} t_{h_d} + \delta^{(2)} t_{h_d}$	
$t_{h_u} \to t_{h_u} + \delta^{(1)} t_{h_u} + \delta^{(2)} t_{h_u}$	$\tan\beta \to \tan\beta + \delta^{(1)} \tan\beta + \delta^{(2)} \tan\beta$
$t_{h_s} \to t_{h_s} + \delta^{(1)} t_{h_s} + \delta^{(2)} t_{h_s}$	$v_s \to v_s + \delta^{(1)} v_s + \delta^{(2)} v_s$
$t_{a_d} \to t_{a_d} + \delta^{(1)} t_{a_d} + \delta^{(2)} t_{a_d}$	$\lvert\lambda\rvert \to \lvert\lambda\rvert + \delta^{(1)}\lvert\lambda\rvert + \delta^{(2)}\lvert\lambda\rvert$
$t_{a_s} \to t_{a_s} + \delta^{(1)} t_{a_s} + \delta^{(2)} t_{a_s}$	$\lvert\kappa\rvert \to \lvert\kappa\rvert + \delta^{(1)}\lvert\kappa\rvert + \delta^{(2)}\lvert\kappa\rvert$
$M_W^2 \to M_W^2 + \delta^{(1)} M_W^2 + \delta^{(2)} M_W^2$	$\text{Re}A_\kappa \to \text{Re}A_\kappa + \delta^{(1)}\text{Re}A_\kappa + \delta^{(2)}\text{Re}A_\kappa$
$M_Z^2 \to M_Z^2 + \delta^{(1)} M_Z^2 + \delta^{(2)} M_Z^2$	$\varphi_y \to \varphi_y + \delta^{(1)}\varphi_y + \delta^{(2)}\varphi_y$
$e \to e(1 + \delta^{(1)} Z_e + \delta^{(2)} Z_e)$	$\varphi_z' \to \varphi_z' + \delta^{(1)}\varphi_z' + \delta^{(2)}\varphi_z'$
$M_{H^\pm}^2 \to M_{H^\pm}^2 + \delta^{(1)} M_{H^\pm}^2 + \delta^{(2)} M_{H^\pm}^2$	

Table 7.1: Counterterms of the Higgs sector.

$$S \to \left(1 + \frac{1}{2}\delta^{(1)} Z_S + \frac{1}{2}\delta^{(2)} Z_S\right) S \ . \tag{7.4c}$$

Inserting these substitutions into the Lagrangian it can be read off that the one-loop renormalized self-energy containing the full momentum dependence can be decomposed as

$$\begin{aligned}\hat{\Sigma}^{(1)}_{h_i h_j}(p^2) =& \Sigma^{(1)}_{h_i h_j}(p^2) + \frac{1}{2}p^2\left[\mathcal{R}\left(\delta^{(1)}\mathcal{Z}^\dagger + \delta^{(1)}\mathcal{Z}\right)\mathcal{R}^T\right]_{ij} + \\ &- \frac{1}{2}\left[\mathcal{R}\left(\delta^{(1)}\mathcal{Z}^\dagger \mathcal{M}_{\text{Higgs}} + \mathcal{M}_{\text{Higgs}}\,\delta^{(1)}\mathcal{Z}\right)\mathcal{R}^T\right]_{ij} - \left[\mathcal{R}\,\delta^{(1)}\mathcal{M}_{\text{Higgs}}\,\mathcal{R}^T\right]_{ij}.\end{aligned} \tag{7.5}$$

Here $\Sigma^{(1)}_{h_i h_j}$ denotes the unrenormalized self-energy at one-loop level taking into account all possible contributions. These include loop contributions from fermions, gauge bosons, Higgs and Goldstone bosons, charginos, neutralinos, sfermions and ghosts. The Higgs mixing matrix $\mathcal{R}$ was defined in Eq. (3.26) and $\mathcal{M}_{\text{Higgs}}$ is the corresponding 5×5 tree-level mass matrix in the interaction eigenbasis, (a, a_s, h_d, h_u, h_s). The wavefunction renormalization constants enter via the diagonal matrix

$$\delta^{(1)}\mathcal{Z} = \text{diag}\big(\sin^2\beta\,\delta^{(1)} Z_{H_d} + \cos^2\beta\,\delta^{(1)} Z_{H_u}, \delta^{(1)} Z_S, \delta^{(1)} Z_{H_d}, \delta^{(1)} Z_{H_u}, \delta^{(1)} Z_S\big)\,. \tag{7.6}$$

Finally, the one-loop counterterm mass matrix $\delta^{(1)}\mathcal{M}_{\text{Higgs}}$ is obtained by expressing the tree-level mass matrix in terms of the set of independent parameters, introducing the counterterms for these parameters, expanding around the counterterms and keeping only the terms linear in the one-loop counterterms. Note that for this procedure it is important to distinguish between the angle β, which is defined via the ratio of the vacuum expectation values of the doublets, and the angles β_n and β_c, which are the angles in the rotation matrices to decouple the Goldstone bosons (see Eq. (3.23) and Eq. (3.28)), since the latter two do not receive a counterterm, whereas the former does.

The two-loop contribution to the renormalized self-energy is calculated at vanishing external momentum and can be decomposed as

$$\begin{aligned}\hat{\Sigma}^{(2)}_{h_i h_j}(0) =& \Sigma^{(2)}_{h_i h_j}(0) - \frac{1}{2}\left[\mathcal{R}\left(\delta^{(2)}\mathcal{Z}^\dagger \mathcal{M}_{\text{Higgs}} + \mathcal{M}_{\text{Higgs}}\,\delta^{(2)}\mathcal{Z}\right)\mathcal{R}^T\right]_{ij} + \\ &- \left[\mathcal{R}\,\delta^{(2)}\mathcal{M}_{\text{Higgs}}\,\mathcal{R}^T\right]_{ij},\end{aligned} \tag{7.7}$$

where $\Sigma^{(2)}_{h_i h_j}(0)$ is the unrenormalized two-loop self-energy at the order $\mathcal{O}(\alpha_s\alpha_t)$ that includes both genuine two-loop diagrams as well as one-loop diagrams with counterterm insertions. Note that both the wavefunction renormalization constant matrix $\delta^{(2)}\mathcal{Z}$ and the counterterm mass matrix $\delta^{(2)}\mathcal{M}_{\text{Higgs}}$ do not contain products of one-loop counterterms. Although such combinations appear in general, they are always of the wrong order[5] and can therefore be neglected. Hence, the wavefunction renormalization constant matrix at two-loop level is defined analogously to the one-loop one as

$$\delta^{(2)}\mathcal{Z} = \text{diag}\big(\sin^2\beta\,\delta^{(2)}Z_{H_d} + \cos^2\beta\,\delta^{(2)}Z_{H_u}, \delta^{(2)}Z_S, \delta^{(2)}Z_{H_d}, \delta^{(2)}Z_{H_u}, \delta^{(2)}Z_S\big)\,. \tag{7.8}$$

The details of the calculation of the higher order corrections will be given in Ch. 8 and Ch. 9.

7.1.2 Explanation for the Choice of Independent Parameters

At this point we would also like to explain the curious combination of introducing counterterms not only for the absolute values and phases of the parameters, but also for the real part, as we do for A_κ. As mentioned earlier this is done to comply with the conventions of the SUSY Les Houches Accord (SLHA). The SLHA specifies that all parameters given in a specific block called "`EXTPAR`" are interpreted to be $\overline{\text{DR}}$ parameters at a given input scale. When the accord was extended to include models with complex parameters the "`EXTPAR`" block was declared to contain the real parts, while the block "`IMEXTPAR`" contains the corresponding imaginary parts. Hence, according to the SLHA the parameters are split into real and imaginary part instead of absolute value and phase. At tree level there is no difference at all and if only $\overline{\text{DR}}$ renormalization was applied there also would not be any difference at higher orders. However, since we also apply on-shell conditions for some parameters we need to take care to comply with SLHA conventions. The relevant parameters which can be specified in these blocks are

$$\text{Re}\lambda,\ \text{Im}\lambda,\ \text{Re}\kappa,\ \text{Im}\kappa,\ \text{Re}\mu_{\text{eff}},\ \text{Im}\mu_{\text{eff}},\ \text{Re}A_\lambda,\ \text{Im}A_\lambda,\ \text{Re}A_\kappa,\ \text{Im}A_\kappa,\ \varphi_u\,, \tag{7.9}$$

where $\mu_{\text{eff}} = v_s\lambda\exp(\text{i}\varphi_s)/\sqrt{2}$. Not all of these are independent. As shown earlier we can use the tadpole equations to eliminate $\text{Im}A_\lambda$ and $\text{Im}A_\kappa$ and therefore do not consider them as input. Replacing $\text{Re}A_\lambda$ by the mass of the charged Higgs boson leads to the following parameter set

$$\underbrace{t_{a_d},\ t_{a_s},\ M^2_{H^\pm}}_{\text{on-shell}},\ \underbrace{\text{Re}\lambda,\ \text{Im}\lambda,\ \text{Re}\kappa,\ \text{Im}\kappa,\ \text{Re}\mu_{\text{eff}},\ \text{Im}\mu_{\text{eff}},\ \text{Re}A_\kappa,\ \varphi_u}_{\overline{\text{DR}}}\,. \tag{7.10}$$

We can exploit that several of these parameters always appear in the same combinations, hence the set of

$$\text{Re}\lambda,\ \text{Im}\lambda,\ \text{Re}\kappa,\ \text{Im}\kappa,\ \text{Re}\mu_{\text{eff}}\,,\text{Im}\mu_{\text{eff}},\ \varphi_u\,, \tag{7.11}$$

can be reduced to

$$v_s,\ |\kappa|,\ |\lambda|,\ \varphi_y,\ \varphi'_z\,. \tag{7.12}$$

Since all of these parameters are defined to be $\overline{\text{DR}}$, simple relation between the counterterms can be found, e.g.

$$\delta\kappa = \delta\text{Re}\kappa + \text{i}\delta\text{Im}\kappa = \big(\cos\varphi_\kappa\delta|\kappa| - \sin\varphi_\kappa|\kappa|\delta\varphi_\kappa\big) + \text{i}\big(\sin\varphi_\kappa\delta|\kappa| + \cos\varphi_\kappa|\kappa|\delta\varphi_\kappa\big)\,. \tag{7.13}$$

[5] There is never an α_s contribution.

However, for A_κ such a replacement is not possible anymore, since the absolute value is neither a pure $\overline{\text{DR}}$ nor a pure on-shell parameter, but rather a mixture that is a function of both $\overline{\text{DR}}$ and on-shell parameters, i.e.

$$\delta|A_\kappa|\left(\delta\text{Re}A_\kappa^{\overline{\text{DR}}}, \delta t_{a_d}^{\text{OS}}, \delta t_{a_s}^{\text{OS}}, \dots\right). \tag{7.14}$$

Hence, we have to keep $\delta\text{Re}A_\kappa$. Please note, that the numerical difference in the Higgs masses is tiny when switching between interpreting the absolute value or the real part of A_κ as a $\overline{\text{DR}}$ parameter. So this is a rather technical issue.

7.2 Calculation of the Mixing Matrix Elements at Higher Orders

At tree level the Higgs mixing matrix is simply the matrix $\mathcal{R}$ that diagonalizes the tree-level mass matrix as defined in Eq. (3.26). Analogously the mixing matrix at higher orders is defined as the matrix that diagonalizes the mass matrix at that order, which is given by

$$\mathcal{M}_{ij}^{\text{loop}}(p^2) = \delta_{ij}\, m_{h_i}^2 - \hat{\Sigma}_{h_i h_j}(p^2) \qquad \text{with} \quad i,j = 1...5\,. \tag{7.15}$$

Here m_{h_i} are the tree-level masses and $\hat{\Sigma}_{h_i h_j}$ are components of the renormalized self-energy including corrections up to the order one is interested in. The mass matrix $\mathcal{M}^{\text{loop}}$ is given in the basis of the tree-level mass eigenstates. Due to the explicit dependence on the external momentum p^2 the matrix cannot be diagonalized straight away without any further assumptions.

7.2.1 Mixing Matrix in the Approximation of Vanishing External Momentum

One commonly used approximation is the $p^2 = 0$ approximation, in which the mass matrix at loop level is diagonalized at vanishing external momentum. The mixing matrix $\mathcal{R}^{p^2=0}$ is then defined as

$$\left[\left(\mathcal{R}^{p^2=0}\right)\left(\mathcal{R}^T \mathcal{M}^{\text{loop}}_{(p^2=0)} \mathcal{R}\right)\left(\mathcal{R}^{p^2=0}\right)^T\right]_{ij} = \delta_{ij}\left(M_{H_i}^{p^2=0}\right)^2. \tag{7.16}$$

Here $\left(\mathcal{R}^T \mathcal{M}^{\text{loop}}_{(p^2=0)} \mathcal{R}\right)$ is the mass matrix at loop level in the basis of the interaction eigenstates and $M_{H_i}^{p^2=0}$ are the eigenvalues of the mass matrix obtained at vanishing external momentum. Naturally those eigenvalues do not coincide with the loop masses obtained via the iterative procedure described in the previous section. In that sense the mixing matrix $\mathcal{R}^{p^2=0}$ that links the mass eigenstates at higher order to the interaction basis is not consistent with the masses obtained via the iterative procedure. However, the great advantage of the $p^2 = 0$ approximation is that it yields a unitary mixing matrix, which can be used to calculate effective couplings that include higher order effects.

7.2.2 External On-Shell Higgs Bosons

If one considers a process with external Higgs bosons and wants to ensure the correct on-shell properties of these external Higgs bosons, one can introduce complex wavefunction normalization constants $\hat{\mathbf{Z}}$ [104, 105] that relate the tree-level mass eigenstates to the eigenstates at higher order. The matrix $\hat{\mathbf{Z}}$ is in general a complex, non-unitary matrix defined as

$$\hat{\mathbf{Z}}_{ij} = \sqrt{\hat{Z}_i}\,\hat{Z}_{ij} \qquad \text{with} \quad i,j = 1...5\,. \tag{7.17}$$

Here

$$\hat{Z}_i = 1 \Big/ \left(\frac{\partial}{\partial p^2}\frac{\mathrm{i}}{\Delta_{ii}}\right)\Big|_{p^2=\mathcal{M}^2_{H_i}} \quad \text{and} \quad \hat{Z}_{ij} = \left.\frac{\Delta_{ij}(p^2)}{\Delta_{ii}(p^2)}\right|_{p^2=\mathcal{M}^2_{H_i}}, \tag{7.18}$$

where Δ is the inverse of the renormalized two-point function $\hat{\Gamma}(p^2)$,

$$\Delta(p^2) = \left[-\hat{\Gamma}(p^2)\right]^{-1}. \tag{7.19}$$

By means of this Z-factor the mixing of the tree-level mass eigenstates (denoted by h_i) to the eigenstates at higher order (denoted by H_i) is given by

$$H_i = \hat{\mathbf{Z}}_{ij}\, h_j\,. \tag{7.20}$$

However, since this Z-factor is non-unitary it cannot be used in the calculation of effective couplings.

Hence, the mixing matrix that is consistent with the masses as obtained via the iterative procedure is given by the product of the Z-factors, which link the loop mass eigenstates to the tree-level mass eigenstates, with the tree-level mixing matrix,

$$\mathcal{R}^{\text{iter}} = \hat{\mathbf{Z}}\mathcal{R}\,. \tag{7.21}$$

Now the question arises how different $\mathcal{R}^{p^2=0}$ actually is from $\mathcal{R}^{\text{iter}}$. In contrast to the masses, for which the approximation of vanishing external momentum yields values that differ significantly from those obtained via the iterative procedure, the mixing matrix elements computed applying the two methods are comparable. The absolute values or the real parts of the elements of $\mathcal{R}^{\text{iter}}$ do not deviate by more than 10% from the respective values of $\mathcal{R}^{p^2=0}$.

CHAPTER 8

Full One-Loop Corrections

The calculation of the one-loop corrections was primarily done during my diploma thesis. For completeness and clarity the main features of the calculation and the chosen renormalization scheme are summarized here. For details on the calculation the reader is referred to my diploma thesis [106] and the resulting publications [5, 6], of which the last one was prepared at the beginning of this PhD.

8.1 Unrenormalized Self-Energy at One-Loop Level

At one-loop level we take into account all possible contributions and retain the full momentum dependence. The generic one-loop diagrams are given in Fig. 8.1. In the loops all particles that couple to the Higgs bosons appear. These are the scalars, such as Higgs bosons, Goldstone bosons and all sfermions. There are also the Z and the W bosons and furthermore the fermions, i.e. the quarks and leptons. Additionally the superpartners such as the charginos and neutralinos contribute. Finally, there are ghost loops.

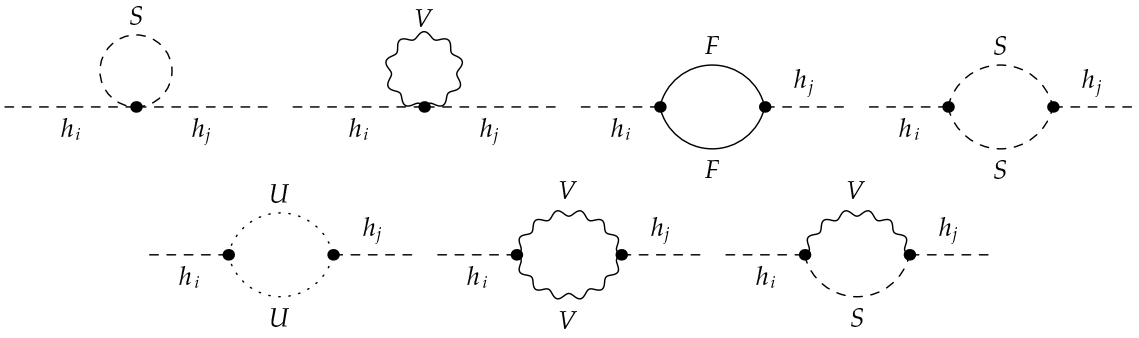

Figure 8.1: Generic diagrams contributing to the one-loop unrenormalized self-energy. There are scalars (S), vector bosons (V), fermions (F) and ghosts (U) in the loop.

To calculate all these contributions we employ the `Mathematica` packages `FeynArts` [107] and `FormCalc` [108] using a model file created by `SARAH` [96–99]. This yields expressions for the unrenormalized one-loop self-energy in terms of the well known one-loop scalar loop functions A_0 and B_0 (see App. A).

8.2 Wavefunction Renormalization Constants

We fix the wavefunction renormalization constants introduced in Eq. (7.4) by applying $\overline{\text{DR}}$ conditions of the form

$$\widetilde{\text{Re}}\frac{\partial \hat{\Sigma}^{(1)}_{h_i h_i}}{\partial p^2}\bigg|^{\text{div}}_{p^2=m^2_{h_i}} = 0\,. \tag{8.1}$$

Taking into account the decomposition of the renormalized self-energy given in Eq. (7.5) this yields

$$\begin{aligned} -\widetilde{\text{Re}}\frac{\partial \Sigma^{(1)}_{h_i h_i}}{\partial p^2}\bigg|^{\text{div}}_{p^2=m^2_{h_i}} =& |\mathcal{R}_{i1}|^2\big(\sin^2\beta\,\delta^{(1)}Z_{H_d} + \cos^2\beta\delta^{(1)}Z_{H_u}\big) + \big(|\mathcal{R}_{i2}|^2 + |\mathcal{R}_{i5}|^2\big)\delta^{(1)}Z_S + \\ &+ |\mathcal{R}_{i3}|^2\delta^{(1)}Z_{H_d} + |\mathcal{R}_{i4}|^2\delta^{(1)}Z_{H_u} \qquad \text{with} \quad i = 1...5\,, \end{aligned} \tag{8.2}$$

where the superscript "div" indicates that only the divergent part is included. As before $\widetilde{\text{Re}}$ only acts on the loop functions. This is an overdetermined system of equations, which can be solved for the three wavefunction renormalization constants $\delta^{(1)}Z_{H_u}$, $\delta^{(1)}Z_{H_d}$ and $\delta^{(1)}Z_S$.

8.3 Fixing of the Counterterms

As already introduced in Tab. 7.1, we define the parameters, which can easily be linked to physical observables as on-shell parameters, while the remaining parameters are renormalized using $\overline{\text{DR}}$ conditions,

$$\underbrace{t_{h_d},\, t_{h_u},\, t_{h_s},\, t_{a_d},\, t_{a_s},\, M_W^2,\, M_Z^2,\, e,\, M_{H^\pm}^2}_{\text{on-shell}},\, \underbrace{\tan\beta,\, v_s,\, |\kappa|,\, |\lambda|,\, \text{Re}A_\kappa,\, \varphi_y,\, \varphi_z'}_{\overline{\text{DR}}}\,. \tag{8.3}$$

For the on-shell parameters the renormalization prescriptions are straightforward and read:

- **tadpole parameters**
  The renormalization conditions for the tadpole parameters are chosen such that the correct minimum of the Higgs potential is preserved also at one-loop level,

  $$\delta^{(1)}t_{\boldsymbol{\phi}} = T^{(1)}_{\boldsymbol{\phi}} \quad \text{with} \quad \boldsymbol{\phi} = h_d, h_u, h_s, a_d, a_s\,, \tag{8.4}$$

  where $T^{(1)}_{\boldsymbol{\phi}}$ denotes the irreducible one-loop tadpole diagrams. The tadpole diagrams are calculated in the mass eigenbasis. The transformation from the mass eigenbasis (denoted by h_i) to the interaction eigenbasis (denoted by ϕ_i) can be easily achieved via $T_{\phi_i} = \mathcal{R}_{ji}T_{h_j}$, where $\mathcal{R}$ denotes the rotation matrix that diagonalizes the Higgs mass matrix defined in Eq. (3.26).

- **masses of the gauge bosons**
  The counterterms for the masses of the gauge bosons are fixed via the transverse part of the respective one-loop self-energy evaluated at the mass of the gauge boson

$$\delta^{(1)} M_W^2 = \widetilde{\mathrm{Re}}\Sigma^{(1),T}_{WW}(M_W^2) \quad \text{and} \quad \delta^{(1)} M_Z^2 = \widetilde{\mathrm{Re}}\Sigma^{(1),T}_{ZZ}(M_Z^2)\,. \tag{8.5}$$

- **electric charge**
  The counterterm for the electric charge is fixed via the fermion-antifermion-photon vertex, in such a way that this vertex does not receive any corrections at the one-loop level for zero momentum transfer (i.e. in the Thomson limit). This yields [109][1]

$$\delta^{(1)} Z_e^{\alpha(0)} = \frac{1}{2} \left.\frac{\partial \Sigma^{(1),T}_{AA}}{\partial p^2}\right|_{p^2=0} + \frac{\sin\theta_W}{\cos\theta_W M_Z^2} \Sigma^{(1),T}_{AZ}(0)\,, \tag{8.6}$$

  with $\Sigma^{(1),T}_{AA}$ and $\Sigma^{(1),T}_{AZ}$ denoting the transverse part of the unrenormalized photon self-energy and the photon-Z-mixing at one-loop level, respectively. The electroweak mixing angle θ_W is defined as $\cos\theta_W = M_W/M_Z$. However, the thus obtained counterterm depends on the masses of the light fermions, which are not well defined. To circumvent this we modify the charge counterterm according to [110]

$$\delta^{(1)} Z_e^{\alpha(M_Z^2)} = \delta^{(1)} Z_e^{\alpha(0)} - \frac{1}{2}\left(\left.\frac{\partial \Sigma^{(1),T,\mathrm{light}}_{AA}}{\partial p^2}\right|_{p^2=0} - \frac{\widetilde{\mathrm{Re}}\Sigma^{(1),T,\mathrm{light}}_{AA}(M_Z^2)}{M_Z^2} \right)\,, \tag{8.7}$$

  where we now use the running value of α at the scale M_Z^2 [111, 112]. The superscript "light" on the transverse part of the self-energies indicates that only diagrams including light fermions in the loop are taken into account, i.e. all quarks and leptons except for the top quark.

- **mass of the charged Higgs boson**
  The counterterm for the mass of the charged Higgs boson is fixed via the on-shell condition

$$\delta^{(1)} M_{H^\pm}^2 = \widetilde{\mathrm{Re}}\Sigma^{(1)}_{H^\pm H^\pm}(M_{H^\pm}^2)\,. \tag{8.8}$$

  This implies that the one-loop mass of the charged Higgs boson remains at the provided input value. And the unrenormalized one-loop self-energy of the charged Higgs boson feeds into the radiative corrections to the masses of the neutral Higgs bosons.

The $\overline{\mathrm{DR}}$ parameters are fixed via the following conditions:

- **ratio of the vacuum expectation values tanβ**
  The one-loop counterterm $\delta^{(1)}\tan\beta$ is fixed via the wavefunction renormalization constants of the doublets [113–118]

$$\delta^{(1)}\tan\beta = \frac{1}{2}\tan\beta \left(\delta^{(1)} Z_{H_u} - \delta^{(1)} Z_{H_d}\right)\big|_{\mathrm{div}}\,. \tag{8.9}$$

[1] Please note, that this reference uses a different sign convention in the Feynman rules, which leads to a relative minus sign in front of the second term compared to our result.

- **remaining $\overline{\text{DR}}$ parameters**
  There are different possibilities how to fix the remaining $\overline{\text{DR}}$ counterterms, which are $\delta^{(1)}|\kappa|$, $\delta^{(1)}|\lambda|$, $\delta^{(1)}\text{Re}A_\kappa$, $\delta^{(1)}v_s$, $\delta^{(1)}\varphi_y$ and $\delta^{(1)}\varphi'_z$. The most convenient way is to check that demanding finite renormalized self-energies in the Higgs sector yields a consistent solution. This means solving the equations

$$\hat{\Sigma}^{(1)}_{h_i h_j}\Big|_{\text{div}} = 0 \qquad \text{with} \quad i,j = 1...5\,. \tag{8.10}$$

  Of course there are more equations than counterterms. However, choosing a subset of six equations leads to a consistent solution that renders all components of the renormalized self-energy finite. An alternative approach is to utilize conditions obtained from other sectors, for example the chargino and neutralino sector, and check that the thus obtained divergence structure also renders the Higgs sector finite. The latter approach was used in [5] and [6] as it provides a non-trivial cross-check of the calculation.

The check whether the renormalization procedure was performed correctly and all divergences cancel is done numerically individually for each parameter point considered. The numerical evaluation revealed that the counterterms for the phases always vanish, i.e. $\delta^{(1)}\varphi_y = \delta^{(1)}\varphi'_z = 0$ holds in general.

CHAPTER 9

Two-Loop Corrections of the Order $\alpha_s\alpha_t$

The corrections with the largest impact at two-loop level are those of the order $\alpha_s\alpha_t$, since the top-Yukawa coupling and the strong coupling constant are considerably larger than the other couplings. We compute the two-loop corrections via the Feynman diagrammatic approach but with vanishing external momentum, which is equivalent to a calculation in the effective potential approach. Furthermore, we work in the gaugeless limit, i.e. the electroweak gauge couplings are neglected, a precise definition of this limit will be specified later. We also assume a vanishing bottom quark mass. The renormalization scheme we apply is consistent with the one utilized in the one-loop part of the calculation and mixes on-shell and $\overline{\text{DR}}$ conditions. The calculation and results presented here are published in [7].

9.1 Unrenormalized Self-Energy at Two-Loop Level

The unrenormalized two-loop self-energy of the order $\alpha_s\alpha_t$ consists of genuine two-loop diagrams and one-loop diagrams with counterterm insertions. Let us first consider the genuine two-loop diagrams.

The different classes of genuine two-loop diagrams are shown in Fig. 9.1. The coupling of the Higgs bosons to tops or their superpartners, the stops, ensures the proportionality to α_t. The proportionality to α_s originates from the couplings of the tops or stops to the gluon or gluino or alternatively from the four-stop-vertex. Hence, the particles in the loops are tops, stops, gluons and gluinos. In the Higgs couplings we neglect the parts proportional to the electroweak gauge couplings but keep the parts proportional to the top-Yukawa coupling and the coupling λ (gaugeless limit). The amplitude was computed using `FeynArts`, the manipulation of the Dirac algebra was performed in `FeynCalc` [119] and the reduction to master integrals was done with `TARCER` [120]. `TARCER` is a `Mathematica` package that is part of `FeynCalc` and uses the reduction algorithms proposed by Tarasov [121, 122]. Throughout the calculation we apply dimensional reduction. At one-loop level this is proven to preserve SUSY [123–127]. At two-loop level no general proof exits. However, there are some dedicated investigations regarding the corrections of the order $\mathcal{O}(\alpha_s\alpha_t + \alpha_s\alpha_b + \alpha_t^2 + \alpha_t\alpha_b + \alpha_b^2)$ in the

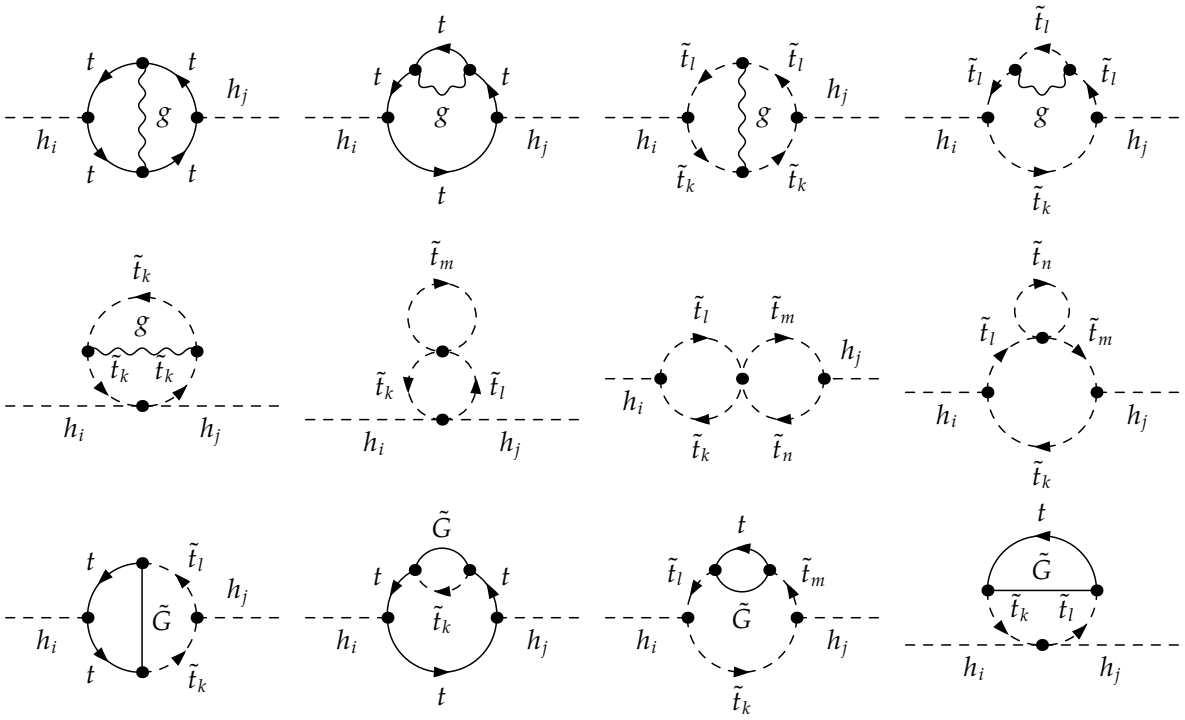

Figure 9.1: Generic diagrams for the genuine two-loop contributions at $\alpha_s\alpha_t$ to the self-energy of the neutral Higgs bosons. The particles in the loops are tops (t), stops ($\tilde{t}_1, \tilde{t}_2$), gluons (g) and gluinos ($\tilde{G}$) and $k, l, m, n = 1, 2$; $i, j = 1...5$.

MSSM [128]. Since there are no structurally new terms in the NMSSM, which could violate SUSY, the application of dimensional reduction should be SUSY preserving for our calculation and no SUSY restoring counterterms are required. Hence, we consider the momenta to be in $D = 4 - 2\epsilon$ dimensions, while the fields are kept four dimensional and our divergences are parametrized by the single pole $1/\epsilon$ and the double pole $1/\epsilon^2$. After performing all the traces and contracting all the indices we encounter integrals of the form

$$I^{(D),\alpha\beta\gamma}_{\nu_1\nu_2\nu_3}(m_1^2, m_2^2, m_3^2) = \left(\frac{(2\pi\mu_R)^{2\epsilon}}{\mathrm{i}\pi^2}\right)^2 \int \frac{\mathrm{d}^D q_1\, \mathrm{d}^D q_2 \quad (q_1^2)^\alpha (q_2^2)^\beta (q_1 q_2)^\gamma}{(q_1^2 - m_1^2)^{\nu_1}(q_2^2 - m_2^2)^{\nu_2}((q_1 - q_2)^2 - m_3^2)^{\nu_3}}\,. \quad (9.1)$$

Here the approximation $p^2 = 0$ was already taken into account. With the help of the Tarasov algorithm these integrals can be reduced to some combination of the two-loop vacuum bubble integral, which is the special case of the general integral given above and will from now on be denoted as $I^{(D)}(m_1^2, m_2^2, m_3^2) \equiv I^{(D),000}_{111}(m_1^2, m_2^2, m_3^2)$, and the product of two one-loop tadpole integrals, denoted by $A_0^{(D)}(m_i^2)$, i.e.

$$I^{(D),\alpha\beta\gamma}_{\nu_1\nu_2\nu_3}(m_1^2, m_2^2, m_3^2) = c_0^{(D)} I^{(D)}(m_1^2, m_2^2, m_3^2) + c_{ij}^{(D)} A_0^{(D)}(m_i^2) A_0^{(D)}(m_j^2)\,. \quad (9.2)$$

Here $c_0^{(D)}$ and $c_{ij}^{(D)}$ are some generic coefficients that can also depend on $D = 4 - 2\epsilon$. Expanding the products of these coefficients and the loop functions in terms of the regularization parameter ϵ yields the prefactors of the finite part and the poles of the original general two-loop integral $I^{(D),\alpha\beta\gamma}_{\nu_1\nu_2\nu_3}(m_1^2, m_2^2, m_3^2)$. The D dimensional loop functions, $I^{(D)}$ and $A_0^{(D)}$, are known analytically and can be expanded in the regularization parameter ϵ. For the two-loop bubble function [129–135] the relevant pieces are the finite part and the prefactors of the single and the double pole. For the one-loop one-point function [136] also the part proportional

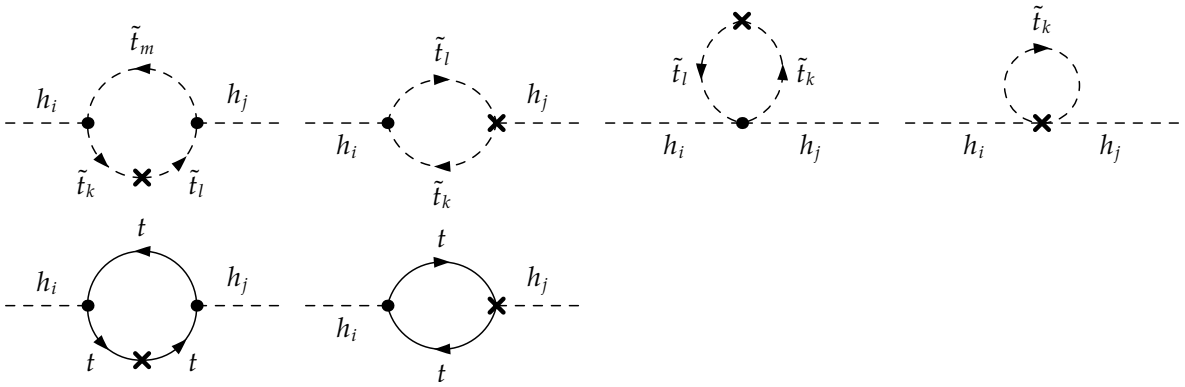

Figure 9.2: Generic one-loop diagrams with counterterm insertions of the order $\alpha_s\alpha_t$. The particles in the loop are tops (t) and stops ($\tilde{t}_1, \tilde{t}_2$) and $k, l, m, n = 1, 2$; $i, j = 1...5$

to ϵ contributes to the finite result (when multiplied with the $1/\epsilon$ pole of the second $A_0^{(D)}$) of the general two-loop integral after performing the limit $\epsilon \to 0$. Hence, the decompositions read

$$\begin{aligned} I^{(D)}(m_1^2, m_2^2, m_3^2) =& \left(\frac{(2\pi\mu_R)^{2\epsilon}}{\mathrm{i}\pi^2}\right)^2 \int \frac{\mathrm{d}^D q_1\, \mathrm{d}^D q_2}{(q_1^2 - m_1^2)(q_2^2 - m_2^2)((q_1 - q_2)^2 - m_3^2)} \\ =& I_{\text{fin}}(m_1^2, m_2^2, m_3^2) + I_{\text{div1}}(m_1^2, m_2^2, m_3^2)\frac{1}{\epsilon} + I_{\text{div2}}(m_1^2, m_2^2, m_3^2)\frac{1}{\epsilon^2}\,, \end{aligned} \tag{9.3}$$

$$\text{and} \quad A_0^{(D)}(m_i^2) = \left(\frac{(2\pi\mu_R)^{2\epsilon}}{\mathrm{i}\pi^2}\right) \int \frac{\mathrm{d}^D q_1}{(q_1^2 - m_i^2)} = \epsilon A_\epsilon(m_i^2) + A_0(m_i^2) + m_i^2\frac{1}{\epsilon}\,. \tag{9.4}$$

Inserting these expansions into the two-loop expression the extraction of the finite contribution and the coefficients of the single and double poles is straightforward.

The generic diagrams for the one-loop diagrams with counterterm insertions are shown in Fig. 9.2. The proportionality to α_t is once again provided via the Higgs couplings to tops and stops. Hence, these are the particles running in the loops. The α_s enters via the counterterms of the top and stop sector, which appear as counterterm insertions on the propagators and vertices. Therefore, the renormalization procedure including the one-loop corrections of the order α_s to the top and stop sector has to be carried out. This calculation is equivalent to existing results in the MSSM (see e.g. [137, 138]) and is shortly summarized in Sec. 9.1.1. In addition to the loop functions defined above, also the one-loop two-point function $B_0^{(D)}$ [136, 139] contributes. It can be decomposed as

$$\begin{aligned} B_0^{(D)}(p^2, m_1^2, m_2^2) =& \left(\frac{(2\pi\mu_R)^{2\epsilon}}{\mathrm{i}\pi^2}\right) \int \frac{\mathrm{d}^D q_1}{(q_1^2 - m_1^2)((q_1 + p)^2 - m_2^2)} \\ =& \epsilon B_\epsilon(p^2, m_1^2, m_2^2) + B_0(p^2, m_1^2, m_2^2) + \frac{1}{\epsilon}\,. \end{aligned} \tag{9.5}$$

Inserting the expansions in ϵ for the loop functions and the counterterms of the top and stop sector, the coefficients for the finite part and the poles can once again be read off.

After obtaining similar expressions for the counterterms of the Higgs sector and the wave-function renormalization constants, the cancellation of the UV-divergent poles can be checked explicitly.

9.1.1 Renormalization of the Top and Stop Sector

For the calculation of the counterterm inserted diagrams of the order $\alpha_s\alpha_t$ the counterterms of the order α_s of the top and stop sectors are required. The renormalization conditions presented are the same as in the MSSM and well known in the literature (see e.g. [137,138]).

The renormalization of the top mass is straightforward and yields for the on-shell counterterm

$$\delta m_t = \frac{1}{2}\widetilde{\mathrm{Re}}\left(m_t\Sigma_t^{VL}(m_t^2) + m_t\Sigma_t^{VR}(m_t^2) + \Sigma_t^{SL}(m_t^2) + \Sigma_t^{SR}(m_t^2)\right), \tag{9.6}$$

where Σ_t^{VL}, Σ_t^{VR}, Σ_t^{SL} and Σ_t^{SR} are parts of the one-loop self-energy of the top quark at order α_s according to the decomposition

$$\begin{aligned}\Sigma_t(p^2) =& \not{p}P_L\Sigma_t^{VL}(p^2) + \not{p}P_R\Sigma_t^{VR}(p^2) + P_L\Sigma_t^{SL}(p^2) + P_R\Sigma_t^{SR}(p^2),\\ &\text{with}\quad P_R = \frac{1+\gamma_5}{2}\quad\text{and}\quad P_L = \frac{1-\gamma_5}{2}.\end{aligned} \tag{9.7}$$

In the stop sector the renormalization is a bit more involved. At tree level and in the gaugeless limit, i.e. if the D-Terms are neglected, the mass matrix of the stop sector in the basis $(\tilde{t}_L, \tilde{t}_R)$ reads

$$\mathcal{M}_{\tilde{t}} = \begin{pmatrix} m_{\tilde{Q}_3}^2 + m_t^2 & m_t\left(A_t^* e^{-i\varphi_u} - \frac{\mu_{\text{eff}}}{\tan\beta}\right) \\ m_t\left(A_t e^{i\varphi_u} - \frac{\mu_{\text{eff}}^*}{\tan\beta}\right) & m_{\tilde{t}_R}^2 + m_t^2 \end{pmatrix}, \tag{9.8}$$

where $m_{\tilde{Q}_3}$ and $m_{\tilde{t}_R}$ are the soft SUSY breaking masses, A_t is the complex soft SUSY breaking trilinear coupling and

$$\mu_{\text{eff}} = \frac{\lambda v_s e^{i\varphi_s}}{\sqrt{2}}. \tag{9.9}$$

We denote the unitary rotation matrix that relates the interaction eigenstates to the mass eigenstates and diagonalizes the mass matrix by $\mathcal{U}_{\tilde{t}}$,

$$(\tilde{t}_1, \tilde{t}_2)^T = \mathcal{U}_{\tilde{t}}\,(\tilde{t}_L, \tilde{t}_R)^T, \tag{9.10a}$$

$$\mathrm{diag}(m_{\tilde{t}_1}^2, m_{\tilde{t}_2}^2) = \mathcal{U}_{\tilde{t}}\,\mathcal{M}_{\tilde{t}}\,\mathcal{U}_{\tilde{t}}^\dagger. \tag{9.10b}$$

The one-loop counterterms for the parameters $\tan\beta$, μ_{eff} and φ_u have already been fixed via the Higgs sector (see Ch. 8) and are not of the order α_s. Hence, they do not contribute here and the independent set of parameters we are left with is

$$m_t,\ m_{\tilde{Q}_3}^2,\ m_{\tilde{t}_R}^2\quad\text{and}\quad A_t\,. \tag{9.11}$$

The counterterm for m_t has already been fixed above. By demanding on-shell conditions for the masses of the stops and no further mixing at loop level the counterterms for the remaining parameters can be derived. For the trilinear soft SUSY breaking parameter this yields[1]

$$\begin{aligned}\delta A_t = \frac{e^{-\mathrm{i}\varphi_u}}{m_t}\Big[&\mathcal{U}_{\tilde{t}_{11}}\mathcal{U}_{\tilde{t}_{12}}^*(\delta m_{\tilde{t}_1}^2 - \delta m_{\tilde{t}_2}^2) + \mathcal{U}_{\tilde{t}_{11}}\mathcal{U}_{\tilde{t}_{22}}^*(\delta Y)^* + \mathcal{U}_{\tilde{t}_{21}}\mathcal{U}_{\tilde{t}_{12}}^*\delta Y + \\ &- \big(A_t e^{\mathrm{i}\varphi_u} - \frac{\mu_{\text{eff}}^*}{\tan\beta}\big)\delta m_t\Big],\end{aligned} \tag{9.12}$$

[1] Please note, that δA_t is in general complex.

with the counterterms to the stop masses being fixed via the one-loop self-energies of the order α_s according to

$$\delta m^2_{\tilde{t}_1} = \Sigma_{\tilde{t}_1\tilde{t}_1}(m^2_{\tilde{t}_1})\,, \tag{9.13a}$$

$$\text{and} \quad \delta m^2_{\tilde{t}_2} = \Sigma_{\tilde{t}_2\tilde{t}_2}(m^2_{\tilde{t}_2})\,. \tag{9.13b}$$

The counterterm for the off-diagonal elements of the stop mass matrix reads

$$\delta Y \equiv \left[\mathcal{U}_{\tilde{t}}\delta\mathcal{M}_{\tilde{t}}\mathcal{U}^\dagger_{\tilde{t}}\right]_{12} = \left[\mathcal{U}_{\tilde{t}}\delta\mathcal{M}_{\tilde{t}}\mathcal{U}^\dagger_{\tilde{t}}\right]^*_{21} = \frac{1}{2}\widetilde{\mathrm{Re}}\left(\Sigma_{\tilde{t}^*_1\tilde{t}^*_2}(m^2_{\tilde{t}_1}) + \Sigma_{\tilde{t}^*_1\tilde{t}^*_2}(m^2_{\tilde{t}_2})\right). \tag{9.14}$$

For the soft SUSY breaking masses one obtains

$$\delta m^2_{\tilde{Q}_3} = |\mathcal{U}_{\tilde{t}_{11}}|^2\delta m^2_{\tilde{t}_1} + |\mathcal{U}_{\tilde{t}_{12}}|^2\delta m^2_{\tilde{t}_2} - \mathcal{U}_{\tilde{t}_{22}}\mathcal{U}^*_{\tilde{t}_{12}}\delta Y - \mathcal{U}_{\tilde{t}_{12}}\mathcal{U}^*_{\tilde{t}_{22}}(\delta Y)^* - 2m_t\delta m_t\,, \tag{9.15a}$$

$$\delta m^2_{\tilde{t}_R} = |\mathcal{U}_{\tilde{t}_{21}}|^2\delta m^2_{\tilde{t}_1} + |\mathcal{U}_{\tilde{t}_{22}}|^2\delta m^2_{\tilde{t}_2} - \mathcal{U}_{\tilde{t}_{11}}\mathcal{U}^*_{\tilde{t}_{21}}(\delta Y)^* - \mathcal{U}_{\tilde{t}_{21}}\mathcal{U}^*_{\tilde{t}_{11}}\delta Y - 2m_t\delta m_t\,. \tag{9.15b}$$

In the above equations the counterterms for on-shell renormalization were given. Alternatively one could also apply $\overline{\text{DR}}$ conditions, i.e. include only the divergent parts in the counterterms. For our two-loop calculation we chose to implement both renormalization schemes. In order to compare the two schemes it is necessary to convert the input parameters accordingly. The link between an on-shell and the corresponding $\overline{\text{DR}}$ parameter can be made via the bare parameter. Let us consider some parameter X. The bare parameter can then be decomposed either according to on-shell or according to $\overline{\text{DR}}$ renormalization

$$X^{\text{bare}} = X^{\text{OS}} + \delta X^{\text{OS}} = X^{\overline{\text{DR}}} + \delta X^{\overline{\text{DR}}}\,, \tag{9.16}$$

where the on-shell counterterm contains also a finite part, whereas the $\overline{\text{DR}}$ counterterm only includes the divergent part,

$$\delta X^{\text{OS}} = \frac{1}{\epsilon}\delta X_{\text{pole}} + \delta X_{\text{fin}}\,, \tag{9.17}$$

$$\delta X^{\overline{\text{DR}}} = \frac{1}{\epsilon}\delta X_{\text{pole}}\,. \tag{9.18}$$

Hence, up to higher order corrections this yields the relation

$$X^{(\text{OS})} = X^{(\overline{\text{DR}})} - \delta X_{\text{fin}}\,. \tag{9.19}$$

The SLHA defines the parameters A_t, $m_{\tilde{Q}_3}$ and $m_{\tilde{t}_R}$ to be $\overline{\text{DR}}$ parameters. Therefore, we convert them when on-shell renormalization for the stop sector is chosen according to

$$A_t^{(\text{OS})} = A_t^{(\overline{\text{DR}})} - \delta A_t^{\text{fin}}\,, \tag{9.20a}$$

$$(m^2_{\tilde{Q}_3})^{(\text{OS})} = (m^2_{\tilde{Q}_3})^{(\overline{\text{DR}})} - \delta(m^2_{\tilde{Q}_3})^{\text{fin}}\,, \tag{9.20b}$$

$$(m^2_{\tilde{t}_R})^{(\text{OS})} = (m^2_{\tilde{t}_R})^{(\overline{\text{DR}})} - \delta(m^2_{\tilde{t}_R})^{\text{fin}}\,. \tag{9.20c}$$

Please note, that the counterterms should be calculated using on-shell parameters. Therefore, Eq. (9.20) needs to be solved iteratively. The top mass is given as an on-shell input and we use the procedure described in App. B to compute the respective $\overline{\text{DR}}$ mass in case $\overline{\text{DR}}$ renormalization is applied in the top and stop sector.

Please note, that in the decomposition of the on-shell counterterm as given in Eq. (9.17) we left out the term proportional to ϵ on purpose. For the on-shell renormalization at one-loop level itself it does not matter anyway since it vanishes when ϵ is taken to zero. However, if one calculates the diagrams of the Higgs self-energy of the order $\alpha_s\alpha_t$ with counterterm insertions, the product of a term proportional to ϵ appearing in a counterterm of the top or stop sector and a $1/\epsilon$ pole of the one-loop functions would yield a finite contribution. But we use our freedom of choosing an appropriate renormalization scheme to omit such terms. The reason for this omission will become clear in the next section.

9.2 Wavefunction Renormalization Constants

Analogously to the one-loop case the wavefunction renormalization constants are fixed via $\overline{\text{DR}}$ conditions and by the derivatives of the Higgs self-energy with respect to p^2. The resulting conditions are

$$\delta^{(2)} Z_{H_d} = - \left. \frac{\partial \Sigma^{(2)}_{h_d h_d}}{\partial p^2} \right|_{\text{div}} (p^2 \to 0)\,, \tag{9.21a}$$

$$\delta^{(2)} Z_{H_u} = - \left. \frac{\partial \Sigma^{(2)}_{h_u h_u}}{\partial p^2} \right|_{\text{div}} (p^2 \to 0)\,, \tag{9.21b}$$

$$\delta^{(2)} Z_S \;\; = - \left. \frac{\partial \Sigma^{(2)}_{h_s h_s}}{\partial p^2} \right|_{\text{div}} (p^2 \to 0)\,, \tag{9.21c}$$

where $\Sigma^{(2)}_{h_d h_d}$, $\Sigma^{(2)}_{h_u h_u}$ and $\Sigma^{(2)}_{h_s h_s}$ are components of the two-loop Higgs self-energy in the interaction basis which can be obtained by rotating the self-energy in the tree-level mass eigenstates basis, e.g. $\Sigma^{(2)}_{h_u h_u} = \mathcal{R}_{h_i h_u} \Sigma^{(2)}_{h_i h_j} \mathcal{R}_{h_j h_u}$. At order $\alpha_s\alpha_t$ the wavefunction renormalization constants $\delta^{(2)} Z_{H_d}$ and $\delta^{(2)} Z_S$ vanish. For the wavefunction renormalization constant of H_u we obtain

$$\delta^{(2)} Z^{\overline{\text{DR}}}_{H_u} = \frac{\alpha_s(m_t^2)^{\overline{\text{DR}}}}{4\pi^3 v^2 \sin^2\beta} \left(\frac{1}{\epsilon^2} - \frac{1}{\epsilon} \right)\,, \tag{9.22}$$

which is equivalent to the respective MSSM result [140]. The superscript $\overline{\text{DR}}$ indicates that $\overline{\text{DR}}$ renormalization in the top sector was applied in the computation of this wavefunction renormalization constant. Hence, the $\overline{\text{DR}}$ top mass is used in the calculation. If instead on-shell renormalization for the top mass is applied, this leads to additional contributions stemming from the counterterm inserted diagrams, that depend on the finite part of the top mass counterterm. The wavefunction renormalization for this case will be denoted by $\delta^{(2)} Z^{\text{OS}}_{H_u}$, which should not be confused with an on-shell condition for the wavefunction renormalization constant itself, i.e. the inclusion of a finite part. The wavefunction renormalization constant then reads

$$\delta^{(2)} Z^{\text{OS}}_{H_u} = \frac{\alpha_s(m_t^2)^{\text{OS}}}{4\pi^3 v^2 \sin^2\beta} \left(\frac{1}{\epsilon^2} - \frac{1}{\epsilon} \right) - \frac{3}{4\pi^2} \frac{m_t^{\text{OS}} (\delta m_t)_{\text{fin}}}{v^2 \sin^2\beta} \frac{1}{\epsilon}\,. \tag{9.23}$$

At this point a closer look at the complete wavefunction renormalization constant originating from top and stop contributions reveals why we chose to omit terms proportional to ϵ in the counterterms of the top and stop sector. The sum of the one-loop and two-loop contributions

for the different renormalization schemes is given by

$$\delta Z_{H_u}^{\overline{\text{DR}}} = \underbrace{-\frac{3(m_t^2)^{\overline{\text{DR}}}}{8\pi^2 v^2 \sin^2\beta}\frac{1}{\epsilon}}_{\text{one-loop}} + \underbrace{\frac{\alpha_s(m_t^2)^{\overline{\text{DR}}}}{4\pi^3 v^2 \sin^2\beta}\left(\frac{1}{\epsilon^2}-\frac{1}{\epsilon}\right)}_{\text{two-loop}}, \tag{9.24}$$

$$\delta Z_{H_u}^{\text{OS}} = \underbrace{-\frac{3(m_t^2)^{\text{OS}}}{8\pi^2 v^2 \sin^2\beta}\frac{1}{\epsilon}}_{\text{one-loop}} + \underbrace{\frac{\alpha_s(m_t^2)^{\text{OS}}}{4\pi^3 v^2 \sin^2\beta}\left(\frac{1}{\epsilon^2}-\frac{1}{\epsilon}\right) - \frac{3}{4\pi^2}\frac{m_t^{\text{OS}}(\delta m_t)_{\text{fin}}}{v^2\sin^2\beta}\frac{1}{\epsilon}}_{\text{two-loop}}. \tag{9.25}$$

Inserting the relation $m_t^{\overline{\text{DR}}} = m_t^{\text{OS}} + (\delta m_t)_{\text{fin}}$ it is evident that the two expressions agree up to higher orders. If, however, we had included parts proportional to ϵ in the on-shell counterterm, i.e. if the relation $m_t^{\overline{\text{DR}}} = m_t^{\text{OS}} + (\delta m_t)_{\text{fin}} + \epsilon(\delta m_t)_\epsilon$ is used, this equality would be destroyed and the on-shell $\delta Z_{H_u}^{\text{OS}}$ as derived from $\delta Z_{H_u}^{\overline{\text{DR}}}$ would gain an additional finite part, originating from the product of the one-loop $1/\epsilon$ pole and the $\epsilon(\delta m_t)_\epsilon$ term[2]. This is very counter intuitive. Hence, we want to avoid this. Please note, that the physical result for the renormalized two-loop self-energy of the order $\alpha_s\alpha_t$ remains the same in any case. If one does include the parts proportional to ϵ in δm_t and accepts the finite contribution in $\delta Z_{H_u}^{\text{OS}}$, then the result for the renormalized self-energy will not change, because the finite contribution from $\delta Z_{H_u}^{\text{OS}}$ will cancel against the additional finite contributions from the counterterm inserted diagrams. Hence, either way the final result for the renormalized self-energy will not depend on terms originating from the parts proportional to ϵ in δm_t. Therefore, we discard these parts from the very beginning.

9.3 Fixing of the Counterterms

As already mentioned we work in the gaugeless limit when calculating the $\alpha_s\alpha_t$ corrections. For the renormalization of the parameters of the Higgs sector at this order, it is therefore important to define this limit properly. In general the gaugeless limit means vanishing gauge couplings $g_1, g_2 \to 0$. Of course this entails a vanishing electric coupling and vanishing gauge boson masses. However, the Higgs mass matrix contains ratios of these parameters, therefore a precise definition of the limit is necessary. In fact, it is easier to carry out the limit when modifying the parameter set of Eq. (3.35) slightly. Instead of M_W^2 and M_Z^2 one can write everything in terms of the vacuum expectation value v and the sine and cosine of the electroweak mixing angle $\theta_W = \arccos M_W/M_Z$. Then the gaugeless limit can be defined as the limit in which $e \to 0$, while the vacuum expectation value v and the ratio of the vector boson masses, and thereby the electroweak mixing angle, remain constant. If this is applied to the Higgs mass matrix, all terms involving the electroweak mixing angle drop out and only terms proportional to v remain. Hence, instead of introducing the counterterms $\delta^{(2)}Z_e$, $\delta^{(2)}M_W^2$ and $\delta^{(2)}M_Z^2$ it is sufficient to introduce one counterterm $\delta^{(2)}v$. The remaining counterterms are as described in Tab. 7.1.

The on-shell counterterms are fixed similarly to the one-loop case with the main difference being that the external momentum is taken to zero.

- **tadpole parameters**
  The two-loop counterterms for the tadpole parameters are determined via the irre-

[2] By the way, the same thing would happen for the counterterms $\delta^{(2)}\tan\beta$ and $\delta^{(2)}\lambda$, which are related to δZ_{H_u} as we will see in the next section.

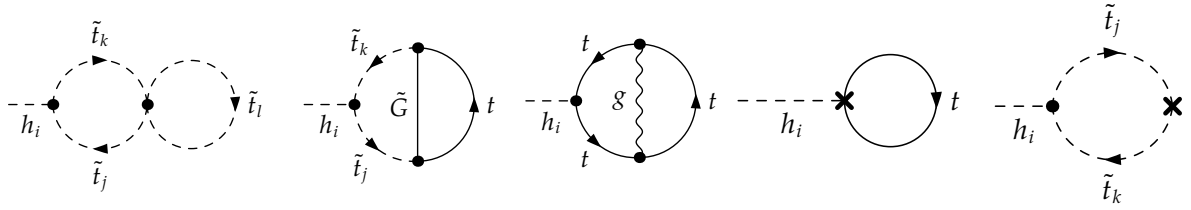

Figure 9.3: Example diagrams for the tadpole diagrams of the order $\alpha_s\alpha_t$.

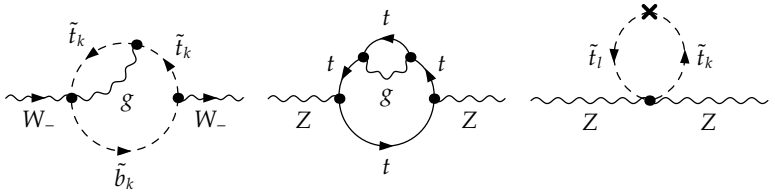

Figure 9.4: Sample diagrams for the W and Z boson self-energy at the order $\alpha_s\alpha_t$.

ducible two-loop tadpole diagrams $T^{(2)}_{\phi}$ of the order $\alpha_s\alpha_t$,

$$\delta^{(2)} t_{\phi} = T^{(2)}_{\phi} \quad \text{with} \quad \phi = h_d, h_u, h_s, a_d, a_s\,. \tag{9.26}$$

Some subset of sample diagrams is given in Fig. 9.3. Just as for the self-energy there are contributions from genuine two-loop diagrams, with tops, stops, gluons and gluinos in the loops, as well as contributions from counterterm inserted one-loop diagrams.

- **the vacuum expectation value**
  The two-loop counterterm of the vacuum expectation value at the order $\alpha_s\alpha_t$ is fixed via the counterterms $\delta^{(2)} M_Z^2$ and $\delta^{(2)} M_W^2$ by

$$\delta^{(2)} v = \frac{2}{v}\left(\cos^4\theta_W \frac{\delta^{(2)} M_Z^2}{e^2} + (1 - 2\cos^2\theta_W)\,\frac{\delta^{(2)} M_W^2}{e^2}\right), \tag{9.27}$$

  where the counterterms of the gauge boson masses are given by the transverse parts of the respective self-energy, which are now evaluated at vanishing external momentum[3], i.e.

$$\delta^{(2)} M_W^2 = \Sigma^{(2),T}_{WW}(0) \quad \text{and} \quad \delta^{(2)} M_Z^2 = \Sigma^{(2),T}_{ZZ}(0)\,. \tag{9.28}$$

  The gauge boson self-energies (example diagrams depicted in Fig. 9.4) are proportional to e^2 and therefore vanish in the gaugeless limit, unless they appear as the ratios $\Sigma^{(2),T}_{WW}(0)/e^2$ and $\Sigma^{(2),T}_{ZZ}(0)/e^2$, as they do in the expression for $\delta^{(2)} v$. In the computation of the self-energy of the W boson we set the bottom quark mass to zero, since our calculation does not include $\alpha_s\alpha_b$ corrections so far. In the limit of vanishing bottom quark mass the left-handed and right-handed sbottoms do not mix, and only the left-handed sbottom enters in our calculation. The counterterm $\delta m^2_{\tilde{b}_L}$, entering the counterterm inserted diagrams, is identical to $\delta m^2_{\tilde{Q}_3}$, which was already determined via the stop sector. The explicit evaluation of the UV-divergent part of $\delta^{(2)} v$ revealed that it is related to the wavefunction renormalization constant via the relation

$$\delta^{(2)} v\big|_{\text{div}} = \frac{1}{2}\, v\, \sin^2\beta\, \delta^{(2)} Z_{H_u}\,, \tag{9.29}$$

  which is to be expected according to [141, 142].

[3] Due to this the $\widetilde{\text{Re}}$ that appeared in the one-loop equations is not necessary here. Since the loop functions are automatically real for vanishing external momentum.

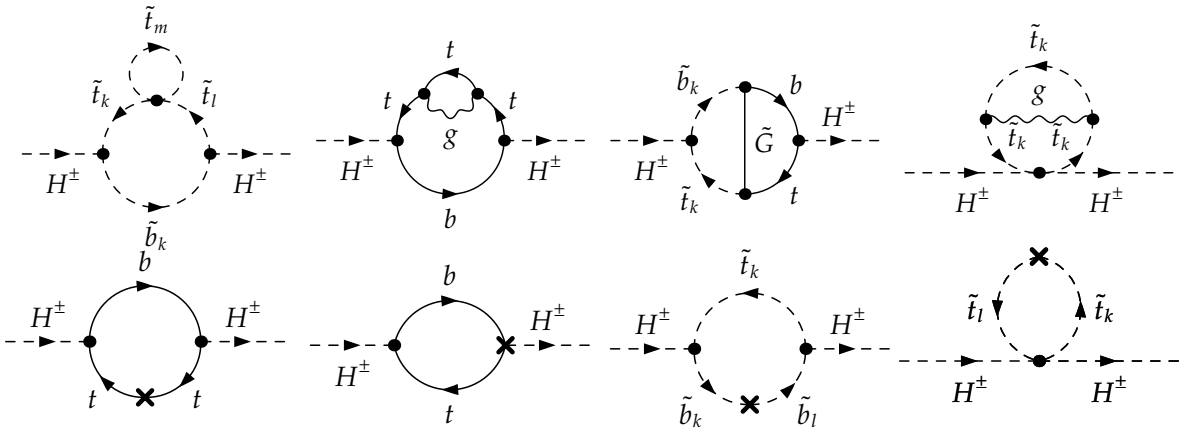

Figure 9.5: Example diagrams for the self-energy of the charged Higgs boson at the order $\alpha_s\alpha_t$.

- **mass of the charged Higgs boson**
  The counterterm to the mass of the charged Higgs boson is fixed via the condition

$$\hat{\Sigma}^{(2)}_{H^\pm H^\pm}(0) = 0\,, \tag{9.30}$$

  where $\hat{\Sigma}^{(2)}_{H^\pm H^\pm}(0)$ is the renormalized self-energy of the charged Higgs boson at order $\alpha_s\alpha_t$ evaluated at vanishing external momentum. Solving this for the counterterm yields

$$\delta^{(2)} M^2_{H^\pm} = \Sigma^{(2)}_{H^\pm H^\pm}(0) - M^2_{H^\pm}\, \cos^2\beta\, \delta^{(2)} Z_{H_u} \tag{9.31}$$

  where we already inserted that the only non-vanishing wavefunction renormalization constant at the order $\alpha_s\alpha_t$ is $\delta^{(2)} Z_{H_u}$. The dependence of $\delta^{(2)} M^2_{H^\pm}$ on $\delta^{(2)} Z_{H_u}$ is due to the fact that the renormalized self-energy is evaluated at vanishing external momentum and not at $p^2 = M^2_{H^\pm}$. If it was evaluated at $p^2 = M^2_{H^\pm}$, the wavefunction renormalization constants would drop out as expected for on-shell renormalization prescriptions. Please keep in mind that $\delta^{(2)} Z_{H_u}$ is purely divergent. Hence, it is necessary to cancel the poles correctly, but does not contribute to the finite part of $\delta^{(2)} M^2_{H^\pm}$. This is only determined by the contributions of the unrenormalized self-energy of the charged Higgs boson at the order $\alpha_s\alpha_t$, which is denoted by $\Sigma^{(2)}_{H^\pm H^\pm}(0)$ and for which some example diagrams are given in Fig. 9.5. The particles in the loops are top and bottom quarks and squarks plus gluons and gluinos. As before $m_b = 0$ so that only the left-handed sbottom contributes.

The conditions for the $\overline{\text{DR}}$ parameters are also determined analogously to the one-loop case.

- **ratio of the vacuum expectation values tanβ**
  The two-loop counterterm for $\tan\beta$ is fixed via the wavefunction renormalization constant $\delta^{(2)} Z_{H_u}$ at this order,

$$\delta^{(2)} \tan\beta = \frac{1}{2} \tan\beta\, \delta^{(2)} Z_{H_u}\big|_{\text{div}}\,. \tag{9.32}$$

- **remaining $\overline{\text{DR}}$ parameters**
  By demanding a finite renormalized self-energy for the neutral Higgs bosons, we end up with the following two-loop counterterms

$$\delta^{(2)}|\lambda| = \frac{-|\lambda|}{2}\big(\delta^{(2)} Z_{H_u} \cos^2\beta + 2\frac{\delta^{(2)} v}{v}\Big|_{\text{div}}\big) = \frac{-|\lambda|}{2}\delta^{(2)} Z_{H_u}\,, \tag{9.33a}$$

$$\delta^{(2)}|\kappa| = \frac{-|\kappa|}{2}\big(-\delta^{(2)} Z_{H_u} \sin^2\beta + 2\frac{\delta^{(2)} v}{v}\Big|_{\text{div}}\big) = 0\,, \tag{9.33b}$$

$$\delta^{(2)} v_s = \frac{-v_s}{2}\Big(- \delta^{(2)} Z_{H_u} \sin^2\beta + 2\frac{\delta^{(2)} v}{v}\Big|_{\text{div}}\Big) = 0\,, \tag{9.33c}$$

$$\delta^{(2)} |A_\kappa| = 0\,, \tag{9.33d}$$

$$\delta^{(2)} \varphi_y = 0\,, \tag{9.33e}$$

$$\delta^{(2)} \varphi_z' = 0\,. \tag{9.33f}$$

All counterterms with the exception of $\delta^{(2)}|\lambda|$ actually vanish at the order $\alpha_s\alpha_t$. For the two phases this is not surprising, since they also do not need to be renormalized at one-loop level as we saw earlier. For the other parameters this can also be understood easily. The corrections of the order $\alpha_s\alpha_t$ we calculated depend on λ, since it appears in the couplings entering the self-energies and tadpole diagrams we compute. However, the other parameters do not enter and therefore they do not need to be renormalized at the order $\alpha_s\alpha_t$.

9.4 Differences Compared to the Respective MSSM Calculation

The most obvious difference compared to the MSSM is of course the presence of the additional singlet. Hence, the self-energy has more components. Still, at first sight one could assume that the components of the self-energy that involve only doublet fields are equal, because the doublet part of the couplings are unchanged. At the level of the unrenormalized self-energy this is true, i.e.

$$\Sigma^{\text{NMSSM}}_{\phi_i\phi_j} = \Sigma^{\text{MSSM}}_{\phi_i\phi_j} \text{ at order } \alpha_s\alpha_t \quad \text{with} \quad \phi = (a, h_u, h_d)\,. \tag{9.34}$$

However, this does not hold for the renormalized self-energy. The difference originates from the finite contributions of the two-loop counterterm mass matrix. The explicit form of this counterterm mass matrix $\delta^{(2)}\mathcal{M}_{\text{Higgs}}$ is given in App. C. The important fact is that it contains terms involving $\delta^{(2)} v$. Such terms do not appear in the MSSM. A look at the explicit form of $\delta^{(2)}\mathcal{M}_{\text{Higgs}}$ reveals that these terms are proportional to $|\lambda|$, i.e. they vanish in the MSSM limit[4].

Aside from these additional contributions to the finite part of the renormalized self-energy, there is also a difference when it comes to the cancellation of the divergences. In the MSSM the explicit form of $\delta^{(2)} Z_{H_u}$ at the order $\alpha_s\alpha_t$ is not important, since – at least in the calculation with vanishing external momentum – the dependence on the Z-factor drops out. This means it is sufficient to determine the other counterterms in terms of $\delta^{(2)} Z_{H_u}$. Inserting these relations into the renormalized self-energy will lead to a finite result that does not depend on the explicit form of $\delta^{(2)} Z_{H_u}$. In the NMSSM this is not the case. Although the Z-factor dependence drops out in most components of the renormalized self-energy, it remains in the $h_d h_s$ component. Hence, in the NMSSM the explicit form of the Z-factor is important to check for the cancellation of the poles.

9.5 Performed Cross-Checks

To validate our calculation we performed thorough cross-checks. First of all the complete calculation was performed by two persons independently (by Dao Thi Nhung and myself).

[4]The MSSM limit is obtained by $|\lambda| \to 0$ and $|\kappa| \to 0$, while at the same time $v_s \to \infty$ such that $|\mu_{\text{eff}}| = v_s|\lambda|/\sqrt{2} = \text{const}$.

However, we relied on the same tools and methods (see description Sec. 9.1). Therefore, some additional checks for the calculation of the self-energy have been performed using in-house `Mathematica` routines and the `Mathematica` packages `OneCalc` and `TwoCalc` [132, 143] (calculation performed by Heidi Rzehak). The results of all of these computations were in full agreement.

Furthermore, we compared to existing results. On the one hand we checked against the results obtained in the complex MSSM [137], i.e. we compared the components of the Higgs self-energy involving doublet-doublet mixing while neglecting the NMSSM specific $\delta^{(2)}v$ terms. We took care to set all possible CP-violating phases to non-zero values during our checks. In the MSSM there is no physical CP-violating phase at tree level, hence one has to be careful to match the phases appearing in the NMSSM correctly to the corresponding MSSM phases, in particular $\varphi_\mu^{\text{MSSM}} = \varphi_\lambda + \varphi_s + \varphi_u$. Our calculation reproduces the MSSM-like corrections of the order $\alpha_s\alpha_t$. On the other hand we compared with the existing NMSSM calculation [85], which holds for the real NMSSM and uses $\overline{\text{DR}}$ conditions everywhere. Our result is in full agreement with this calculation as well[5].

[5]Please note, that Ref. [85] did not include the necessary $\delta^{(2)}v$ term in the conversion from the on-shell value v^{OS} to the $\overline{\text{DR}}$ value $v^{\overline{\text{DR}}}$ entering their calculation.

CHAPTER 10

The Program-Package NMSSMCALC

The Fortran program package `NMSSMCALC` [8] calculates the loop-corrected Higgs boson masses, the decay widths and the branching ratios of the Higgs bosons in the CP-conserving and in the CP-violating NMSSM. It is a combination of two independent programs, one for the calculation of the higher order masses and one for the computation of the decay widths.

During my diploma thesis I already computed the full one-loop corrections to the Higgs boson masses as presented in Ch. 8, but originally the calculation was implemented in a `Mathematica` program. `Mathematica` is convenient due to its interactive evaluation, if one wants to validate the calculation procedure. But it is not well suited for numerical evaluations and linking it to other programs is not straightforward. Therefore, the first project of my PhD thesis was to implement the one-loop corrections to the Higgs boson masses in the NMSSM into a Fortran program. This program features the SLHA [69, 70] conventions[1] for the input and output files and can therefore be easily linked to existing computer tools. By now also the corrections of the order $\alpha_s\alpha_t$ as described in Ch. 9 are included in the published program. In addition to the mixed renormalization scheme described so far, a second slightly changed renormalization scheme is available within the program. Instead of the mass of the charged Higgs boson the real part of the soft SUSY breaking parameter A_λ is considered as an input parameter. In the first scheme the mass of the charged Higgs boson, being an on-shell input, does not receive any radiative corrections, since this is the definition of an on-shell parameter and the counterterm for the mass of the charged Higgs boson is chosen accordingly. However, in the second scheme, where the real part of A_λ is considered as a $\overline{\text{DR}}$ input, the mass of the charged Higgs boson does receive radiative corrections and the pole mass at higher order is determined by iteratively solving the equation

$$\left(M_{H^\pm}^{\text{loop}}\right)^2 = \left(M_{H^\pm}^{\text{tree}}\right)^2 - \hat{\Sigma}_{H^\pm H^\pm}\Big(\left(M_{H^\pm}^{\text{loop}}\right)^2\Big)\,, \tag{10.1}$$

where $\hat{\Sigma}_{H^\pm H^\pm}$ is the renormalized self-energy of the charged Higgs boson, which is given by

$$\hat{\Sigma}_{H^\pm H^\pm}(p^2) = \Sigma_{H^\pm H^\pm}(p^2) + \left(p^2 - \left(M_{H^\pm}^{\text{tree}}\right)^2\right)\left(\sin^2\beta\,\delta Z_{H_d} + \cos^2\beta\,\delta Z_{H_u}\right) - \delta M_{H^\pm}^2\,. \tag{10.2}$$

[1] As described in Sec. 7.1.2 this was the reason why we changed our renormalization scheme slightly compared to our first publications.

Here the counterterm $\delta M^2_{H^\pm}$ is a function of the counterterms of the second renormalization scheme.

The program that calculates the decay widths and branching ratios of the NMSSM Higgs bosons is based on `HDECAY` [144, 145], which was extended to incorporate the additional Higgs singlet field[2]. All decay widths include the dominant higher order QCD corrections. The decays of the neutral Higgs bosons into a pair of bottom quarks include higher order SUSY-QCD and approximate SUSY-electroweak corrections up to one-loop order. The decay into a pair of strange quarks includes the dominant resummed SUSY-QCD corrections, while the decay into a τ pair includes the dominant resummed SUSY-electroweak corrections. For the real NMSSM the SUSY-QCD corrections to the decays into top and bottom squarks are taken into account. All relevant off-shell decays, namely those into massive gauge bosons, into gauge boson and Higgs boson, into Higgs pairs and into pairs of heavy quarks, are included. For detailed explanations and formulas see [8].

In the future we plan to include further higher order corrections. For the Higgs boson masses two-loop corrections, for example those of the orders $\alpha_s\alpha_b$, α_t^2 or α_b^2, will be added. Also the calculation for the corrections up to order $\alpha_s\alpha_t$ to the trilinear Higgs-coupling is ongoing. I contributed to this effort by performing the full one-loop calculation as a cross-check. The one-loop calculation was the main topic of a diploma thesis [13] in our group and the results were published in [12]. Furthermore, the full one-loop corrections to the decay of a CP-odd Higgs boson into two stops was the topic of a diploma thesis in our group [15]. I contributed by calculating the electroweak corrections as a cross-check. These correction will also be included in `NMSSMCALC` in the near future. In addition to these higher order corrections we also plan to implement the renormalization group running of the input parameters, which is not included so far[3].

10.1 The SUSY Les Houches Accord

The SUSY Les Houches Accord [69] was developed to standardize the input and output files of programs performing calculations in supersymmetric models, e.g. spectrum generators, etc. It has been extended to SLHA2 [70] and now features the complex MSSM and the real NMSSM. However, the complex NMSSM is not yet included. The form of the input and output files we use in `NMSSMCALC` is based on the suggested form for the complex MSSM, but we made some slight changes that we would like to mention here. In the input file the required blocks for the real NMSSM are the blocks "`MODSEL`", "`SMINPUTS`" and "`EXTPAR`". In case of the complex NMSSM the additional blocks "`IMEXTPAR`" and "`CMPLX`" are necessary, where the latter is a block we introduced specifically for the NMSSM. In the block "`MODSEL`" the user has the possibility to configure a few options. Depending on whether the entry 5 is set to "0" or "2" the calculation is carried out in the CP-conserving or CP-violating NMSSM[4]. Via entry 6 the user can choose up to which order the Higgs masses and mixing matrices should be calculated ("1": one-loop level and "2": two-loop level). Entry 7 finally allows to fix the renormalization scheme of the top and stop sector ("1": $\overline{\text{DR}}$ scheme and "2": on-shell scheme). If one of these entries is missing the defaults are the inclusion of the two-loop corrections and the $\overline{\text{DR}}$ renormalization of the top and stop sector. In the block "`SMINPUTS`"

[2] These modification were mainly made by J. Baglio, R. Gröber and M. Mühlleitner.

[3] The input parameters are assumed to be given at the renormalization scale.

[4] Setting entry 5 to "1" corresponds to including only CP-violating effects originating from the elements of the CKM matrix. However, this is not supported by `NMSSMCALC`.

we added an entry for the pole mass of the W boson (entry 9) as we require the pole mass for our renormalization scheme, the rest is as defined by SLHA. In the block "`EXTPAR`" the input parameters of the Higgs sector are set. In the entry 0 the input scale can be set. This also fixes the renormalization scale, denoted by μ_R, used in the mass calculation. If the input scale, denoted by M_{inp}, is not explicitly given it is set to the geometric mean of the soft SUSY breaking masses of the stop sector,

$$M_{\text{inp}} = \mu_R = \sqrt{m_{\tilde{Q}_3} m_{\tilde{t}_R}}\,. \tag{10.3}$$

By providing either the mass of the charged Higgs boson or the real part of A_λ the user can choose which renormalization scheme is going to be applied. If $M_{H^\pm}$ is supplied in entry 27 of "`EXTPAR`" the first scheme is used, i.e. the mass of the charged Higgs boson is renormalized using on-shell conditions. If the real part of A_λ is given in entry 63 the second renormalization scheme is applied. In case both $M_{H^\pm}$ and A_λ are wrongly provided the program issues a warning and uses the mass of the charged Higgs boson, while the given value for A_λ is ignored. If the complex NMSSM is considered the block "`EXTPAR`" contains the real parts of the parameters, whereas the block "`IMEXTPAR`" contains the respective imaginary parts. Please note, that there are some parameters, like the soft SUSY breaking masses of the squark and slepton sector, that are always real and are therefore not represented in "`IMEXTPAR`". Furthermore, the imaginary parts of A_λ and A_κ should not be given as input. Since they are not part of the set of independent parameters we chose, they are calculated from the other input parameters. In case the user supplies them nevertheless, a warning is issued and the given values are ignored. Finally, the block "`CMPLX`" contains just one entry, namely the phase φ_u. The calculated masses and branching ratios are written to output files following the SLHA conventions.

CHAPTER 11

Numerical Analysis

In order to illustrate the importance of the $\alpha_s\alpha_t$ corrections to the masses of the Higgs bosons we discuss one benchmark scenario. The results presented here are published in [7]. The parameter point we selected displays a typical behavior we found for scenarios that were obtained from a parameter scan which searched for phenomenologically valid points. We used the programs `HiggsBounds` [146–148] and `HiggsSignals` [149] to ensure that our scenarios are in accordance with the current experimental Higgs results. The program `HiggsBounds` tests whether the Higgs spectrum is excluded at the 95% confidence level (CL) by the exclusion bounds obtained from LEP, Tevatron and LHC measurements[1]. The program `HiggsSignals` checks whether the Higgs spectrum contains a Higgs boson whose mass and signal strengths are compatible with the Higgs boson observed at the LHC. `HiggsSignals` returns a p-value, which we demand to be at least 0.05, corresponding to a non-exclusion at 95% CL. Both programs accept the input in the SLHA format. In addition to the standard blocks, blocks which include the effective couplings normalized to the respective SM value are introduced. These effective couplings are then used to calculate the production cross sections of the NMSSM Higgs bosons by rescaling the respective cross sections of a SM Higgs boson of the same mass. We compute the effective coupling to gluons by taking the ratio of the partial decay widths of Higgs to gluons in the NMSSM and the SM. The signal strength values for the different channels are then calculated by `HiggsBounds` and `HiggsSignals` by multiplying the production cross sections with the respective branching ratios as they are supplied by `NMSSMCALC`. In addition to this we accommodate the constraints coming from SUSY searches [150–160] by choosing our input values for the soft SUSY breaking masses, which give a very good handle on the squark masses, in appropriate ranges.

We use the following SM parameters [28, 161]

$$\begin{aligned} &\alpha(M_Z) = 1/128.962\,, \quad \alpha_s^{\overline{\rm MS}}(M_Z) = 0.1184\,, \quad M_Z = 91.1876\,\text{GeV}\,, \\ &M_W = 80.385\,\text{GeV}\,, \quad m_t = 173.5\,\text{GeV}\,, \quad m_b^{\overline{\rm MS}}(m_b^{\overline{\rm MS}}) = 4.19\,\text{GeV}\,. \end{aligned} \tag{11.1}$$

[1] For the exhaustive list of included analyses see the references within `HiggsBounds`.

	H_1	H_2	H_3	H_4	H_5
mass tree [GeV]	79.15	103.55	146.78	796.62	803.86
main component	h_s	h_u	a_s	h_d	a
mass one-loop [GeV]	103.45	129.15	139.84	796.53	802.94
main component	h_s	a_s	h_u	h_d	a
mass two-loop [GeV]	103.00	126.20	128.93	796.45	803.07
main component	h_s	h_u	a_s	h_d	a

Table 11.1: Masses and main components of the neutral Higgs bosons at tree, one- and two-loop level as obtained using OS renormalization in the top/stop sector.

Applying two-loop SM renormalization group running [162] the strong coupling constant is evolved up to the renormalization scale and then converted from $\overline{\text{MS}}$ to $\overline{\text{DR}}$ [163]. If $\overline{\text{DR}}$ renormalization is chosen for the top and stop sector, the top pole mass is converted to the respective $\overline{\text{DR}}$ running mass at the renormalization scale (see App. B). The light quark masses are chosen as

$$m_u = 2.5\,\text{MeV}\,, \quad m_d = 4.95\,\text{MeV}\,, \quad m_s = 101\,\text{MeV} \quad \text{and} \quad m_c = 1.27\,\text{GeV}\,. \tag{11.2}$$

Please note, that their influence on the higher order corrections is very small. Therefore, the fact that they are not well defined does not pose a problem. The input parameters of the Higgs sector are set to

$$\begin{aligned} &|\lambda| = 0.629\,, \quad |\kappa| = 0.208\,, \quad |A_\kappa| = 179.7\,\text{GeV}\,, \quad |\mu_{\text{eff}}| = 173.7\,\text{GeV}\,, \\ &\varphi_\lambda = \varphi_{\mu_{\text{eff}}} = \varphi_u = 0\,, \quad \varphi_\kappa = \pi\,, \quad \tan\!\beta = 4.02\,, \quad M_{H^\pm} = 788\,\text{GeV}\,. \end{aligned} \tag{11.3}$$

Instead of the vacuum expectation value v_s and the phase φ_s we give the absolute value and phase of μ_{eff} as defined in Eq. (9.9), from which the first two can be derived. The soft SUSY breaking masses and trilinear couplings are set to

$$\begin{aligned} &m_{\tilde{u}_R,\tilde{c}_R} = m_{\tilde{d}_R,\tilde{s}_R} = m_{\tilde{Q}_{1,2}} = m_{\tilde{L}_{1,2}} = m_{\tilde{e}_R,\tilde{\mu}_R} = 3\ \text{TeV}\,,\ m_{\tilde{t}_R} = 1170\,\text{GeV}\,, \\ &m_{\tilde{Q}_3} = 1336\,\text{GeV}\,,\ m_{\tilde{b}_R} = 1029\,\text{GeV}\,,\ m_{\tilde{L}_3} = 2465\,\text{GeV}\,,\ m_{\tilde{\tau}_R} = 300.5\,\text{GeV}\,, \\ &|A_{u,c,t}| = 1824\,\text{GeV}\,,\ |A_{d,s,b}| = 1539\,\text{GeV}\,,\ |A_{e,\mu,\tau}| = 1503\,\text{GeV}\,, \\ &|M_1| = 862.3\,\text{GeV},\ |M_2| = 201.5\,\text{GeV}\,,\ |M_3| = 2285\,\text{GeV}\,, \\ &\varphi_{A_{d,s,b}} = \varphi_{A_{e,\mu,\tau}} = \pi\,,\ \varphi_{A_{u,c,t}} = \varphi_{M_1} = \varphi_{M_2} = \varphi_{M_3} = 0\,. \end{aligned} \tag{11.4}$$

As the renormalization scale we choose

$$\mu_R = \sqrt{m_{\tilde{Q}_3} m_{\tilde{t}_R}} \approx 1250\,\text{GeV}\,. \tag{11.5}$$

In this scenario all phases are multiples of π, hence there is no CP-violation. However, since we will move to non-trivial phases later on, we use the convention for the complex NMSSM already here. This means we do not distinguish between CP-even and CP-odd Higgs states but simply label all five Higgs states by ascending mass. This avoids confusing changes of notation when we actually turn on CP-violating phases in this scenario.

The masses obtained for this scenario at tree level, at one-loop level and at two-loop level when applying on-shell renormalization in the top and stop sector are displayed in Tab. 11.1. The table also lists the main component of the Higgs bosons at the respective orders. This

	H_1	H_2	H_3	H_4	H_5
mass tree [GeV]	79.15	103.55	146.78	796.62	803.86
main component	h_s	h_u	a_s	h_d	a
mass one-loop [GeV]	102.80	120.52	128.80	796.36	803.09
main component	h_s	h_u	a_s	h_d	a
mass two-loop [GeV]	103.09	124.52	128.91	796.36	803.03
main component	h_s	h_u	a_s	h_d	a

Table 11.2: Masses and main components of the neutral Higgs bosons at tree, one- and two-loop level as obtained using $\overline{\text{DR}}$ renormalization in the top/stop sector.

main component is important since it helps us to identify which of the masses at different orders we should actually compare with each other to determine the size of the corrections. Aside from their masses the main properties of the Higgs bosons are given by their couplings. Their coupling properties depend on which mixture of the interaction eigenstates forms the respective mass eigenstate. Hence, by comparing the Higgs bosons with the same main component, we compare the Higgs bosons with similar couplings. In this particular scenario the Higgs boson with a large h_u component is at tree level the next-to-lightest Higgs boson. At one-loop level, however, H_3 is the h_u-like Higgs boson, while at two-loop it is once again the next-to-lightest Higgs boson. This happens because the one-loop corrections to the mass of the Higgs boson that is h_u-like (H_2 at tree level) are positive and rather large $\sim 35\%$ while the one-loop corrections to the mass of the a_s-like (H_3 at tree level) Higgs boson are negative and with $\sim 12\%$ also sizeable. This causes an interchange in the mass ordering of these two states[2]. Including the $\alpha_s\alpha_t$ two-loop corrections the a_s-like state hardly receives any corrections, while the ones for the h_u state are quite large again ($\sim 10\%$) but negative so that the tree-level mass ordering is restored. Overall, the typical behavior can be observed that the one-loop corrections are sizeable for all light Higgs bosons, while the heavy ones with masses around 800 GeV are not affected much. Including the two-loop corrections of the order $\alpha_s\alpha_t$ does influence the mass of the h_u-like Higgs boson, but has hardly any effect on the other masses. This is to be expected since the interaction eigenstate h_u is the one coupling to top quarks and we only include corrections involving tops and stops at two-loop order. Please note, that for this choice of parameters, or more precisely for this value of $\tan\beta$, the h_u-like Higgs boson is the one whose couplings are closest to those of the SM Higgs boson. Hence, the chosen scenario with a h_u-like Higgs boson with a mass of 126 GeV at two-loop order is compatible with the current experimental Higgs results. The other light Higgs bosons are singlet-like and can therefore have escaped detection at the colliders so far, while the remaining Higgs bosons are rather heavy and thereby evade the exclusion bounds.

If one now uses $\overline{\text{DR}}$ renormalization in the top and stop sector, the picture at two-loop level remains the same (see Tab. 11.2). The mass of the h_u-like Higgs boson is slightly – but not significantly – changed to 124.5 GeV, while the other masses are only affected at the per mille level. At one-loop order, however, the mass of the h_u-like Higgs boson displays a strong dependence on the choice of renormalization scheme for the top and stop sector. Using on-shell renormalization it is close to 140 GeV, whereas it is roughly 120.5 GeV for $\overline{\text{DR}}$ conditions.

To investigate this dependence on the renormalization scheme applied in the top and stop

[2]This change in mass ordering is not specific to this scenario. This can occur generically if two Higgs bosons close in mass are present.

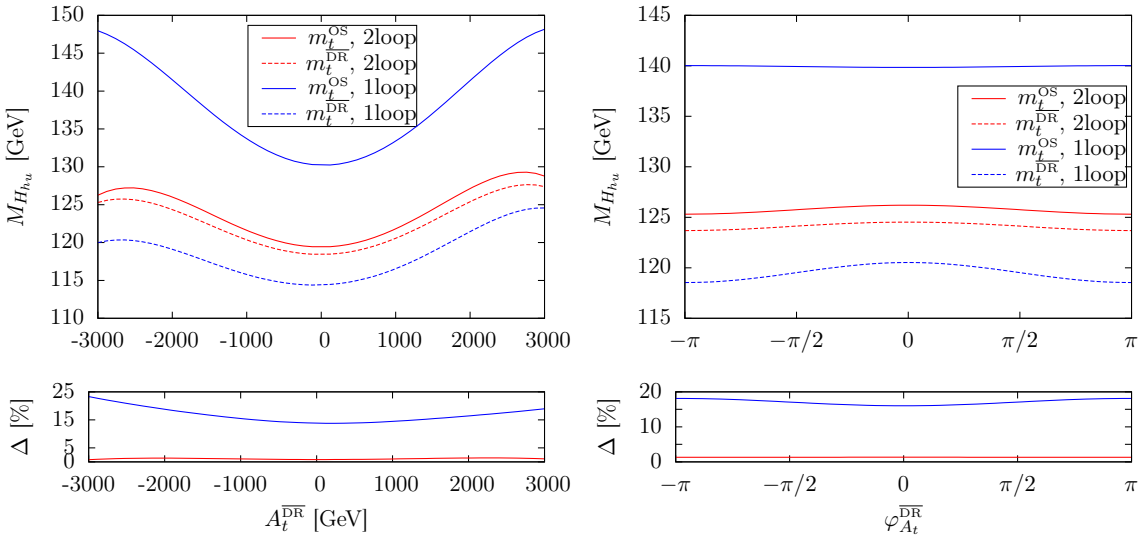

Figure 11.1: Upper Panels: Dependence of the one-loop (blue) and two-loop (red) mass of the h_u-like ($\widehat{=}$ SM-like here) Higgs boson on the variation of the absolute value of A_t (left-hand side) and the phase (right-hand side). For the renormalization in the stop/top sector either on-shell conditions (solid lines) or $\overline{\rm DR}$ conditions (dashed lines) are applied. Lower Panels: Relative difference – i.e. $\Delta = |M_{H_{h_u}}^{m_t(\overline{\rm DR})} - M_{H_{h_u}}^{m_t({\rm OS})}|/M_{H_{h_u}}^{m_t(\overline{\rm DR})}$ – in percent of the two renormalization schemes at one-loop (blue) and two-loop level (red). Already published in [7].

sector further we started with our benchmark point and varied the absolute value and the phase of the soft SUSY breaking trilinear coupling A_t while keeping all other parameters fixed. Figure 11.1 shows the dependence of the mass of the Higgs boson with the largest h_u admixture on the varied quantities at one-loop and two-loop level for the two different renormalization schemes in the top and stop sector. The relative difference Δ between the renormalization schemes is plotted in the lower panels. At one-loop level the relative difference is quite large and varies between $15 - 25\%$. Including the $\alpha_s\alpha_t$ corrections reduces this dependence significantly to less than 2%. As the difference between two renormalization schemes is a hint at the missing higher order corrections, this illustrates nicely that the theoretical error due to missing higher order corrections of the top and stop sector is significantly reduced by the $\alpha_s\alpha_t$ corrections. What is also striking is that the convergence for the $\overline{\rm DR}$ scheme seems to be better than for the on-shell scheme, i.e. the one-loop and two-loop results are closer to each other in the $\overline{\rm DR}$ scheme. This is a general feature we observe and can be explained by the fact, that in the $\overline{\rm DR}$ scheme some of the $\alpha_s\alpha_t$ corrections are actually already included in the one-loop result, because they enter in the conversion of the top pole mass to the running mass. Whereas in the on-shell scheme these corrections enter only at two-loop level via the counterterm inserted diagrams, which include terms proportional to the finite part of the counterterm of the top quark mass.

Now, we would like to investigate the dependence on the phases that appear explicitly in the two-loop corrections. The important ones are – just as in the MSSM – the phase of the gluino sector φ_{M_3}, the phase of the soft SUSY breaking trilinear coupling φ_{A_t} and the phase $\varphi_{\mu_{\rm eff}}$. With the very last one caution is required. The issue is that we want to avoid CP-violating effects appearing at tree level for this discussion, since they can be quite extreme and we are explicitly interested in the effect induced by the two-loop corrections. However, recall that the following relation holds $\varphi_{\mu_{\rm eff}} = \varphi_\lambda + \varphi_s$ and that these two phases enter the CP-violating

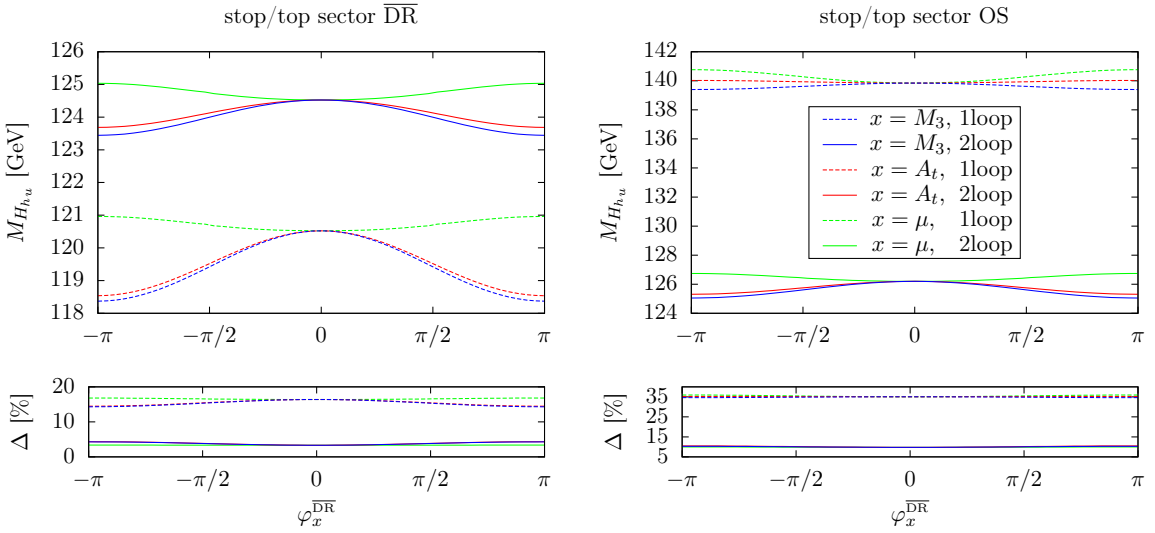

Figure 11.2: Upper Panels: Dependence of the one-loop (dashed line) and two-loop (solid line) masses of the h_u-like ($\widehat{=}$ SM-like here) Higgs boson on the variation of the phases φ_{M_3} (blue), φ_{A_t} (red) and φ_μ (green) applying either $\overline{\text{DR}}$ (left-hand side) or on-shell renormalization (right-hand side) for the stop/top sector. Lower Panels: Relative correction of the n^{th} order to the mass of the h_u-like Higgs boson with respect to the $(n-1)^{st}$ order – i.e. $\Delta = |M^{(n)}_{H_{h_u}} - M^{(n-1)}_{H_{h_u}}|/M^{(n-1)}_{H_{h_u}}$ – in percent as a function of the phases φ_{M_3} (blue), φ_{A_t} (red) and φ_μ (green) for $n = 2$ (solid line) and $n = 1$ (dashed line). Already published in [7]

phase of the tree-level Higgs sector $\varphi_y = \varphi_\lambda - 2\varphi_s + \varphi_u - \varphi_\kappa$. The phases φ_u and φ_κ are kept as in Eq. (11.3). Hence, they are multiples of π and do not contribute to a CP-violating φ_y. In order to obtain a value of φ_y that is CP-conserving at tree level, while generating a value of $\varphi_{\mu_{\text{eff}}}$ that causes CP-violation at higher orders we choose $\varphi_\lambda = 2\varphi_s = 2/3\varphi_{\mu_{\text{eff}}}$. The dependence of the mass of the h_u-like Higgs boson on the variation of these three phases is displayed in Fig. 11.2. In the left panels $\overline{\text{DR}}$ renormalization was applied in the top and stop sector, whereas on-shell renormalization was chosen in the right panels. Both the dependence at one-loop and at two-loop level is shown. The lower panels show the corrections of the n^{th} order relative to the $(n-1)^{st}$ order, i.e.

$$\Delta = \frac{|M^{(n)}_{H_{h_u}} - M^{(n-1)}_{H_{h_u}}|}{M^{(n-1)}_{H_{h_u}}} \,. \tag{11.6}$$

The tree-level mass values necessary for this comparison do not depend on the variation of these phases. They are the same for every point of the variations and given in Tab. 11.1 and Tab. 11.2. Although the dependence of the higher order masses on the variation of the phases is clearly visible the impact on the relative corrections is rather small. Adopting the on-shell scheme for the top and stop sector the one-loop corrections amount to $\sim 35\%$, while for the $\overline{\text{DR}}$ scheme they are roughly 15%. At two-loop order they vary between $5-10\%$ depending on the renormalization scheme and the specific parameter point. The dependence of the mass on the phases at two-loop level is very similar for both renormalization schemes. The dependence on φ_{A_t} and φ_{M_3} is quite pronounced, whereas the curve for $\varphi_{\mu_{\text{eff}}}$ is flatter. The overall form and the size of the dependence on these phases is more generic and is similarly observed for other scenarios. However, which of the three phases has the most impact is scenario specific. Furthermore, we would also like to point out that the three phases actually only appear in

two linearly independent phase combinations[3] in the $\alpha_s\alpha_t$ corrections, namely

$$\varphi_1 = \varphi_{\mu_{\text{eff}}} + \varphi_{A_t} \quad \text{and} \quad \varphi_2 = \varphi_{M_3} - \varphi_{A_t}\,. \tag{11.7}$$

Finally, let us discuss the phase dependencies displayed at one-loop level. The dependence on the phases $\varphi_{\mu_{\text{eff}}}$ and φ_{A_t} is expected, since they appear in the stop sector, which enters the one-loop corrections. However, the dependence on φ_{M_3}, i.e. the phase of the gluino sector, is slightly puzzling at first sight, because corrections involving gluinos in the loop enter only at two-loop order. But the dependence at one-loop order is actually induced by parameter conversions that do depend on the phase of the gluino sector. If $\overline{\text{DR}}$ renormalization is adopted in the top and stop sector the top pole mass is converted to the running $\overline{\text{DR}}$ mass and this conversions includes SUSY corrections that involve gluinos in the loop. In the case of on-shell renormalization the input parameters of the stop sector, i.e. A_t, $m_{\tilde{Q}_3}$ and $m_{\tilde{t}_R}$, which are $\overline{\text{DR}}$ parameters according to the SLHA convention need to be converted to on-shell parameters according to Eq. (9.20).

Furthermore, it is interesting to examine the impact of the NMSSM specific corrections and the finite contributions stemming from the $\delta^{(2)}v$ terms, which have been neglected in earlier calculations of the $\alpha_s\alpha_t$ corrections. In order to do so we varied the coupling λ, while at the same time adapting v_s so that μ_{eff} remains constant. For this investigation we chose the on-shell scheme for the top and stop sector. The upper part of Fig. 11.3 shows the difference of the masses obtained if only the MSSM-like $\alpha_s\alpha_t$ contributions are taken into account and the masses obtained if the full NMSSM corrections are included (solid lines). Furthermore, the mass difference between the approximation that neglects the finite $\delta^{(2)}v$ contribution and the full result is plotted (dashed lines). The upper-left panel is for the light Higgs bosons, while the upper-right panel features the heavy Higgs bosons. As a reference the lower panel gives the masses of the Higgs bosons including the full NMSSM corrections as a function of λ. Note, that in these plots we varied λ for illustrative purposes beyond the perturbativity limit, which is given by $\sqrt{\lambda^2+\kappa^2} \lesssim 0.7$ [164], and also consider parameter points that are excluded by the experimental data. While applying the two approximations does not lead to a large difference compared to the full result – the difference is actually below 1 GeV – it does rise with λ. This is to be expected, since $\lambda \to 0$ is the MSSM limit, in which the singlet decouples completely. Hence, the larger λ the larger the NMSSM specific effect. As stated earlier the $\delta^{(2)}v$ terms appearing in the counterterm mass matrix are proportional to λ, and are therefore more important for large values of λ. It is interesting to note that for the CP-odd Higgs bosons the lines for the two approximations lie nearly on top of each other. This implies that for the CP-odd Higgs bosons the most important NMSSM specific contributions actually originate from the $\delta^{(2)}v$ terms. Furthermore, it is peculiar that neglecting the $\delta^{(2)}v$ terms can lead to a result, that is further away from the full result than the result obtained by just including the MSSM corrections is. This is the case for the h_u-like and the h_s-like Higgs bosons in this scenario. Please note, that the peaks in δM_{H_i} at $\lambda \approx 0.475$ are caused by a cross-over in the masses of the h_u-like and h_s-like Higgs bosons. All other cross-overs that occur for this variation of λ are between CP-even and CP-odd Higgs bosons. But since no CP-violating phases were included here the CP-even and CP-odd Higgs bosons do not mix and the cross-overs do not become evident in δM_{H_i}.

Let us finally turn to the impact of the two-loop corrections on the effective couplings. Effective couplings are computed by inserting the higher order mixing matrices into the tree-level

[3] This means if those phases are kept constant the two-loop corrections do not change.

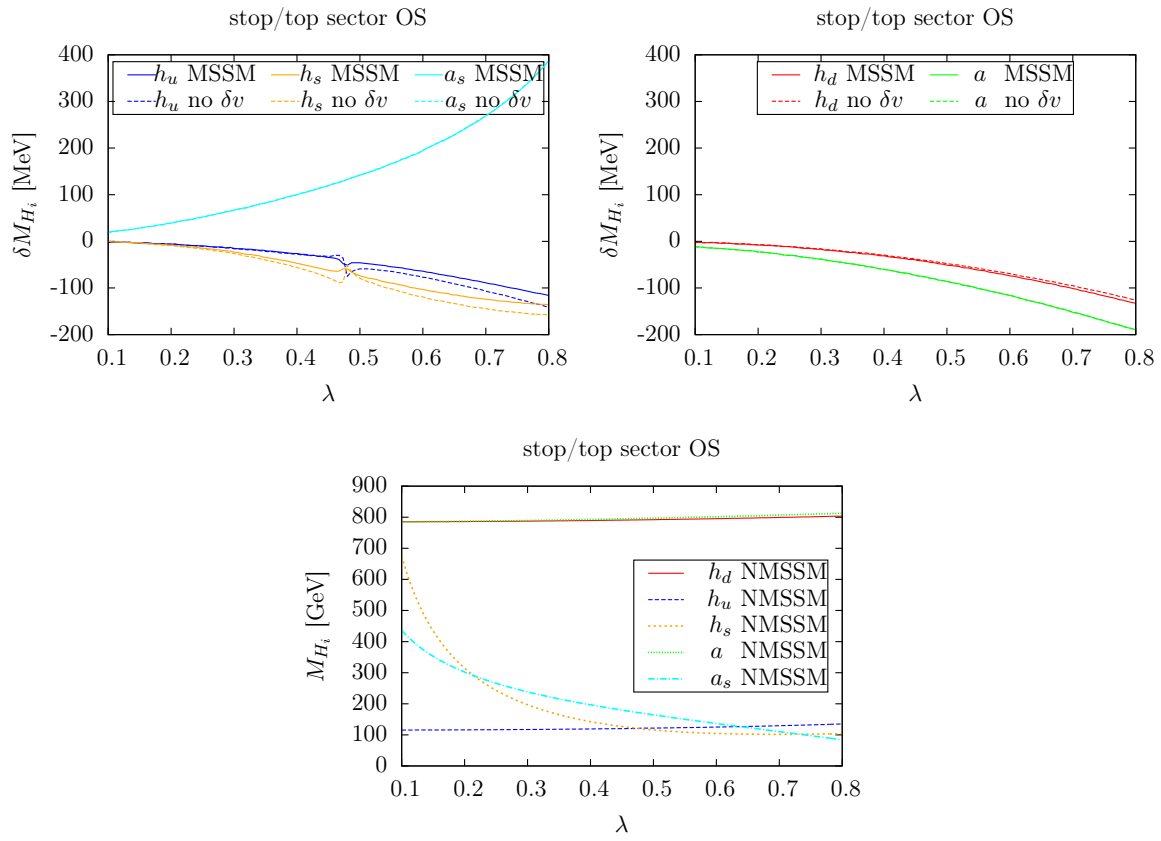

Figure 11.3: Upper Panels: Absolute deviation δM_{H_i} to the full NMSSM result of the Higgs masses obtained (a) if only MSSM-like $\alpha_s\alpha_t$ corrections are included (solid lines) and (b) if the finite contribution of the $\delta^{(2)}v$ term is omitted (dashed line) as a function of λ. The left-hand side shows the deviations for the Higgs bosons which are mainly h_u-like (blue), mainly h_s-like (orange) and mainly a_s-like (cyan). The right-hand side displays δM_{H_i} for the mainly h_d-like (red) and mainly a-like (green) Higgs bosons. Lower Panel: Masses of the Higgs bosons including the full $\alpha_s\alpha_t$ NMSSM corrections as a function of λ. Already published in [7].

couplings. This way it is possible to incorporate some higher order corrections in the couplings. The mixing matrix elements we use here are obtained via the $p^2 = 0$ approximation as described in Sec. 7.2. The coupling of the Higgs boson H_i, which is a mass eigenstate, to massive vector bosons ($V = W, Z$) normalized to the respective SM coupling reads

$$C_V(H_i) = \mathcal{R}_{ih_d} \cos\beta + \mathcal{R}_{ih_u} \sin\beta \,. \tag{11.8}$$

Hence, the coupling to vector bosons depends on the value of $\tan\beta$ and on the admixtures of h_d and h_u to the mass eigenstate. This admixture changes when including the loop corrections. The left-hand side of Fig. 11.4 shows the square of the coupling to vector bosons for the lightest and next-to-lightest Higgs state at one-loop and at two-loop level as a function of A_t. In the top and stop sector $\overline{\text{DR}}$ renormalization was applied. On the right-hand side the relative difference between the one-loop and the two-loop result is plotted

$$\Delta C_V^2 = \frac{(C_V^2)^{(\text{2loop})} - (C_V^2)^{(\text{1loop})}}{(C_V^2)^{(\text{1loop})}} \,. \tag{11.9}$$

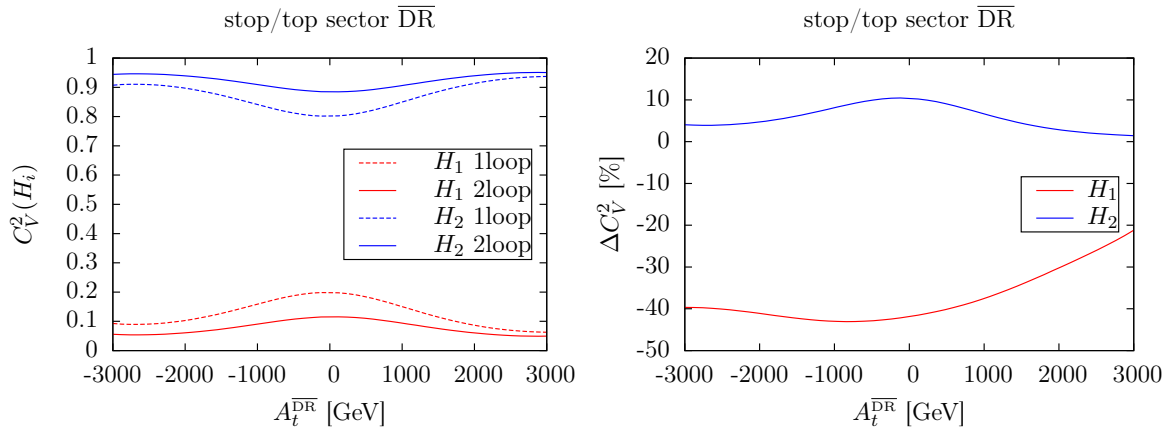

Figure 11.4: Left: Square of the effective coupling to massive vector bosons ($V = W, Z$) normalized to the respective SM coupling for the lightest (red) and the next-to-lightest (blue) Higgs boson at one-loop order (dashed line) and at two-loop order (solid line). Right: Difference between the effective two-loop and one-loop coupling squared to massive vector bosons relative to the one-loop coupling for the lightest (red) and the next-to-lightest (blue) Higgs boson; i.e. $\Delta C_V^2 = [(C_V^2)^{(2\text{loop})} - (C_V^2)^{(1\text{loop})}]/(C_V^2)^{(1\text{loop})}$. Already published in [7].

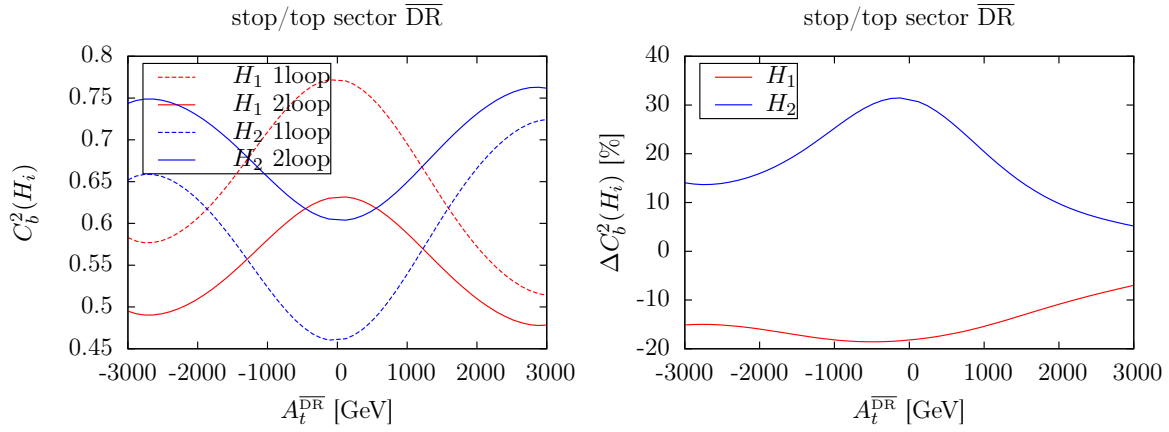

Figure 11.5: Left: Square of the effective coupling to bottom quarks normalized to the respective SM coupling for the lightest (red) and the next-to-lightest (blue) Higgs boson at one-loop order (dashed line) and at two-loop order (solid line). Right: Difference between the effective two-loop and one-loop coupling squared to bottom quarks relative to the one-loop coupling for the lightest (red) and the next-to-lightest (blue) Higgs boson; i.e. $\Delta C_b^2 = [(C_b^2)^{(2\text{loop})} - (C_b^2)^{(1\text{loop})}]/(C_b^2)^{(1\text{loop})}$. Already published in [7].

As was already commented on earlier H_2 displays a coupling close to the SM value in this scenario. The two-loop corrections amount to $5-10\%$ and render the coupling more SM-like. The mass eigenstate H_1 is mainly h_s-like and therefore couples only weakly to vector bosons and the two-loop corrections lower this coupling even further. This effect can be up to 40%.

Figure 11.5 deals with the coupling to bottom quarks, which for a scalar Higgs boson is given by

$$C_b(H_i) = \frac{\mathcal{R}_{ih_d}}{\cos\beta}\,. \tag{11.10}$$

Since the h_d admixtures of the lightest and next-to-lightest Higgs boson are not that different

from each other – for both this is not the main component – their couplings to bottom quarks are of the same order. They range from 0.45 to 0.8. Once again the two-loop corrections render the H_2 coupling more SM-like, while diminishing the coupling of H_1. Also here the relative corrections can be up to 30%.

For the coupling of a scalar Higgs boson to up-type quarks, which is defined as

$$C_u(H_i) = \frac{\mathcal{R}_{ih_u}}{\sin\beta}\,, \tag{11.11}$$

a similar behavior is observed and we refrain from showing them explicitly here. The H_2 coupling is rendered more SM-like due to the two-loop corrections and the corrections can amount to some 40%.

These investigations proof that the inclusion of the $\alpha_s\alpha_t$ corrections is not only important to reduce the theoretical error of the Higgs boson masses, but has also an essential influence on the couplings, which in turn can affect the phenomenological discussions significantly.

Part III

Phenomenological Investigations of the NMSSM Higgs Sector

CHAPTER 12

Introduction to Part III

In July 2012 the two LHC experiments ATLAS and CMS both reported the observation of a new resonance at ~ 125 GeV [1, 2]. Since then a huge effort has been made to pin down the exact properties of this new bosonic particle, such as its spin, its CP quantum number and its couplings. By now it is established that it is most likely a CP-even spin-0 particle, whose mass is determined with a remarkable precision. The current values provided by ATLAS [165] and CMS [4] are

$$\begin{aligned} m_h^{\text{ATLAS}} &= 125.36^{\pm 0.37}(\text{stat})^{\pm 0.18}(\text{syst})\ \text{GeV}\,, \\ m_h^{\text{CMS}} &= 125.02^{+0.26}_{-0.27}(\text{stat})^{+0.14}_{-0.15}(\text{syst})\ \text{GeV}\,. \end{aligned}$$

Recently a combination relying on the data of both experiments in the channels $h \to \gamma\gamma$ and $h \to ZZ \to 4l$ was published [166]

$$m_h^{\text{comb}} = 125.09^{\pm 0.21}(\text{stat})^{\pm 0.11}(\text{syst})\ \text{GeV}\,.$$

The signal strength measurements are in good agreement with the SM expectation. However, the precision is not yet as high as for the mass and there is still some room for physics beyond the SM. But even if the signal strengths are very close to those of the SM, this does not necessarily mean that the observed Higgs boson can only be "the" SM Higgs. BSM models featuring extended Higgs sectors and/or modified couplings can also contain a Higgs boson, which is compatible with the experimental observations. Therefore, we want to analyze the NMSSM in light of the experimental results.

Firstly, it is interesting to investigate how such a 125 GeV Higgs boson can be realized in the NMSSM. To be more precise this means investigating questions like: Which of the three scalar Higgs bosons is the one at 125 GeV? Can the signal maybe be explained by the superposition of two mass degenerate Higgs bosons? What part of the parameter space allows for a 125 GeV Higgs? What are the predicted signal strength values for this Higgs boson? These questions will be addressed in Ch. 13.

Secondly, the inevitable question about the discovery prospects of the other Higgs bosons poses itself. To discuss this we consider the standard search channels, as well as channels

that involve Higgs-to-Higgs decays and can lead to exotic final states. For the latter we present some selected benchmark points. Furthermore, the possibility of making use of coupling sum rules is discussed. This analysis of the discovery prospects of the NMSSM Higgs bosons during the 13 TeV run of the LHC is performed in Ch. 14.

The results presented here are based on three publications [9–11], the last one of which is a general review on BSM physics, where I contributed to the NMSSM part. All presented results are derived from data obtained from two extensive scans over the NMSSM parameter space. Both scans were performed using the program `NMSSMTools` [73–75]. `NMSSMTools` calculates the spectrum and branching ratios in the framework of the real NMSSM. For the spectrum calculation the Higgs mass corrections up to the order $\mathcal{O}(\alpha_s\alpha_t + \alpha_s\alpha_b)$ computed in the effective potential approach are included. The computation of the branching ratios is based on a modified version of the program `HDECAY` [144, 145]. `NMSSMTools` is very convenient for our purposes, since some checks against experimental results are already included, for example among other things the exclusion bounds on the Higgs mass as supplied by LEP and Tevatron and some B-physics observables. Furthermore, a link to `micrOMEGAS` [167] allows the computation of the relic density.

The two scans were performed under different objectives. For the first one, to which we will refer from now on as Scan A, we were mainly interested in discussing the possibility of a 125 GeV scalar Higgs boson within the NMSSM. While Scan B only shortly investigates the 125 GeV NMSSM Higgs boson itself, but otherwise focuses on the discovery prospects of the other Higgs bosons. Due to these different points of view, we performed a grid scan for Scan A, while the results of Scan B have been obtained from a random scan. A grid scan seemed more appropriate to systematically raster the investigated parameter space. However, due to the many parameters in the NMSSM we had to restrict ourselves to a small part of this parameter space and could only use rough steps. In contrast to this the random scan makes scanning larger parameter ranges feasible. We should also remark that the scans are separated by roughly two years. Hence, they are based on different experimental constraints and signal strength measurements. Scan B includes nearly the full set of 7 and 8 TeV data, whereas Scan A is based on the full set of 7 TeV data, but includes only part of the 8 TeV data. In the following the set-up of the two scans – i.e. chosen parameter ranges, applied conditions and such – will be described in detail.

12.1 Set-up Parameter Scan A

Parameter Scan A was performed as a grid scan and the results were presented in [9]. For a parameter point to be accepted we demanded:

1. the presence of a CP-even Higgs boson (from here on denoted as h) within the mass range $124\ \text{GeV} \leq m_h \leq 127\ \text{GeV}$;
2. the signal rate of this Higgs boson in the final state $\gamma\gamma$ should be at least 80% of the SM value; i.e. $\mu_{\gamma\gamma}(h) \geq 0.8$;
3. the other Higgs bosons (i.e. $H_i \neq h$) are not excluded by the experimental results of LEP, Tevatron and LHC; the LHC exclusion bounds that were available at the time of our analysis and which we implemented in `NMSSMTools` are [168–177].

The motivations for the first and the last condition are obvious, however the second condition might require some explanation. At the time of the analysis the signal strength measurements

Experiment	Final state	$(\sqrt{s},\ \mathrm{L})$	$\mu = \sigma/\sigma_{\mathrm{SM}}$
ATLAS	$\gamma\gamma$	(7 TeV, 4.8 fb^{-1})+(8 TeV, 5.9 fb^{-1})	1.8 ± 0.5 [168]
	WW	(8 TeV, 13 fb^{-1})	1.5 ± 0.6 [169]
	ZZ	(7 TeV, 4.8 fb^{-1})+(8 TeV, 5.8 fb^{-1})	1.4 ± 0.6 [170]
	bb	(7 TeV, 4.7 fb^{-1})+(8 TeV, 13 fb^{-1})	-0.4 ± 1.1 [171]
	$\tau\tau$	(7 TeV, 4.6 fb^{-1})+(8 TeV, 13 fb^{-1})	0.7 ± 0.7 [172]
CMS	$\gamma\gamma$	(7 TeV, 5.1 fb^{-1})+(8 TeV, 5.3 fb^{-1})	1.56 ± 0.43 [173]
	WW	(7 TeV, 4.9 fb^{-1})+(8 TeV, 12.1 fb^{-1})	0.74 ± 0.25 [174]
	ZZ	(7 TeV, 5.1 fb^{-1})+(8 TeV, 12.2 fb^{-1})	$0.8^{+0.35}_{-0.28}$ [175]
	bb	(7 TeV, 5 fb^{-1})+(8 TeV, 12 fb^{-1})	$1.3^{+0.7}_{-0.6}$ [176]
	$\tau\tau$	(7 TeV+8 TeV, 17 fb^{-1})	0.72 ± 0.52 [177]

Table 12.1: Best fit values for the signals rates and 1σ errors as reported by ATLAS and CMS at the end of 2012, when we performed the analysis of Scan A.

had not reached the level of precision they currently[1] have, but were still very vague. However, both experiments reported an enhanced signal in the $\gamma\gamma$ channel (see Tab. 12.1). Therefore, we aimed at presenting scenarios featuring a sizeable signal in the $\gamma\gamma$ channel. We did not pose any constraints on the signal strength values of the other search channels.

The input parameters of the Higgs sector and the soft SUSY breaking parameters of the other sectors are considered to be $\overline{\mathrm{DR}}$ parameters at the input scale $M_{\mathrm{input}} = 1$ TeV, with the exception of $\tan\beta$ which is given at the scale M_Z. For the parameters of the Higgs sector we scanned over the following parameter ranges,

$$\begin{aligned} \tan\beta = 2 \text{ and } 4\,, \quad 0.55 \leq \lambda \leq 0.8\,, \quad 10^{-4} \leq \kappa \leq 0.4\,, \\ -500 \text{ GeV} \leq A_\kappa \leq 0 \text{ GeV}\,, \quad 200 \text{ GeV} \leq A_\lambda \leq 800 \text{ GeV}\,, \quad 100 \text{ GeV} \leq \mu_{\mathrm{eff}} \leq 200 \text{ GeV}\,. \end{aligned} \tag{12.1}$$

For $\tan\beta$ we chose two discrete rather low values[2], while the values for λ are rather large. This combination has the advantage that it maximizes the tree-level mass of the lightest non-singlet-like scalar Higgs boson (see Eq. (3.6)), and thereby reduces fine-tuning. Fine-tuning considerations also lead to the upper bound on μ_{eff}, whereas the lower bound is motivated by exclusion bounds on the lightest chargino mass. If one wants to ensure perturbativity of both λ and κ up to the GUT scale, this leads to an upper bound on the parameters at the input scale of 1 TeV. These constraints can be derived from the two-loop renormalization group running and depend in addition to the values of κ and λ also on the value of $\tan\beta$ [164]. The inclusion of exotic extra matter at the TeV scale can relax these bounds a bit. In the search for valid scenarios these bounds on κ and λ were not enforced. But we will discuss later how many of the valid scenarios actually respect these bounds. The trilinear soft SUSY breaking couplings A_λ and A_κ were varied in ranges that typically lead to valid scenarios as we knew from experience. The obtained results validate these ranges also in hindsight.

[1] spring 2015

[2] Please note, that in the discussion later on we will only show explicit results for $\tan\beta = 2$. The results for $\tan\beta = 4$ are rather similar.

channel	best fit value	$2 \times 1\sigma$ error
$VH \to Vbb$	0.97	± 1.06
$H \to \tau\tau$	1.02	± 0.7
$H \to \gamma\gamma$	1.14	± 0.4
$H \to WW$	0.78	± 0.34
$H \to ZZ$	1.11	± 0.46

Table 12.2: Combination of the best fit values for the signal strength values and errors reported by ATLAS and CMS [186, 187] at the time of the analysis of Scan B. Combination performed according to Eq. (5) of [188].

For the trilinear soft SUSY breaking parameters of the sfermion sector we chose discrete values,

$$A_U = 0 \text{ and } 1 \text{ TeV}\,, \quad A_D = A_E = 1 \text{ TeV}\,. \tag{12.2}$$

In the analysis later on, we will restrict ourselves mostly to the case of A_U=1 TeV. For the respective plots for $A_U = 0$ the reader is referred to [9]. At the time of the analysis the exclusion bounds for the SUSY particles were not very strict yet [178–180]. We conservatively set the soft SUSY breaking masses of the first and second generation to 2.5 TeV.

$$m_{\tilde{u}_R} = m_{\tilde{c}_R} = m_{\tilde{D}_R} = m_{\tilde{Q}_{1,2}} = m_{\tilde{e}_R} = m_{\tilde{\mu}_R} = m_{\tilde{L}_{1,2}} = 2.5 \text{ TeV} \tag{12.3}$$

For the soft SUSY breaking masses of the stop and stau sectors we chose in accordance with the experimental results [151, 152, 181–185]

$$500 \text{ GeV} \leq m_{\tilde{Q}_3} = m_{\tilde{t}_R} \leq 800 \text{ GeV}\,, \quad m_{\tilde{\tau}_R} = m_{\tilde{L}_3} = 300 \text{ GeV}\,. \tag{12.4}$$

The choice of the parameters of the stop sector results in relatively light stop masses and therefore low fine-tuning. Finally, the soft SUSY breaking masses of the gauginos have been set to

$$M_1 = 150 \text{ GeV}\,, \quad M_2 = 300 \text{ GeV}\,, \quad M_3 = 1 \text{ TeV}\,. \tag{12.5}$$

The influence of M_1 and M_2 on the Higgs masses is marginal. Therefore, we decided to keep them fixed. However, they strongly influence the relic density. Keeping this in mind, it does not make sense to demand that our scenarios reproduce the correct relic density. As this could simply be achieved by tuning M_1 and M_2, which essentially leads to a scenario that still displays the same features in the Higgs sector, but at the same time yields the correct relic density.

12.2 Set-up Parameter Scan B

This random scan aimed at exploring larger ranges for the input parameters and the results were presented in [10]. All points that do not fulfill the following criteria were discarded:

1. at least one CP-even Higgs boson within the mass range $124 \text{ GeV} \leq m_h \leq 127 \text{ GeV}$;
2. signal rates of this Higgs boson are compatible with the experimental observations (see Tab. 12.2), i.e. deviate less than two times the 1σ error[3]:
   $|\mu_{XX}^{\text{scan}}(h) - \mu_{XX}^{\text{exp}}| \leq 2 \times 1\sigma$ with $X = b, \tau, \gamma, W, Z$;

[3] Restricting the allowed range to the 1σ error seemed too strict, as then not even the SM itself would fulfill this criterion. Since the experiments typically do not report the 2σ error, we chose two times the 1σ error as our allowed range.

3. the other Higgs bosons (i.e. $H_i \neq h$ and A_j) are still allowed according to the exclusion bounds provided by LEP, Tevatron and LHC; in addition to the LHC bounds already included for Scan A [168–177] the following analyses were taken into account [189–198] ;
4. the predicted relic density $\Omega_c h^2$ is smaller than the result reported by Planck [27][4] ,

Although the precision of the experimentally measured Higgs mass has of course increased, we did not narrow the mass interval, in which we demand a CP-even Higgs boson. This is sensible since the typically quoted error for the theoretical prediction of the Higgs mass is ~ 3 GeV.

For the parameters of the Higgs sector we chose the following parameter ranges,

$$\begin{aligned} 1 \leq \tan\beta \leq 30\,, \qquad & 0 \leq \lambda \leq 0.7\,, \qquad & -0.7 \leq \kappa \leq 0.7\,, \\ -2 \text{ TeV} \leq A_\kappa \leq 2 \text{ TeV}\,, \qquad & -2 \text{ TeV} \leq A_\lambda \leq 2 \text{ TeV}\,, \qquad & -1 \text{ TeV} \leq \mu_{\text{eff}} \leq 1 \text{ TeV}\,. \end{aligned} \tag{12.6}$$

To ensure perturbativity of λ and κ up to the GUT scale we conservatively discarded points with $\sqrt{\lambda^2 + \kappa^2} \geq 0.7$. The trilinear soft SUSY breaking couplings were varied independently in the range,

$$-2 \text{ TeV} \leq A_U, A_D, A_E \leq 2 \text{ TeV}\,. \tag{12.7}$$

The soft SUSY breaking masses of the first two generations and the soft SUSY breaking mass of the right-handed sbottom were set to fixed values,

$$m_{\tilde{u}_R} = m_{\tilde{c}_R} = m_{\tilde{D}_R} = m_{\tilde{Q}_{1,2}} = m_{\tilde{e}_R} = m_{\tilde{\mu}_R} = 3 \text{ TeV}\,, \tag{12.8}$$

while we included some variation for the other soft SUSY breaking masses of the third generation,

$$600 \text{ GeV} \leq m_{\tilde{Q}_3} = m_{\tilde{t}_R}, m_{\tilde{L}_3} = m_{\tilde{\tau}_R} \leq 3 \text{ TeV}\,. \tag{12.9}$$

Note, that the soft SUSY breaking masses of the stop sector are not varied independently but are always set to the same value. The same applies to the soft SUSY breaking masses of the stau sector. Finally, the soft SUSY breaking masses of the gauginos are chosen as

$$100 \text{ GeV} \leq M_1 \leq 1 \text{ TeV}\,, \quad 200 \text{ GeV} \leq M_2 \leq 1 \text{ TeV}\,, \quad 1.3 \text{ TeV} \leq M_3 \leq 3 \text{ TeV}\,. \tag{12.10}$$

[4] Imposing this condition does not necessarily mean discarding the idea of SUSY as a solution to the dark matter problem. In fact, the argument given at the very end of the previous section, still applies, i.e. by tuning of M_1 and M_2 we can generate a scenario with the correct relic density that in the Higgs sector still displays the main features of the original scenario.

CHAPTER 13

A 125 GeV Higgs Boson in the NMSSM

This chapter concentrates on the properties of the 125 GeV Higgs boson within the NMSSM. The discussion of the properties of the other Higgs bosons is deferred to Ch. 14. After investigating in which parameter subspace phenomenologically valid scenarios are typically realized, we present the signal strength values these scenarios feature at 8 TeV and analyze whether there exist correlations between the different final states. Furthermore, we discuss how an enhanced signal in the two photon final state can arise.

13.1 Distribution of Valid Scenarios in the Parameter Space

The majority of scenarios obtained from Scan A features the next-to-lightest CP-even Higgs boson as the one with a mass of 125 GeV, but scenarios with M_{H_1} in the required mass range also exist. In Scan B, which probed a larger part of the parameter space, this picture was reversed. Here the majority of points was for $h = H_1$ (as before h denotes the Higgs boson in the mass range $124 - 127$ GeV), while there were only a few with $h = H_2$. To understand this feature let us first have a closer look at the distribution of the valid parameter points of Scan A in the λ-κ plane.

Figure 13.1 shows this distribution for $A_t = 0$ TeV (upper row) and $A_t = 1$ TeV (lower row) and $\tan\beta = 2$. The plots on the left-hand side are for $h = H_1$, while on the right-hand side $h = H_2$. The color code indicates the total number of points in each bin[1]. Comparing the plots for the same A_t value with each other, it becomes evident that $h = H_1$ generally requires slightly larger values of λ and considerably larger values of κ than $h = H_2$. This can be understood by recalling that κ was introduced as the dimensionless coupling in front of the term cubic in the singlet field in the superpotential. Thus κ mainly influences the mass of the Higgs boson with the largest singlet component[2], whereas all other Higgs masses are insensitive to κ. In fact, the tree-level mass of the CP-even singlet-like Higgs state is

[1] The bin size reflects the step size used to raster the parameter intervals.
[2] It usually grows with increasing κ.

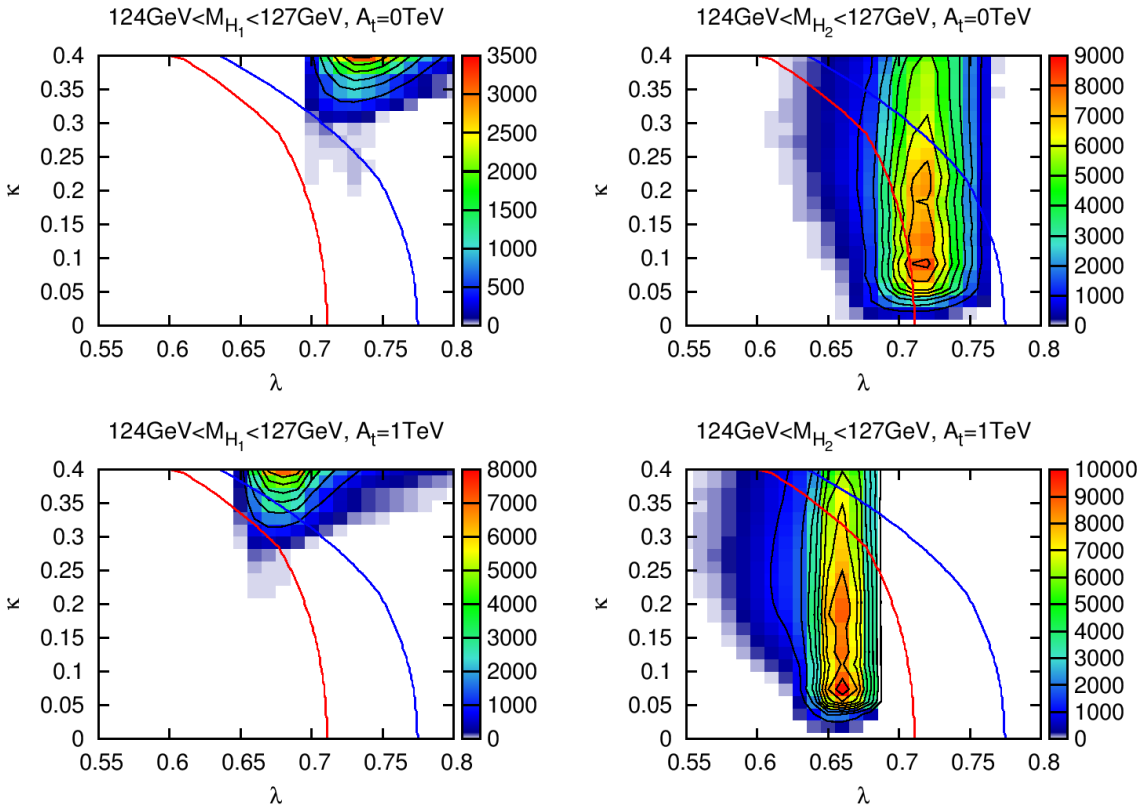

Figure 13.1: Distribution of the allowed parameter points in the λ-κ plane. The color code indicates the number of points. The upper row displays the distributions for $A_t = 0$ TeV, while the lower row is for $A_t = 1$ TeV. In the plots on the left-hand side H_1 is the 125 GeV Higgs boson, while on the right-hand side H_2 takes on this role. The red/blue line indicates the perturbativity bound without/with extra matter at the 1 TeV scale. Based on data of Scan A [9].

approximately set by $\kappa\mu_{\text{eff}}/\lambda$. In the parameter space we chose for Scan A this yields a mass that is lighter than 125 GeV, which results in H_1 being mostly singlet-like, whereas $h = H_2$. Only for κ values at the upper bound of the considered interval scenarios with $h = H_1$ are realized. Please note, that we always expect either the lightest or next-to-lightest CP-even Higgs boson to be singlet-like, because these are usually in the mass ranges probed by the collider experiments. If both H_1 and H_2 were MSSM-like, the scenario would likely be excluded by the experiments. However, the couplings of a singlet-dominated Higgs boson are reduced compared to the SM values and it can thus evade the exclusion bounds. Comparing the plots for the different values of A_t reveals, that $A_t = 1$ TeV seems to require smaller values of λ than $A_t = 0$ TeV. This is to be expected, since a higher value of λ in general means a higher tree-level mass for the h-like Higgs boson. Hence, the radiative corrections necessary to reach the 125 GeV are smaller. The contributions from stops to the radiative corrections are important and proportional to the stop mixing, which is controlled by A_t. So the smaller A_t is, the smaller are the radiative corrections stemming from the stop sector, and therefore larger values of λ are favored, because these lead to a larger tree-level mass. The red line in Fig. 13.1 indicates the upper bound on λ and κ originating from perturbativity requirements. Assuming extra exotic matter at the TeV scale leads to the more relaxed blue bound. For $h = H_1$ it is very difficult to find scenarios in this parameter subspace which respect the perturbativity bound. Furthermore, it can be said that the lower the A_t value is, the more

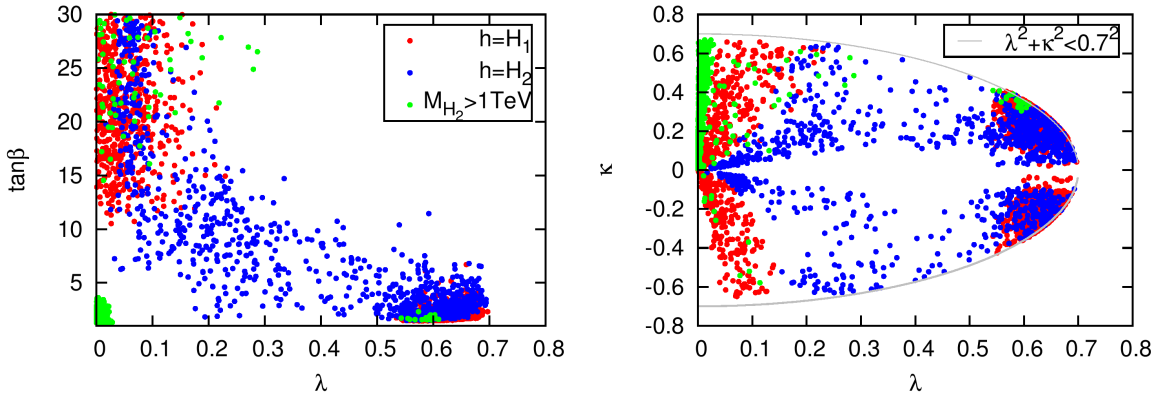

Figure 13.2: Distribution of allowed parameter points in the λ-tanβ (left) and λ-κ plane (right). Red and green points are for $h = H_1$, but the green points feature a very high mass for H_2. Blue points are for $h = H_2$. Based on data of Scan B [10].

difficult it gets to respect the perturbativity bound. For scenarios with tan$\beta = 4$ (plots not shown here) the situation is even worse, since the higher tanβ value generally requires larger values of λ in order to maximize the tree-level mass.

To disentangle the situation in Scan B it is necessary to analyze the distribution in the λ-tanβ plane as well. This distribution together with the distribution in the λ-κ plane is shown in Fig. 13.2. We observe two main regions in the λ-tanβ plane: one around small values of tanβ ($\sim 1-5$) and large values of λ ($\sim 0.5-0.7$), and one around a wide range of large tanβ values ($\sim 10-30$) and small λ values (< 0.1). In between there are only a few scattered points. For Scan A we were in the first region. Due to the large λ values these parameter points display an NMSSM specific phenomenology, because they allow for significant doublet-singlet mixing. In the region with low λ values the doublet-singlet mixing is very small, leading to scenarios in which the singlet mostly decouples. Therefore, these scenarios are phenomenologically similar to the MSSM. This in mind it is not surprising to find that those scenarios require large tanβ values, just like the MSSM. In both regions either H_1 or H_2 can be the 125 GeV Higgs boson. For small λ values the majority of points features the lightest Higgs boson as the 125 GeV Higgs. This becomes even more obvious in the λ-κ plane (right side of Fig. 13.2). The next-to-lightest CP-even Higgs as the 125 GeV one, is for small values of λ only realized if also κ is small. The peculiar shape in the λ-κ plane is due to the fact, that we imposed the condition $\sqrt{\lambda^2 + \kappa^2} < 0.7$ as a conservative constraint to ensure perturbativity of λ and κ up to the GUT scale. At this point we should explain the green points. These are parameter points where the mass of the next-to-lightest scalar Higgs boson is larger than 1 TeV. Detailed investigations revealed that nearly all of such points are highly fine-tuned in the sense, that changing any input parameter just a tiny bit changes the resulting mass spectrum considerably. This instability occurs for small values of λ and is caused by the way we fix the input parameters. Recall that instead of setting v_s, we chose to fix $\mu_{\text{eff}} = \lambda v_s/\sqrt{2}$. So very small λ values lead to large values of v_s. As long as v_s appears in combination with λ this has no effect. However, there are terms proportional to κv_s, which then grow very large. For the discussion of the predicted signal strength values we discarded these fine-tuned points.

In addition to the distribution in the parameter planes, it is also useful to analyze, which parameter intervals are favored. Figure 13.3 shows how the phenomenologically valid scenarios of Scan B are distributed over the parameter ranges of tanβ, λ, κ and A_t. The distributions

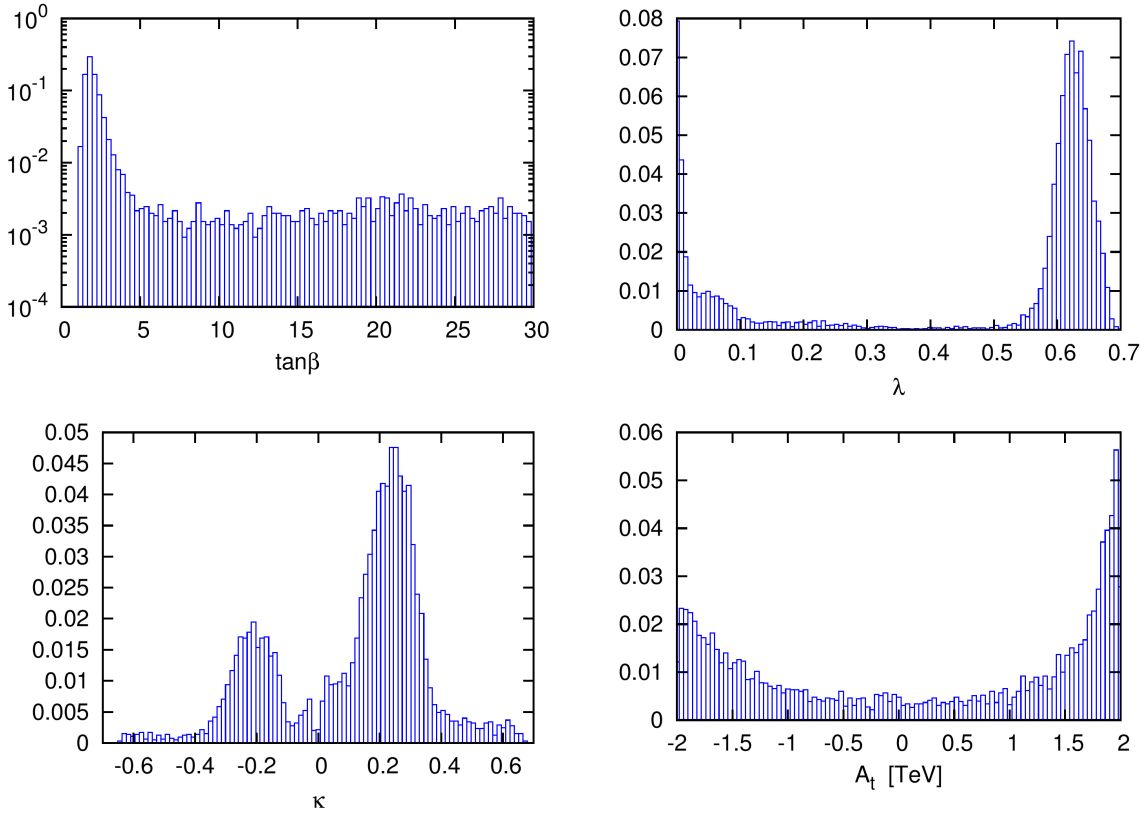

Figure 13.3: Distributions of the tanβ (upper left), λ (upper right), κ (lower left) and A_t (lower right) values normalized to the total number of valid parameter points. Based on data of Scan B [10].

for tanβ and λ prove nicely that our choice for the parameter ranges in Scan A was well motivated. Small values of tanβ are clearly favored (please note, that the plot for tanβ is logarithmically on the y-axis). The distribution among the higher values of tanβ is more or less homogenous. For λ there are two peaks, corresponding to the regions mentioned earlier when discussing the correlations between the parameters. The majority of points is clustered in the region of large λ values ($0.55 < \lambda < 0.7$). The scan yielded the most scenarios for absolute values of κ of around ~ 0.25 and the positive values dominated over negative ones. In the distribution for A_t we see a clear rise for larger values of A_t, i.e. large mixing in the stop sector is favored. This entails larger radiative mass corrections, which might be necessary to achieve a mass of 125 GeV, but can also result in large fine-tuning.

Finally, after discussing the distributions for the individual scans, we can explain why Scan A yielded more valid scenarios for $h = H_2$, whereas Scan B lead to scenarios, of which the majority features $h = H_1$. Of course, this cannot be attributed to one single fact, but is an interplay of several influences. First of all, in Scan B we chose a considerably wider range for μ_{eff} and larger absolute values of μ_{eff} lead to a larger mass for the mass eigenstate with a large singlet admixture. The singlet-like scalar Higgs boson is then heavier than 125 GeV and the lightest scalar Higgs boson takes on the role of the 125 GeV Higgs (i.e. $H_1 = h$). Second, in Scan B we also included large tanβ values and small λ values, which favors $h = H_1$. Furthermore, the larger mixing in the stop sector, which leads to larger radiative corrections, is also a factor that makes it easier to realize scenarios with $h = H_1$.

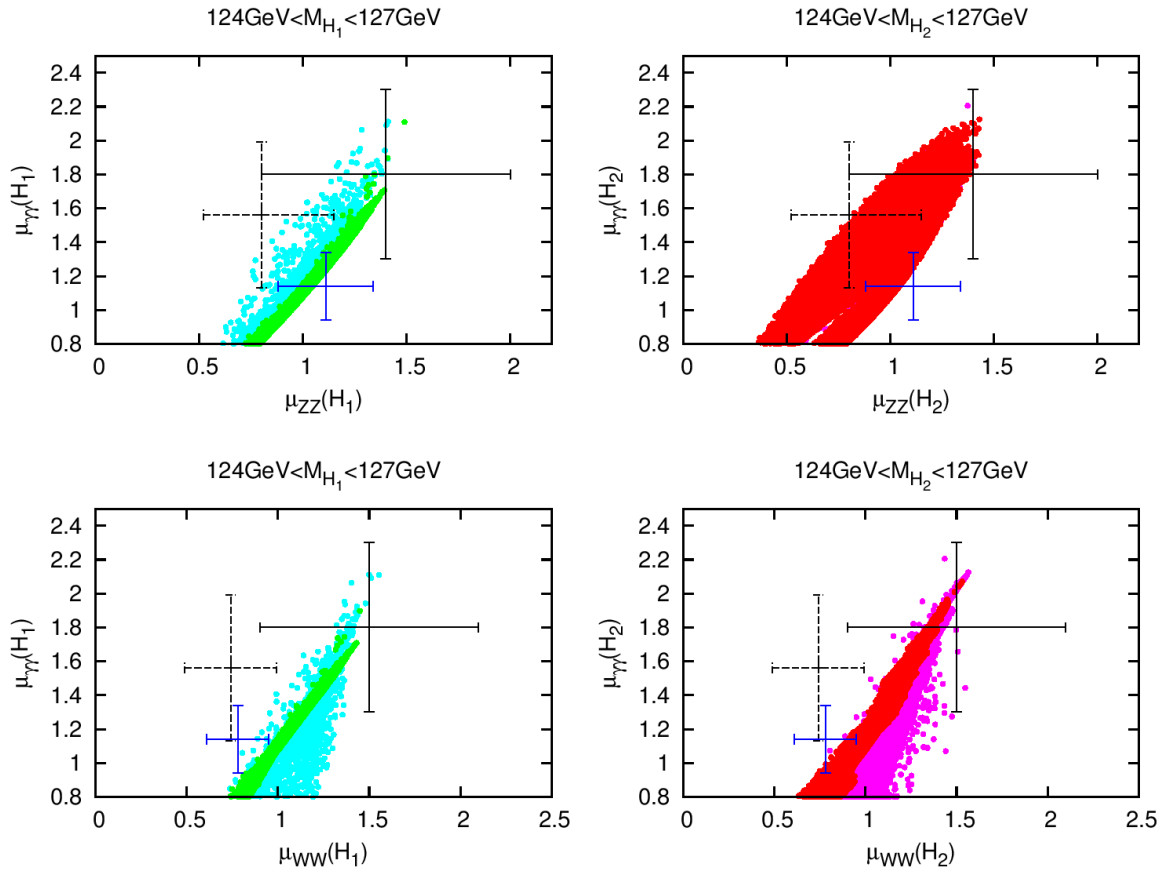

Figure 13.4: Predicted signal strength values for the $\gamma\gamma$ final state versus the signal strength values for the ZZ (upper panels) and WW (lower panels) final states for all valid scenarios with $\tan\beta = 2$ and $A_t = 1$ TeV both for $h = H_1$ (left) and $h = H_2$ (right). Cyan and pink points indicate the points where signals of Higgs bosons close in mass overlap and the resulting combined signal strength value deviates by more than 10% from the signal of the individual Higgs boson. For the green and red points the signal superposition does not play a role. Experimental best fit values and errors are indicated by a black solid cross (ATLAS), by a black dashed cross (CMS) and by a blue cross (more up-to-date combined value). Based on data of Scan A [9].

13.2 Correlations Between the Signal Strength Values

In this section we discuss the signal strength values as predicted for the scalar Higgs boson at 125 GeV in the NMSSM. All results presented here are based on the data of Scan A [9]. The given signal strength values are calculated at 8 TeV using the inclusive cross section. The possible superposition of signals of Higgs bosons, which are close in mass, is taken into account as well. The procedures used to calculate the different ingredients are described in detail in Ch. 5. It is interesting to not only study the predictions of the signal strength values for the individual channels but also whether there is a correlation between the different channels.

Figures 13.4 and 13.5 investigate the correlations of the $\mu_{\gamma\gamma}$ value with the μ-values of the final states ZZ, WW, bb and $\tau\tau$. The plots on the left-hand side include all valid parameter points with $A_t = 1$ TeV and $\tan\beta = 2$ for which $h = H_1$, while the plots on the right-hand side are for $h = H_2$. The color code signifies whether at least one of the μ-values after superposition,

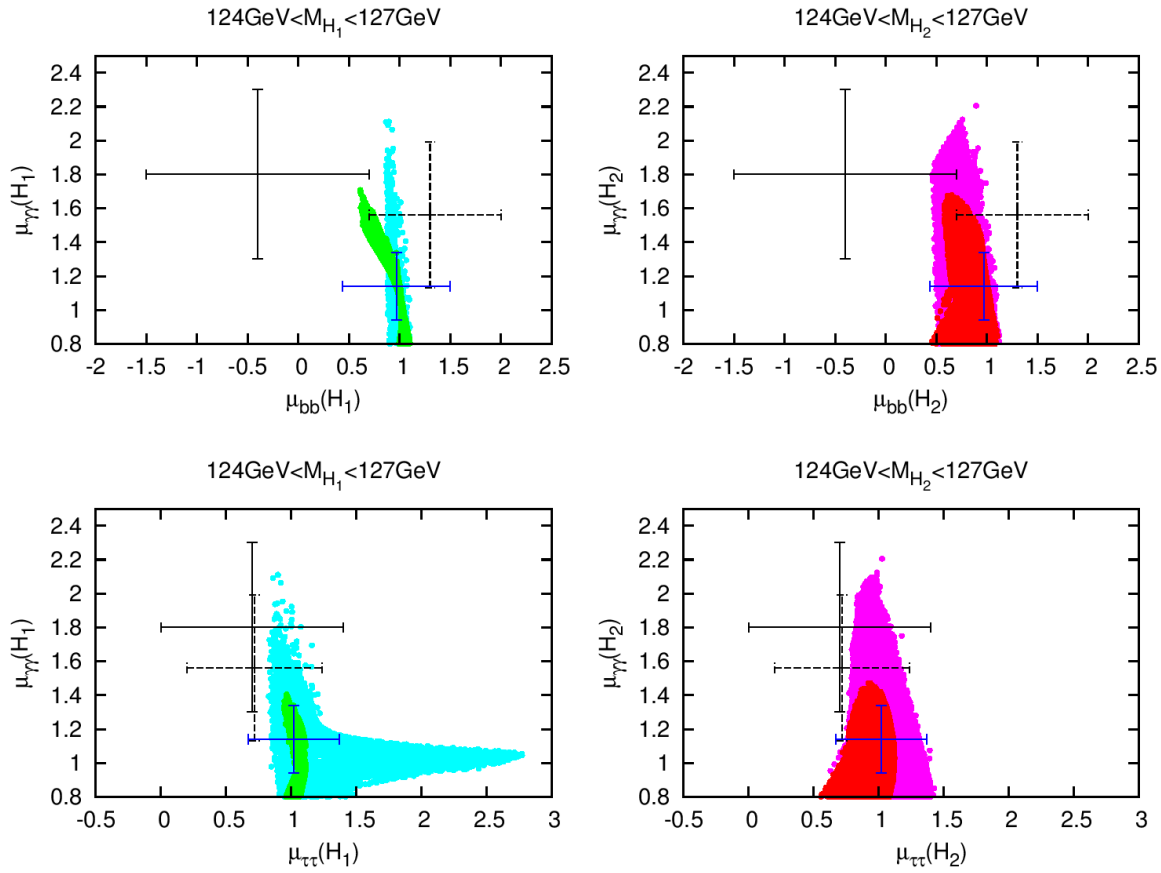

Figure 13.5: Predicted signal strength values for the $\gamma\gamma$ final state versus the signal strength values for the bb (upper panels) and $\tau\tau$ (lower panels) final states for all valid scenarios with $\tan\beta = 2$ and $A_t = 1$ TeV both for $h = H_1$ (left) and $h = H_2$ (right). Cyan and pink points indicate the points where signals of Higgs bosons close in mass overlap and the resulting combined signal strength value deviates by more than 10% from the signal of the individual Higgs boson. For the green and red points the signal superposition does not play a role. Experimental best fit values and errors are indicated by a black solid cross (ATLAS), by a black dashed cross (CMS) and by a blue cross (more up-to-date combined value). Based on data of Scan A [9].

i.e either $\mu_{\gamma\gamma}$ or that on the x-axis, deviates by more than 10% from the μ-value, that takes only the signal strength of the 125 GeV Higgs boson itself into account. The crosses and error bars indicate the experimental best fit values and the respective 1σ errors as reported at the time of Scan A by ATLAS (full, black) and CMS (dashed, black) and the combined values we used in Scan B (blue)[3].

We see a correlation between $\mu_{\gamma\gamma}$ and the μ-values of the bosonic final states, i.e. ZZ (Fig. 13.4, upper panels) and WW (Fig. 13.4, lower panels), whereas there is no such correlation for the fermionic final states, i.e. bb (Fig. 13.5, upper panels) and $\tau\tau$ (Fig. 13.5, lower panels). This behavior can be understood by investigating the origin of the enhancement in the $\gamma\gamma$ rate, which can be up to ~ 2.4. For now let us defer the detailed discussion to the next section and just use the outcome, which is the observation that the enhancement in the $\gamma\gamma$ rate is mainly due to a suppression of the coupling to bottom quarks. This reduced coupling to bottom quarks leads to a smaller total width, which in turn leads to an enhanced branching

[3] for exact values see Tab. 12.1 and Tab. 12.2.

ratio into $\gamma\gamma$. The same argument also applies to the other bosonic final states. However, for the fermionic final states the diminished coupling to bottom quarks does not only affect the total width, but also leads to a suppressed partial decay width, which compensates the reduced total width. Therefore, there is no correlation between the predicted signal strength values of the fermionic and bosonic final states whereas there is some correlation between the different bosonic final states.

Naively one would expect that the signal strength values for the WW and ZZ final states are equal, because the couplings of the Higgs boson to WW and ZZ are modified by the same factor compared to the respective SM couplings (see Eq. (5.2)). Since all the other ratios appearing in μ (see Eq. (5.4)), namely the ratios of the total widths and the production cross sections, are also the same for the ZZ and WW final states, the μ-values as calculated for each individual Higgs boson are indeed the same for the two final states. However, the mass resolution of the ZZ channel is far better than that of the WW channel. Therefore, taking into account the superposition of Higgs signals, the combined μ-values for the two final states are not the same. In the fermionic final states, to which the same argument applies, since there is a universal reduced coupling for all down-type fermions, this behavior is even more pronounced. The superposition of signals leads to the "nose" in the $\mu_{\tau\tau}(H_1)$, whereas there is no such structure in $\mu_{bb}(H_1)$, due to the better mass resolution. The fact that the superposition is more important for the $\tau\tau$ and bb finals states than for the WW and ZZ final states can be traced back to the distribution of the coupling to vector bosons among the NMSSM Higgs bosons. Coupling sum rules require the reduced couplings to the massive vector bosons of all scalar Higgs bosons to add up to one. By requiring $\mu_{\gamma\gamma}(h) > 0.8$ we favor scenarios with a large h_u component in the 125 GeV Higgs boson, since this coupling is important to achieve a large production cross section in gluon fusion. For the small $\tan\beta = 2$ we chose here, a large h_u admixture maximizes the coupling to massive vector bosons. This leads to rather small couplings to massive vector bosons for the other Higgs bosons, which in turn means that their signals in the ZZ and WW channels are small as well. Since the 125 GeV Higgs boson is mainly h_u-like, it has only a small h_d admixture. Another Higgs boson close in mass can therefore easily produce a signal of equal size in the $\tau\tau$ and bb final states. In general, we observe that the superposition of signals has a significant effect. As the resolution at the experiments increases, the superposition of signals will lose in importance. However, for studies of this early data it has to be taken into account to obtain a realistic picture.

13.2.1 Enhanced Signal in the $\gamma\gamma$ Final State

When the ATLAS and CMS experiments both reported enhanced signals in the $\gamma\gamma$ rate this triggered a lot of investigations of how such an enhanced rate could be realized in different BSM models (see for example [199–207][4]). Of course this observed enhancement was not significant and although by now with more data available the enhancement has nearly vanished and the reported value is very close to the SM, we would like to discuss the mechanisms that lead to an enhancement in the NMSSM. To investigate the origin of the enhancement, the left-hand side of Fig. 13.6 shows the branching ratio of the 125 GeV Higgs boson into $\gamma\gamma$ versus the inclusive production cross section. Both quantities are normalized to the respective SM values. For the subset of scenarios we selected here, i.e. $h = H_2$, $\tan\beta = 2$ and $A_t = 1$ TeV, the enhancement originates only from an enhanced branching ratio, which

[4]This is by far not an exhaustive list.

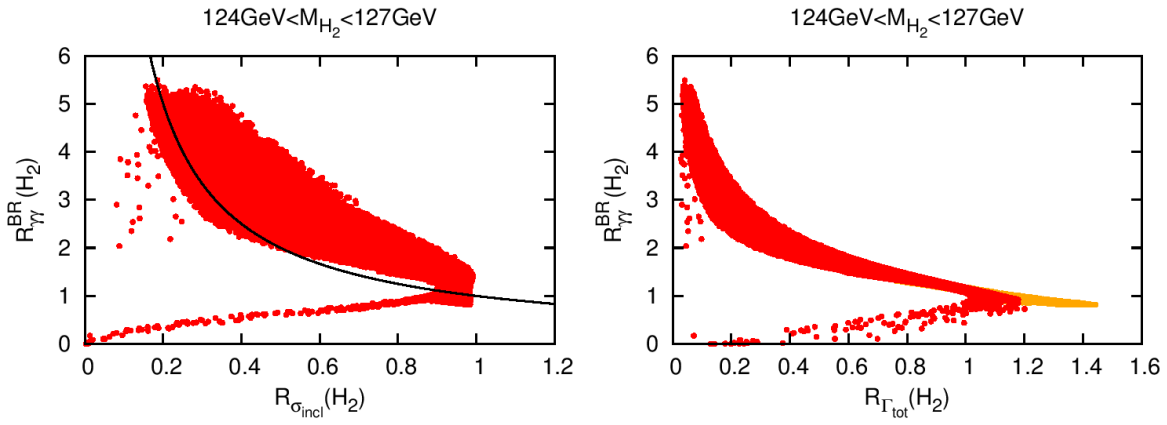

Figure 13.6: Left: Branching ratio of h into $\gamma\gamma$ normalized to the SM versus the inclusive production cross section normalized to the SM. All scenarios above the black line feature an enhanced $\mu_{\gamma\gamma}$ value. Right: Branching ratio into $\gamma\gamma$ normalized to the SM versus the total width normalized to the SM. Orange points indicate scenarios, in which decays into non-SM particles occur. Both plots are for scenarios with $h = H_2$, $\tan\beta = 2$ and $A_t = 1$ TeV. Based on data of Scan A [9].

can be up to 5.5 times the SM value, but not from an enhanced production cross section. However, we should remark that in principle the NMSSM can also yield an enhancement in the production cross section. We observed this for $A_t = 0$. But in general the enhancement in the branching ratio is more common. As can be inferred from the right-hand side plot of Fig. 13.6, the enhancement of the branching ratio is caused by a suppression of the total width. This suppression in turn is created by a suppressed coupling to bottom quarks. As the orange points indicate there are also scenarios, which allow for decays into non-SM particles[5]. However, the presence of non-SM decays increases the total width and therefore does not lead to an enhanced branching ratio into $\gamma\gamma$. Finally, let us remark on the tail for small $R^{\mathrm{BR}}_{\gamma\gamma}$ values, which is present in both plots. It is obvious that these points do not reproduce the demanded $\mu_{\gamma\gamma} > 0.8$ signal on their own. Nevertheless, these points pass the constraints because another Higgs boson with a large signal in the $\gamma\gamma$ channel is sufficiently close in mass.

[5]This could for example be a decay into a pair of lighter Higgs bosons or into a pair of neutralinos.

CHAPTER 14

Discovery Prospects of the NMSSM Higgs Bosons During the LHC Run at 13 TeV

This chapter deals with the predictions for the other Higgs bosons in the scenarios delivered by the two scans that feature a scalar Higgs boson with a mass of 125 GeV. After discussing the masses and admixtures of these Higgs bosons, we investigate the signals in standard search channels at 13 TeV. Here "standard search channels" refers to direct production of the Higgs bosons in different production modes with subsequent decay into a final state of SM particles. Most of these final states were already applied in the search for the SM Higgs boson. Then we move on to discovery channels that involve decay chains including Higgs-to-Higgs decays, which can result in very unique final states, as the benchmark points we supply prove. We close with a short discussion on coupling sum rules.

14.1 Mass Spectrum and Properties of the NMSSM Higgs Bosons

Let us start by investigating the mass spectrum of the other light Higgs bosons, i.e. of A_1 and of H_i with $i = 1, 2$ depending on whether the next-to-lightest or the lightest scalar Higgs boson takes on the role of the 125 GeV Higgs boson. Figure 14.1 conveys the situation for Scan A. In the plot on the left-hand side $H_1 = h$ and the mass of the lightest pseudoscalar is plotted versus the mass of the next-to-lightest scalar Higgs boson. There is one region that features nearly mass degenerate Higgs bosons, i.e. the mass of the next-to-lightest Higgs boson is around 125 GeV as well. After that there is a gap and only masses $M_{H_2} \gtrsim 160$ GeV are allowed again. The mass of H_2 ranges up to 240 GeV. The mass gap is caused by the LHC exclusion limits. First of all because the provided exclusion limits are strictest in this mass region. Moreover, since we take into account the possibility of superposed signals, the signal of $H_1 = h$ contributes to the superposed signal of H_2, causing an overall signal which is excluded. For the same reason the mass of A_1 only starts at about 130 GeV for $H_1 = h$ and goes up to 350 GeV. The majority of parameter points cluster around $(M_{H_2}, M_{A_1}) = (175, 170)$ GeV. The plot on the right-hand side of Fig. 14.1 shows the mass of A_1 plotted versus the mass of H_1 for scenarios with $H_2 = h$. The mass of the lightest scalar Higgs boson can be as small as 10 GeV

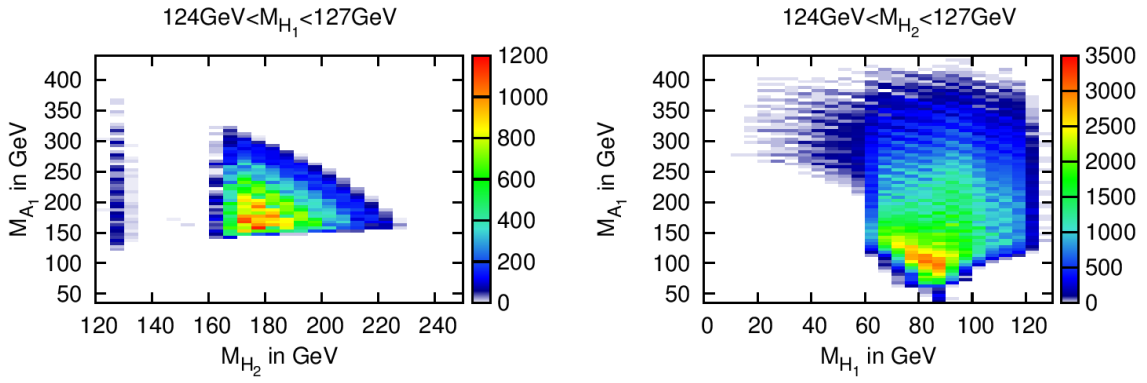

Figure 14.1: Mass spectrum of A_1 and the non SM-like light scalar Higgs boson, i.e. H_2 on the left-hand side and H_1 on the right-hand side for scenarios of Scan A with $\tan\beta = 2$ and $A_t = 1$ TeV. Color code indicates the number of points. Based on data of Scan A [9].

and is just bounded by the 125 GeV at which the labeling convention changes. It is striking that the distribution for M_{H_1} fades out for masses below 62 GeV. This is due to the decay of H_2 into a pair of H_1's, which is kinematically allowed for $M_{H_1} \lesssim 62$ GeV. The availability of this new decay channel causes a reduction of the SM-like branching ratios, thereby diminishing the respective signals, so that it is more difficult to satisfy the condition $\mu_{\gamma\gamma} > 0.8$, which we impose. The mass of the lightest pseudoscalar ranges from $40 - 400$ GeV, but lighter values are favored. The majority of points cluster around $(M_{H_1}, M_{A_1}) = (85, 110)$ GeV. The masses of the heavier Higgs bosons, H_3 and A_2 range from 300 to 500 GeV.

Turning to the respective plot for Scan B, Fig. 14.2 combines both types of scenarios, i.e. $H_1 = h$ and $H_2 = h$. The mass of the non 125 GeV light scalar Higgs boson, denoted by H_i is plotted versus the mass of the lightest pseudoscalar. Due to the enlarged parameter ranges[1] of Scan B the masses of both M_{A_1} and M_{H_i} can go up to $\mathcal{O}$(TeV) – the plot only depicts values up to 1 TeV, but there are a few points even above. We once again observe mass gaps caused by the application of the LHC exclusion limits. For M_{H_i} the mass gap is between $115-170$ GeV. For M_{A_1} it is located between $115-130$ GeV for scenarios with $H_1 = h$. The color code of Fig. 14.2 indicates whether the $\tan\beta$ value is above or below 5. The motivation of this distinction is that scenarios with $\tan\beta < 5$ typically feature a large λ value as we saw earlier, which leads to an NMSSM specific phenomenology. Scenarios with $\tan\beta > 5$ are expected to display a phenomenology which is similar to that of the MSSM. For scenarios with $H_2 = h$ the mass spectrum of A_1 covers

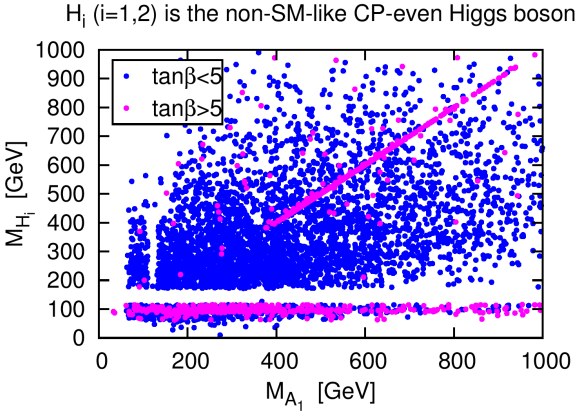

Figure 14.2: Mass spectrum of A_1 and H_i, where H_i denotes the non 125 GeV light scalar, i.e. $H_j = h$ with $i, j = 1, 2$ but $i \neq j$. Blue/pink points are for scenarios with $\tan\beta$ values below/above 5. Based on data of Scan B [10].

[1] Mostly, this can be attributed to the larger μ_{eff} values.

$\tan\beta < 5$	$H_{j=1} = h$	$H_{j=2} = h$
$H_{i=1,2\neq j} \neq h$	singlet	singlet - up to almost doublet
H_3	doublet	doublet
A_1	mostly singlet (few doublet)	mostly singlet (few doublet)
A_2	mostly doublet (few singlet)	mostly doublet (few singlet)

$\tan\beta \geq 5$	$H_{j=1} = h$	$H_{j=2} = h$
$H_{i=1,2\neq j} \neq h$	mostly doublet	singlet - up to almost doublet
H_3	singlet (few doublet)	doublet
A_1	doublet or singlet (for small M_{A_1})	doublet or singlet (for small M_{A_1})
A_2	singlet or doublet	singlet or doublet

Table 14.1: The approximate singlet-/doublet-composition of the NMSSM Higgs bosons for $\tan\beta$ smaller (upper part) and larger (lower part) than 5 and scenarios with either $H_1 = h$ (left) or $H_2 = h$ (right). Based on data of Scan B [10].

the whole mass range independently of the specific tanβ value. However, for $H_1 = h$ there seems to be a correlation between the mass of H_i and M_{A_1} for tan$\beta > 5$. This is due to the fact that in this case they are both doublet-like.

Table 14.1 shows the approximate decomposition encountered for the different scenarios. The $H_i \neq h$ typically displays a large singlet admixture. Only for some scenarios with $H_1 = h$ and tan$\beta > 5$ the Higgs boson H_2 is doublet-like. In these cases the heavy scalar Higgs boson takes over the singlet component. For scenarios with $H_2 = h$ and tan$\beta < 5$ the singlet-like H_1 can have a large doublet admixture as well. The mixing of the pseudoscalar Higgs bosons leads typically to a singlet-like A_1 for tan$\beta < 5$, while for tan$\beta > 5$ the majority of points features an A_2 with a large singlet admixture. The masses of the heavy Higgs bosons take on values of 300 GeV up to $\mathcal{O}$(TeV).

14.2 Signals in Standard Search Channels at 13 TeV

To investigate the discovery prospects of the additional NMSSM Higgs bosons during the 13 TeV run of the LHC, we consider the signal rates predicted for the production in gluon fusion with a subsequent decay into the final states $\gamma\gamma$, bb, $\tau\tau$, WW, ZZ and tt. As described in Ch. 5 the values of the production cross section in gluon fusion at a center of mass energy of 13 TeV were obtained by rescaling the SM cross sections as calculated by `HIGLU` with the gluon coupling of the respective NMSSM Higgs boson normalized to the SM. For some scenarios with tan$\beta > 5$, which feature an enhanced coupling to bottom quarks, also the production in association with b-quarks can be sizeable as we will see later. The respective cross section was obtained by rescaling the SM cross section as calculated by `SUSHI` [208] with the coupling to bottom quarks of the NMSSM Higgs boson in units of the respective SM coupling. We refrain from explicitly showing plots for all possible final states here, but only select those that display interesting features and comment shortly on the remaining ones.

Figure 14.3 shows the signals rates for the production of the light scalar Higgs boson, which is not the one at 125 GeV in gluon fusion with subsequent decay into the final states $\gamma\gamma$, bb, ZZ and tt. The plots for the final states $\tau\tau$ and WW (not shown here) display qualitatively a very similar behavior to those of bb and ZZ, respectively. However, the $\tau\tau$ final state is

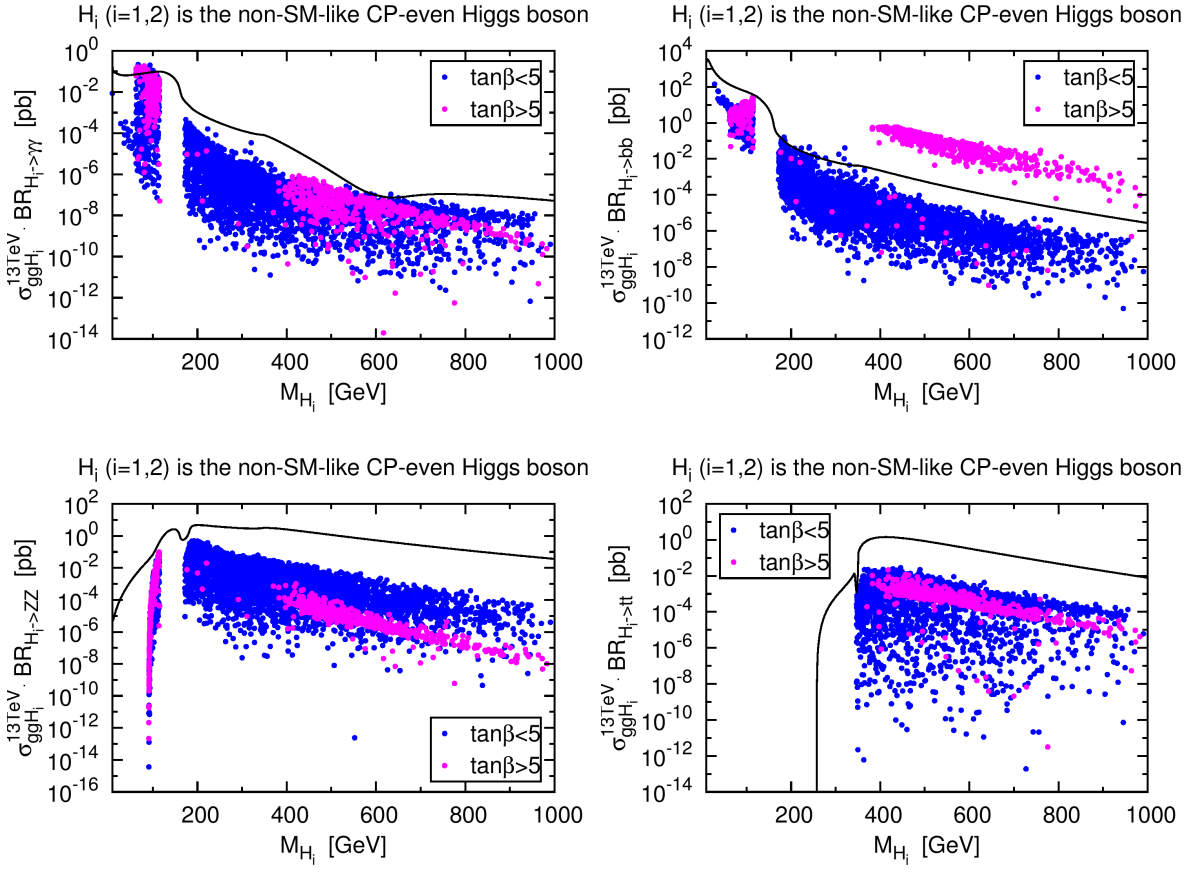

Figure 14.3: Signal rates at a c.m. energy of $\sqrt{s} = 13$ TeV for the production of H_i with $i = 1, 2$ and $H_i \neq h$ in gluon fusion and subsequent decay into the final states $\gamma\gamma$ (upper left), bb (upper right), ZZ (lower left) and tt (lower right) for $\tan\beta < 5$ (blue) and $\tan\beta > 5$ (pink). The respective signal rates for a Higgs boson with the same mass as H_i within the SM (full black line) are given as reference. Based on data of Scan B [10].

suppressed by a factor of roughly 10 compared to the bb state, whereas the WW final state is enhanced by a factor of 10 compared to ZZ. The signal in $\gamma\gamma$ is only of relevance for light Higgs masses. Since the branching ratio into $\gamma\gamma$ is not very large and the production cross section decreases with increasing mass, the overall signal in $\gamma\gamma$ drops soon well below 1 fb, which will make it experimentally very challenging to detect. However, for Higgs masses below the LEP limit of 115 GeV we observe that even signals enhanced compared to the SM can occur. This implies that it is inevitable to also consider the mass regions that were already excluded for a SM-like Higgs boson. At the time of this analysis the experiments had not yet published analyses, which probed this region. However, shortly after our analysis was finalized, first results for the mass region of $65 - 600$ GeV appeared [76]. The exclusion bounds presented there are already very strict. Unfortunately, the inclusion of these bounds in our analysis is not straightforward, since they are given on the fiducial cross section. But it is to be expected that the application of these bounds would probably cut away the points that feature an enhanced signal in the $\gamma\gamma$ final state. For the bb and $\tau\tau$ final states we observe that these can – in addition to the low mass region – also be of interested for larger Higgs masses, since scenarios with $\tan\beta > 5$ can display enhanced signals there. In these scenarios H_2 has a large h_d component (see Tab. 14.1). On the one hand this leads to an enhanced

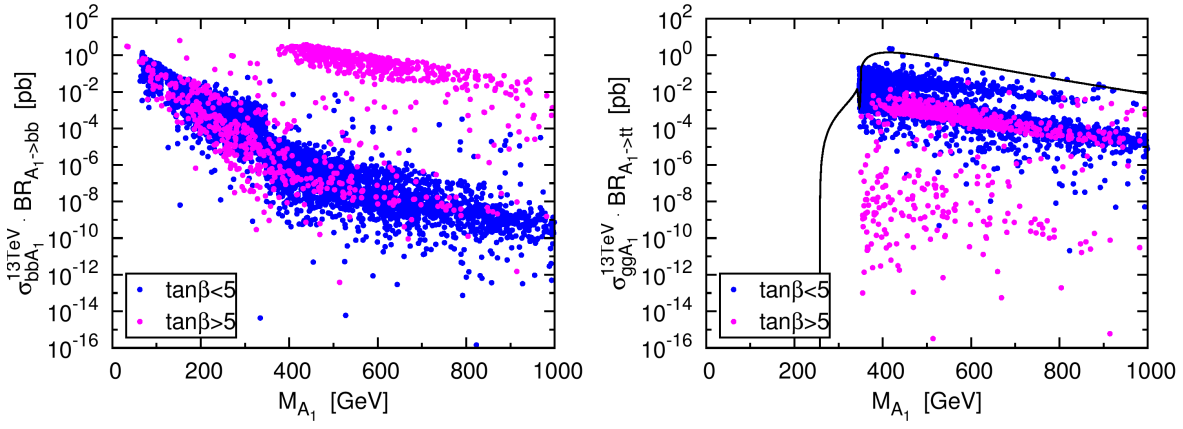

Figure 14.4: Signal rates at a c.m. energy of $\sqrt{s} = 13$ TeV for the production of A_1 in associated production with b-quarks and subsequent decay into the final states bb (left) and in gluon fusion with subsequent decay into tt (right) for $\tan\beta < 5$ (blue) and $\tan\beta > 5$ (pink). The respective signal rate for the production in gluon fusion for a Higgs boson with the same mass as A_1 within the SM (full black line) is given as reference. Based on data of Scan B [10].

coupling to bottom quarks, while on the other hand this leads to a reduced coupling to vector boson pairs. Both factors contribute to an enhanced branching ratio into bb as can easily be seen by starting from Eq. (5.7) and keeping in mind that in the SM the main contribution to the total width of a Higgs boson within this mass range originates from the decays into massive vector bosons

$$R^{\text{BR}}_{bb}(H_2) = C_b^2(H_2)\frac{\Gamma_{H^{\text{SM}}\to WW} + \Gamma_{H^{\text{SM}}\to ZZ} + \cdots}{C_V^2(H_2)\Gamma_{H^{\text{SM}}\to WW} + C_V^2(H_2)\Gamma_{H^{\text{SM}}\to ZZ} + \cdots} \approx \frac{C_b^2(H_2)}{C_V^2(H_2)}\,. \tag{14.1}$$

If one considers production in association with bottom quarks, one can even gain another factor of 10. Of course, the bb final state suffers from a large background. Hence, the $\tau\tau$ final state might be more promising, although it is suppressed by a factor of 10 compared to bb. In the case of $H_1 = h$ the next-to-lightest scalar Higgs bosons could also be searched in final states with massive vector bosons or with a top quark pair. The predicted signals for these, however, are about two orders of magnitude smaller than in the SM, due to the composition of H_2. Because H_2 has either a very large singlet component, which leads to a reduction of all couplings to SM particles, or if it is doublet-like, it has a large h_d component, which results in suppressed couplings to vector bosons and up-type quarks and thereby to reduced signals in these final states. Hence, a discovery via those channels is very challenging. In fact, for scenarios with $\tan\beta < 5$ the only possibility seems to be a combination of the $\tau\tau$, the vector bosons and the tt channels.

Let us look at the situation for the lightest pseudoscalar Higgs boson. Due to its CP nature the decay into massive gauge bosons is forbidden. Furthermore, the signal rate in the $\gamma\gamma$ channel is always well below 10^{-4} pb, even for the low mass region. This leaves the channels bb, $\tau\tau$ and tt. Figure 14.4 shows the signal rate in associated production with b-quarks and subsequent decay into a bottom quark pair (left) and the signal rate for the production in gluon fusion with subsequent decay into a pair of top quarks (right). For $\tan\beta > 5$ and masses above ~ 400 GeV, we observe a similar behavior as for H_2, namely an enhancement in the rate into bb due to an enhanced coupling to bottom quarks. Cross sections up to 4 pb are

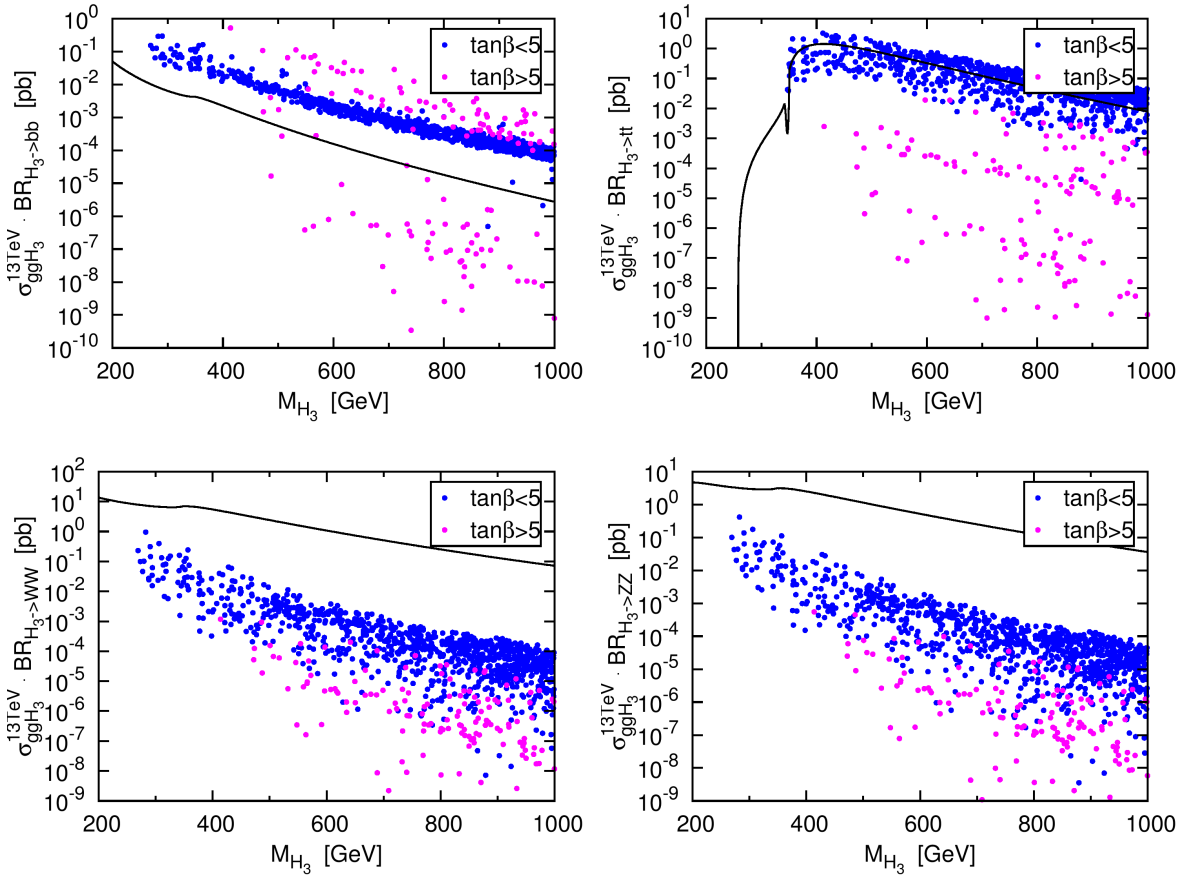

Figure 14.5: Signal rates at a c.m. energy of $\sqrt{s} = 13$ TeV for the production of H_3 in gluon fusion and subsequent decay into the final states bb (upper left), tt (upper right), WW (lower left) and ZZ (lower right) for tan$\beta < 5$ (blue) and tan$\beta > 5$ (pink). The respective signal rates for a Higgs boson with the same mass as H_3 within the SM (full black line) are given as reference. Based on data of Scan B [10].

reached[2]. The signal rate for $\tau\tau$ (not shown here) displays a similar behavior but is reduced by a factor of roughly 10. Hence, all in all the bb and $\tau\tau$ final states might be suitable for the discovery of a pseudoscalar in the low mass range and for large tanβ values also for masses above 400 GeV. However, for scenarios with tan$\beta < 5$ the only search channel left for the high mass region is tt. The signal rates there are at most a few pb, which for this complicated final state makes the search challenging.

For the heavy Higgs bosons the situation can become very difficult for masses above 1 TeV, simply because the production cross sections become too tiny. Figure 14.5 shows the signal rates predicted for the heavy scalar Higgs boson with a mass below 1 TeV in the final states bb, tt, WW and ZZ. The heavy scalar Higgs boson typically has an enhanced coupling to bottom quarks, while the couplings to top quarks and vector bosons are suppressed. The suppressed coupling to the vector bosons entails a diminished total width. Therefore, the signal in bb is enhanced, even though the coupling to gluons, which is relevant to the production is reduced as the signal rates for the massive vector boson final states reveal[3]. Also for the tt final state

[2]The sudden step in the signal rate at $M_{A_1} \approx 350$ GeV appears as the decay channel into top pairs opens up, which leads to a reduction of the branching ratios of the other decays.

[3]A suppressed coupling to vector bosons reduces both the total width and the partial width for the decay into massive vector bosons, leaving the respective branching ratio unaffected.

A (Point ID 3877)	**Scenario**		
$M_{H_1}, M_{H_2}, M_{H_3} = M_{H_s}, M_h, M_H$	90.3 GeV	126.8 GeV	341.3 GeV
$M_{A_1}, M_{A_2} = M_{A_s}, M_A$	118.5 GeV	346.7 GeV	
$\mu_{\tau\tau}(h)$, $\mu_{bb}(h)$	1.09	1.08	
$\mu_{ZZ}(h)$, $\mu_{WW}(h)$, $\mu_{\gamma\gamma}(h)$	0.85	0.85	0.88
$\tan\beta$, λ, κ	1.66	0.64	0.11
A_λ, A_κ, μ_{eff}	338.0 GeV	-71.2 GeV	162.8 GeV
A_t, A_b, A_τ	181.1 GeV	-1530.0 GeV	87.2 GeV
M_1, M_2, M_3	440.0 GeV	813.7 GeV	1710.2 GeV
$M_{Q_3} = M_{t_R}$, M_{b_R}	1827.5 GeV	3 TeV	
$M_{L_3} = M_{\tau_R}$, M_{SUSY}	1663.7 GeV	3 TeV	

Table 14.2: The parameters defining scenario A, together with the Higgs boson masses and the reduced signal rates of h.

the influence of the diminished total width compensates the suppressed coupling to top quarks and the reduced production so that the overall rates are of the order of the SM for $\tan\beta < 5$. The picture for the heavy pseudoscalar is similar, therefore we refrain from explicitly showing the plots here.

In summary it can be said that the general NMSSM predicts quite a few scenarios, which if they are realized in nature, will be very challenging to discover – at least if only search channels involving direct production are taken into account. As a next step we considered the parameter subspace of the natural NMSSM, which is characterized by an approximate Peccei-Quinn symmetry, to analyze whether the 13 TeV run of the LHC will be able to probe this subspace completely. We found that even if no further Higgs bosons are discovered, it will at least be possible to constrain this parameter subspace severely. Which is of interest since this subspace contains a fair amount of the valid scenarios for the general NMSSM. For details on this analysis the reader is referred to [10].

14.3 Search Channels Involving Higgs-to-Higgs Decays

Search channels involving decay chains including Higgs-to-Higgs decays become relevant in two situations. They can either be the means to discover a heavy Higgs boson, in case this heavy Higgs boson decays dominantly into lighter Higgs bosons instead of the typical final states. Or they can be facilitated to search for light Higgs bosons, which due to a large singlet admixture display a very small direct production cross section. For such a Higgs state the production via the decay of a heavier Higgs boson can be larger than the direct production, provided that the direct production of the heavy Higgs boson is sufficiently large. Hence we will consider processes of the following type

$$\sigma(gg\phi_i) \times \text{BR}(\phi_i \to \phi_j\phi_k) \times \text{BR}(\phi_j \to XX) \times \text{BR}(\phi_k \to YY)\,, \tag{14.2}$$

where ϕ_i generically denotes one of the five neutral Higgs bosons. Of course the Higgs-to-Higgs decays have to be allowed kinematically, i.e. $M_{\phi_i} > M_{\phi_j} + M_{\phi_k}$, and by the CP properties of the participating Higgs bosons. The light Higgs bosons then decay further into the usual final states, i.e. $XX, YY = (\gamma\gamma, bb, \tau\tau, WW, ZZ, tt, \ldots)$. In the following we will label the Higgs states not by their mass ordering, but according to their main components. As before the scalar state at 125 GeV, which is doublet-like, is denoted by h. The other doublet-like scalar

A (Point ID 3877)	Rates
$\sigma(ggH_s)$	2.37 pb
$\sigma(ggH_s)\mathrm{BR}(H_s \to b\bar{b})$	2.04 pb
$\sigma(ggH_s)\mathrm{BR}(H_s \to \tau\tau)$	204.82 fb
$\sigma(ggH_s)\mathrm{BR}(H_s \to \gamma\gamma)$	2.74 fb
$\sigma(ggH)$	4.29 pb
$\sigma(ggH)\mathrm{BR}(H \to b\bar{b})$	40.88 fb
$\sigma(ggH)\mathrm{BR}(H \to \tau\tau)$	5.10 fb
$\sigma(ggH)\mathrm{BR}(H \to WW)$	49.13 fb
$\sigma(ggH)\mathrm{BR}(H \to ZZ)$	22.41 fb
$\sigma(ggH)\mathrm{BR}(H \to \tilde{\chi}_1^0\tilde{\chi}_1^0)$	1.27 pb
$\sigma(ggH)\mathrm{BR}(H \to \tilde{\chi}_1^0\tilde{\chi}_2^0)$	686.4 fb
$\sigma(ggH)\mathrm{BR}(H \to H_sH_s)$	458.74 fb
$\sigma(ggH)\mathrm{BR}(H \to H_sH_s \to bb+bb)$	341.12 fb
$\sigma(ggH)\mathrm{BR}(H \to H_sH_s \to bb+\tau\tau)$	68.34 fb
$\sigma(ggH)\mathrm{BR}(H \to H_sH_s \to \tau\tau+\tau\tau)$	3.42 fb
$\sigma(ggH)\mathrm{BR}(H \to H_sH_s \to bb+\gamma\gamma)$	0.92 fb
$\sigma(ggH)\mathrm{BR}(H \to hH_s)$	505.60 fb
$\sigma(ggH)\mathrm{BR}(H \to hH_s \to bb+bb)$	274.92 fb
$\sigma(ggH)\mathrm{BR}(H \to hH_s \to bb+\tau\tau)$	56.46 fb
$\sigma(ggH)\mathrm{BR}(H \to hH_s \to \tau\tau+\tau\tau)$	2.90 fb
$\sigma(ggH)\mathrm{BR}(H \to hH_s \to bb+\gamma\gamma)$	1.34 fb
$\sigma(ggH)\mathrm{BR}(H \to ZA_s)$	1.07 pb
$\sigma(ggH)\mathrm{BR}(H \to ZA_s \to ll+bb)$	31.67 fb
$\sigma(ggH)\mathrm{BR}(H \to ZA_s \to \tau\tau+bb)$	46.59 fb
$\sigma(ggH)\mathrm{BR}(H \to ZA_s \to \tau\tau+\tau\tau)$	3.32 fb

A (Point ID 3877)	Rates
$\sigma(ggA_s)$	914.07 fb
$\sigma(ggA_s)\mathrm{BR}(A_s \to b\bar{b})$	804.77 fb
$\sigma(ggA_s)\mathrm{BR}(A_s \to \tau\tau)$	84.15 fb
$\sigma(ggA_s)\mathrm{BR}(A_s \to \gamma\gamma)$	0.36 fb
$\sigma(ggA)$	3.36 pb
$\sigma(ggA)\mathrm{BR}(A \to t\bar{t})$	1.43 pb
$\sigma(ggA)\mathrm{BR}(A \to \tilde{\chi}_1^0\tilde{\chi}_1^0)$	686.00 fb
$\sigma(ggA)\mathrm{BR}(A \to hA_s)$	472.37 fb
$\sigma(ggA)\mathrm{BR}(A \to hA_s \to bb+bb)$	262.24 fb
$\sigma(ggA)\mathrm{BR}(A \to hA_s \to \tau\tau+bb)$	55.00 fb
$\sigma(ggA)\mathrm{BR}(A \to hA_s \to \tau\tau+\tau\tau)$	2.88 fb
$\sigma(ggA)\mathrm{BR}(A \to hA_s \to WW+bb)$	85.39 fb
$\sigma(ggA)\mathrm{BR}(A \to hA_s \to \gamma\gamma+bb)$	1.04 fb
$\sigma(ggA)\mathrm{BR}(A \to H_sA_s)$	285.76 fb
$\sigma(ggA)\mathrm{BR}(A \to H_sA_s \to bb+bb)$	216.95 fb
$\sigma(ggA)\mathrm{BR}(A \to H_sA_s \to \tau\tau+bb)$	44.42 fb
$\sigma(ggA)\mathrm{BR}(A \to H_sA_s \to \tau\tau+\tau\tau)$	2.27 fb
$\sigma(ggA)\mathrm{BR}(A \to H_sA_s \to \gamma\gamma+bb)$	0.39 fb
$\sigma(ggA)\mathrm{BR}(A \to ZH_s)$	158.13 fb
$\sigma(ggA)\mathrm{BR}(A \to ZH_s \to ll+b\bar{b})$	4.59 fb
$\sigma(ggA)\mathrm{BR}(A \to ZH_s \to \tau\tau+b\bar{b})$	6.66 fb
$\sigma(ggA)\mathrm{BR}(A \to ZH_s \to \tau\tau+\tau\tau)$	0.46 fb

Table 14.3: The signal rates and production cross sections for scenario A.

will be denoted by H, whereas H_s is the scalar Higgs boson with a large singlet admixture. Likewise the state A_s is CP-odd with a large singlet admixture, while A denotes the doublet-like CP-odd state. We will illustrate the possibilities this type of search channel offers by means of three benchmark scenarios. We selected two scenarios for small $\tan\beta$ values with either $h = H_2$ or $h = H_1$ (scenarios A and B) and one scenario with a relatively large $\tan\beta$ value (scenario C). More scenarios can be found in [10].

Scenario A

The input parameters of scenario A and the resulting mass spectrum are listed in Tab. 14.2. This scenario features a very light spectrum, where the doublet-like heavy Higgs bosons have masses of ~ 345 GeV. The light scalar with a mass of 90 GeV has a large singlet admixture, just like the light pseudoscalar with a mass of 118 GeV, leaving the next-to-lightest scalar to take over the role of the 125 GeV Higgs boson. The signal strength values for h do not deviate by more than 15% from those of a SM Higgs boson. The signal rate into the down-type fermions is slightly enhanced, while the rates into the bosonic final states, i.e. into ZZ, WW and $\gamma\gamma$, are reduced.

The relevant signal rates for scenario A are given in Tab. 14.3. Even though the coupling of the singlet-like states to gluons amounts only to about $\mathcal{O}(15\%)$ of the respective SM value

B (Point ID Poi2a)	**Scenario**		
M_h, M_{H_s}, M_H	124.6 GeV	181.7 GeV	322.6 GeV
M_{A_s}, M_A	72.5 GeV	311.7 GeV	
$\mu_{\tau\tau}(h)$, $\mu_{bb}(h)$	1.54	1.01	
$\mu_{ZZ}(h)$, $\mu_{WW}(h)$, $\mu_{\gamma\gamma}(h)$	0.93	0.93	1.01
$\tan\beta, \lambda, \kappa$	1.9	0.628	0.354
$A_\lambda, A_\kappa, \mu_{\text{eff}}$	251.2 GeV	53.8 GeV	158.9 GeV
M_1, M_2, M_3	890 GeV	576 GeV	1219 GeV
A_t, A_b, A_τ	1555 GeV	-1005 GeV	-840 GeV
$M_{Q_3} = M_{t_R}$, M_{b_R}	1075 GeV	1 TeV	
$M_{L_3} = M_{\tau_R}$, M_{SUSY}	530 GeV	2.5 TeV	

Table 14.4: The parameters defining scenario B, together with the Higgs boson masses and the reduced signal rates of h.

their production cross sections in gluon fusion are still large enough to be discovered via direct production. Promising final states are for example $\tau\tau$ and $\gamma\gamma$. Since the CP-even heavy Higgs boson is still comparatively light, the production cross section in gluon fusion is with ~ 4.3 pb sufficiently large. However, H decays dominantly into a pair of the lightest neutralinos (branching ratio of 30%) and also the decay into the lightest and next-to-lightest neutralino is with a branching ratio of 16% relevant. The presence of such non-SM decays leads to a reduction of the branching ratios into the SM particles, rendering the standard search channels less effective. Conveniently the branching ratios $H \to H_s H_s$ and $H \to h H_s$ are sizeable as well, amounting to 11% and 12%, respectively. Even after multiplication with the branching ratios for the decays of the light Higgs bosons the resulting signals are of the same order as those obtained via direct production of H and subsequent decay. The largest signal is obtained for the $4b$-quark final state. But since this suffers from a large background the final states $(bb)(\tau\tau)$, 4τ or even $(bb)(\gamma\gamma)$ might be better suited. Finally, one could also exploit decay chains involving the decay $H \to Z A_s$ (branching ratio of 25%) to search for the heavy scalar. For the heavy pseudoscalar we also observe that the decays into neutralinos and other Higgs states play an important role. However, the dominant decay channel for A is into a top quark pair. But also decay chains involving $A \to h A_s$ and $A \to H_s A_s$ can lead to sizeable signals.

Scenario B

Scenario B also features a relatively light spectrum (see Tab. 14.4) with the masses of the heavy Higgs bosons at 320 GeV for the CP-even and at 310 GeV for the CP-odd Higgs boson. Both heavy states are doublet-like. Here $H_1 = h$, so that the next-to-lightest scalar and the lightest pseudoscalar are singlet dominated. Most of the predicted signal strength values for h are very SM-like in this scenario, with the exception of $\mu_{\tau\tau} = 1.54$, which is enhanced.

With this mass spectrum a lot of different Higgs-to-Higgs decays are kinematically allowed. The rates of the interesting signals are given in Tab. 14.5. The scalar singlet-like state decays to 97% into an A_s pair. Moreover, the A_s state decays dominantly into photon pairs. This combination leads to a final state with four photons and a signal of 190 fb. Since the production cross section of A_s is very small (below 0.1 fb) exploiting this production via the decay of H_s is the only way. For H the standard search channels do exhibit sufficiently large

B (Point ID Poi2a)	**Rates**
$\sigma(ggH_s)$	282.37 fb
$\sigma(ggH_s)\mathrm{BR}(H_s \to WW)$	5.09 fb
$\sigma(ggH_s)\mathrm{BR}(H_s \to A_sA_s)$	274.75 fb
$\sigma(ggH_s)\mathrm{BR}(H_s \to A_sA_s \to b\bar{b}+b\bar{b})$	5.87 fb
$\sigma(ggH_s)\mathrm{BR}(H_s \to A_sA_s \to \gamma\gamma+b\bar{b})$	67.33 fb
$\sigma(ggH_s)\mathrm{BR}(H_s \to A_sA_s \to \gamma\gamma+\gamma\gamma)$	193.22 fb
$\sigma(ggH)$	3.17 pb
$\sigma(ggH)\mathrm{BR}(H \to WW)$	264.73 fb
$\sigma(ggH)\mathrm{BR}(H \to ZZ)$	119.52 fb
$\sigma(ggH)\mathrm{BR}(H \to b\bar{b})$	297.37 fb
$\sigma(ggH)\mathrm{BR}(H \to \tau\tau)$	37.65 fb
$\sigma(ggH)\mathrm{BR}(H \to \tilde{\chi}_1^0\tilde{\chi}_1^0)$	383.33 fb
$\sigma(ggH)\mathrm{BR}(H \to \tilde{\chi}_1^+\tilde{\chi}_1^-)$	403.14 fb
$\sigma(ggH)\mathrm{BR}(H \to hH_s)$	1.609 pb
$\sigma(ggH)\mathrm{BR}(H \to hH_s \to bb+\tau\tau)$	1.44 fb
$\sigma(ggH)\mathrm{BR}(H \to hH_s \to h+A_sA_s \to bb+4\gamma)$	712.47 fb
$\sigma(ggH)\mathrm{BR}(H \to hH_s \to h+A_sA_s \to \gamma\gamma+4b)$	248.02 fb
$\sigma(ggH)\mathrm{BR}(H \to hH_s \to h+A_sA_s \to \tau\tau+4\gamma)$	74.60 fb
$\sigma(ggH)\mathrm{BR}(H \to hH_s \to h+A_sA_s \to \gamma\gamma+4\tau)$	2.47 fb
$\sigma(ggH)\mathrm{BR}(H \to hH_s \to h+A_sA_s \to 6\gamma)$	2.69 fb
$\sigma(ggH)\mathrm{BR}(H \to hH_s \to h+A_sA_s \to \tau\tau+\gamma\gamma+b\bar{b})$	49.55 fb
$\sigma(ggH)\mathrm{BR}(H \to A_sA_s)$	5.59 fb
$\sigma(ggH)\mathrm{BR}(H \to A_sA_s \to 4\gamma)$	3.93 fb
$\sigma(ggA_s)$	0.08 fb
$\sigma(ggA)$	2.51 pb
$\sigma(ggA)\mathrm{BR}(A \to \tau\tau)$	14.42 fb
$\sigma(ggA)\mathrm{BR}(A \to \tilde{\chi}_1^0\tilde{\chi}_1^0)$	963.87 fb
$\sigma(ggA)\mathrm{BR}(A \to \tilde{\chi}_1^+\tilde{\chi}_1^-)$	273.57 fb
$\sigma(ggA)\mathrm{BR}(A \to H_sA_s)$	525.56 fb
$\sigma(ggA)\mathrm{BR}(A \to H_sA_s \to A_sA_s+A_s \to 6\gamma)$	301.58 fb
$\sigma(ggA)\mathrm{BR}(A \to H_sA_s \to A_sA_s+A_s \to bb+4\gamma)$	157.64 fb
$\sigma(ggA)\mathrm{BR}(A \to H_sA_s \to A_sA_s+A_s \to 4b+\gamma\gamma)$	27.47 fb
$\sigma(ggA)\mathrm{BR}(A \to H_sA_s \to A_sA_s+A_s \to \tau\tau+4\gamma)$	14.99 fb
$\sigma(ggA)\mathrm{BR}(A \to H_sA_s \to A_sA_s+A_s \to \tau\tau+bb+\gamma\gamma)$	5.22 fb
$\sigma(ggA)\mathrm{BR}(A \to H_sA_s \to A_sA_s+A_s \to 4\tau+\gamma\gamma)$	0.25 fb
$\sigma(ggA)\mathrm{BR}(A \to hA_s)$	29.96 fb
$\sigma(ggA)\mathrm{BR}(A \to hA_s \to \gamma\gamma+b\bar{b})$	16.25 fb
$\sigma(ggA)\mathrm{BR}(A \to hA_s \to \gamma\gamma+\tau\tau)$	1.70 fb
$\sigma(ggA)\mathrm{BR}(A \to hA_s \to b\bar{b}+b\bar{b})$	2.83 fb
$\sigma(ggA)\mathrm{BR}(A \to ZH_s)$	554.38 fb
$\sigma(ggA)\mathrm{BR}(A \to ZH_s \to bb+A_sA_s \to bb+4\gamma)$	57.36 fb
$\sigma(ggA)\mathrm{BR}(A \to ZH_s \to bb+A_sA_s \to 4b+\gamma\gamma)$	19.99 fb
$\sigma(ggA)\mathrm{BR}(A \to ZH_s \to Z+A_sA_s \to bb+\tau\tau+\gamma\gamma)$	6.35 fb
$\sigma(ggA)\mathrm{BR}(A \to ZH_s \to ll/\tau\tau+A_sA_s \to ll/\tau\tau+4\gamma)$	12.78 fb
$\sigma(ggA)\mathrm{BR}(A \to ZH_s \to ll/\tau\tau+A_sA_s \to ll\tau\tau/4\tau+\gamma\gamma)$	0.42 fb

Table 14.5: The signal rates and production cross sections for scenario B.

C (Point ID 2296)	**Scenario**		
M_h, M_H, M_{H_s}	124.1 GeV	597.7 GeV	3528.3 GeV
M_{A_s}, M_A	311.8 GeV	614.5 GeV	
$\mu_{\tau\tau}(h)$, $\mu_{bb}(h)$	0.97	1.06	
$\mu_{ZZ}(h)$, $\mu_{WW}(h)$, $\mu_{\gamma\gamma}(h)$	0.78	0.78	0.80
$\tan\beta$, λ, κ	17.06	0.08	-0.63
A_λ, A_κ, μ_{eff}	-1766.2 GeV	-24.2 GeV	-217.1 GeV
A_t, A_b, A_τ	1961.8 GeV	-1535.3 GeV	-1211.9 GeV
M_1, M_2, M_3	478.3 GeV	369.2 GeV	2847.8 GeV
$M_{Q_3} = M_{t_R}$, M_{b_R}	977.0 GeV	3 TeV	
$M_{L_3} = M_{\tau_R}$, M_{SUSY}	2797.1 GeV	3 TeV	

Table 14.6: The parameters defining scenario C, together with the Higgs boson masses and the reduced signal rates of h.

signals due to the sizeable cross section in gluon fusion of 3.17 pb. However, the dominant decay mode for H is the decay into hH_s with a branching ratio of 50% and also the decays into neutralinos and charginos with 12% each play an important role. The fact that H_s decays mostly into A_sA_s allows for the construction of a decay chain involving two Higgs-to-Higgs decays in a row. The resulting signatures with multiphoton, multi-b and multi-τ final states are very unique and still deliver signals up to several hundred fb. Similar final states can be constructed for the decay chain $A \to H_sA_s \to A_sA_s + A_s$. Here the six-photon final state even yields a signal of 300 fb.

Scenario C

The mass spectrum and the input parameters for scenario C are given in Tab. 14.6, while the relevant signal rates are listed in Tab. 14.7. This scenario features a large value of $\tan\beta = 17$ and at the same time a small value for $\lambda = 0.08$. This results in a very heavy scalar state at 3.5 TeV, which is almost a pure singlet. This renders a detection of this state nearly impossible. The doublet-like Higgs bosons H and A have a mass of the order of 600 GeV and are nearly completely dominated by the down-type component[4]. This leads to enhanced couplings to bottom quarks, whereas the coupling to top quarks and thereby at the same time the coupling to gluons is close to vanishing. Therefore, the production mode with the largest cross section is, for both H and A, production in association with b-quarks. The cross sections for direct production are sufficiently large for all Higgs bosons with the exception of H_s. Furthermore, the decays $H \to ZA_s$ and $A \to hA_s$ offer additional search channels for A_s. Note, that it is in general more difficult to find scenarios with large $\tan\beta$ values in which Higgs-to-Higgs decays play an important role than it is to find such scenarios for small $\tan\beta$ values. As we saw earlier large $\tan\beta$ values usually go hand in hand with small values of λ. Many of the trilinear Higgs self-couplings are proportional to λ and are therefore very small for scenarios featuring large $\tan\beta$ values.

[4]This is caused by the large value of $\tan\beta$, which requires h to be nearly completely h_u-like in order to have a large coupling to top quarks, which is necessary to acquire a large coupling to gluons. Due to sum rules this leaves only a small h_u component for H.

C (Point ID 2296)	Rates
$\sigma(bbH)$	346.97 fb
$\sigma(bbH)\mathrm{BR}(H \to b\bar{b})$	190.72 fb
$\sigma(bbH)\mathrm{BR}(H \to \tau\tau)$	23.32 fb
$\sigma(bbH)\mathrm{BR}(H \to t\bar{t})$	5.37 fb
$\sigma(bbH)\mathrm{BR}(H \to \tilde{\chi}_1^0\tilde{\chi}_1^0)$	7.00 fb
$\sigma(bbH)\mathrm{BR}(H \to \tilde{\chi}_1^+\tilde{\chi}_1^-)$	16.21 fb
$\sigma(bbH)\mathrm{BR}(H \to ZA_s)$	101.84 fb
$\sigma(bbH)\mathrm{BR}(H \to ZA_s \to ll + b\bar{b})$	3.08 fb
$\sigma(bbH)\mathrm{BR}(H \to ZA_s \to \tau\tau + b\bar{b})$	4.61 fb
$\sigma(bbA_s)$	404.91 fb
$\sigma(bbA_s)\mathrm{BR}(A_s \to b\bar{b})$	364.21 fb
$\sigma(bbA_s)\mathrm{BR}(A_s \to \tau\tau)$	40.17 fb

C (Point ID 2296)	Rates
$\sigma(bbh)$	643.60 fb
$\sigma(bbA)$	282.80 fb
$\sigma(bbA)\mathrm{BR}(A \to b\bar{b})$	151.41 fb
$\sigma(bbA)\mathrm{BR}(A \to \tau\tau)$	18.60 fb
$\sigma(bbA)\mathrm{BR}(A \to t\bar{t})$	5.08 fb
$\sigma(bbA)\mathrm{BR}(A \to \tilde{\chi}_1^0\tilde{\chi}_1^0)$	6.85 fb
$\sigma(bbA)\mathrm{BR}(A \to hA_s)$	76.27 fb
$\sigma(bbA)\mathrm{BR}(A \to hA_s \to bb + bb)$	46.65 fb
$\sigma(bbA)\mathrm{BR}(A \to hA_s \to bb + \tau\tau)$	9.98 fb
$\sigma(bbA)\mathrm{BR}(A \to hA_s \to \tau\tau + \tau\tau)$	0.53 fb

Table 14.7: The signal rates and production cross sections for scenario C.

14.4 Sum Rules

Once the experiments do find another scalar Higgs boson, the question whether this Higgs boson can be described within the framework of the MSSM or NMSSM will arise. In case the couplings of the two Higgs bosons to SM particles have been measured, one possibility to distinguish the NMSSM from the MSSM is the consideration of sum rules, that apply to the couplings. The relevant couplings for this investigation are the coupling of the scalar Higgs bosons to massive vector bosons, denoted by g_{H_iVV}, the coupling to top quarks, denoted by g_{H_itt}, and the coupling to bottom quarks, denoted by g_{H_ibb}. Both in the NMSSM and in the MSSM the couplings normalized to the SM read

$$g_{H_iVV} = \sin\beta\,\mathcal{R}^S_{ih_u} + \cos\beta\,\mathcal{R}^S_{ih_d}\,, \tag{14.3a}$$

$$g_{H_itt} = \frac{\mathcal{R}^S_{ih_u}}{\sin\beta}\,, \tag{14.3b}$$

$$g_{H_ibb} = \frac{\mathcal{R}^S_{ih_d}}{\cos\beta}\,. \tag{14.3c}$$

The only difference is that in the MSSM there are only two scalars, i.e. $i = 1, 2$, and the unitarity[5] of the mixing matrix implies $(\mathcal{R}^S_{ih_u})^2 + (\mathcal{R}^S_{ih_d})^2 = 1$, whereas in the NMSSM there are three scalars, i.e. $i = 1, 2, 3$, and $(\mathcal{R}^S_{ih_u})^2 + (\mathcal{R}^S_{ih_d})^2 + (\mathcal{R}^S_{ih_s})^2 = 1$, which implies that if H_i has a singlet admixture $(\mathcal{R}^S_{ih_u})^2 + (\mathcal{R}^S_{ih_d})^2 < 1$. It is evident that due to the unitarity of the mixing matrix $\mathcal{R}$ the couplings fulfill the following sum rules

$$\sum_{i=1}^{n} g^2_{H_iVV} = 1\,, \tag{14.4a}$$

$$\frac{1}{\sum_{i=1}^{n} g^2_{H_itt}} + \frac{1}{\sum_{i=1}^{n} g^2_{H_ibb}} = 1\,, \tag{14.4b}$$

with $n = 2$ for the MSSM and $n = 3$ for the NMSSM.

[5] In fact, it is even orthogonal.

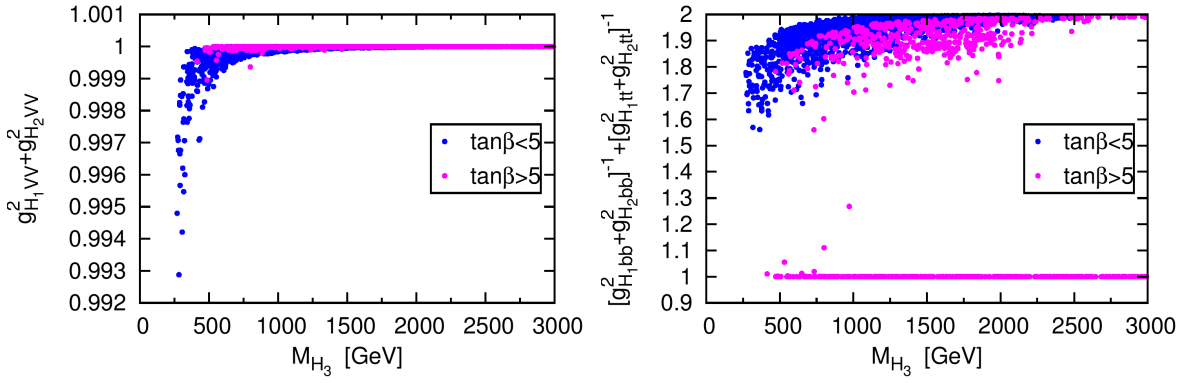

Figure 14.6: Sum rules of for the couplings to vector bosons (left) and the couplings to quarks (right) applied to the two lightest scalar Higgs bosons of valid scenarios versus the mass of the heavy scalar. Based on the data of Scan B [10].

To illustrate the method let us assume that the model realized in nature is the NMSSM, but that the LHC has only discovered the two lightest of the three scalar Higgs bosons so far, but for those the couplings have been measured with sufficient accuracy. Figure 14.6 shows what one obtains if the sum rules are applied to the two lighter scalar Higgs bosons of the scenarios Scan B delivered. First of all, we observe that exploiting the sum rule for the couplings to gauge bosons is not very helpful as the deviations from one are very small. This is due to the fact, that typically the Higgs boson at 125 GeV has a very SM-like coupling to vector bosons, while the other scalar Higgs bosons display only a very small coupling to vector bosons. However, considering the sum rule for the couplings to quarks, we see a clear deviation in a large number of scenarios. Only some scenarios with large $\tan\beta$ values fulfill the sum rule if only the two lightest scalar Higgs bosons are taken into account. In these scenarios the two light Higgs bosons are both MSSM-like and have hardly any singlet admixture at all. However, as soon as one of the light scalars has a sizeable singlet admixture[6], the sum rule for the quark couplings deviates from the value one expects if the whole spectrum is taken into account. Typically the 125 GeV Higgs boson is h_u-like and a large deviation from the sum rule is observed, when the other light scalar is singlet-like, while the h_d-like heavy Higgs boson is not taken into account and therefore its contributions to the sum rule are missing. We discussed this method of considering sum rules already in [10] and [11].

[6]This is equivalent to the statement that the undiscovered heavy Higgs boson has a large doublet admixture

Part IV

To Conclude...

CHAPTER 15

Summary and Conclusion

This thesis discussed the Next-to-Minimal Supersymmetric Extension of the Standard Model. It contributes to the effort of increasing the accuracy of the theoretical predictions available within the framework of the complex NMSSM. Furthermore, a phenomenological analysis interpreting the NMSSM in light of the experimental results was conducted.

Part II presented the calculation of the Higgs bosons masses including higher order corrections up to the order $\alpha_s\alpha_t$ in the complex NMSSM. We focused especially on the two-loop contributions $\mathcal{O}(\alpha_s\alpha_t)$, which were computed in the Feynman diagrammatic approach applying the approximation of vanishing external momentum and the gaugeless limit. To fix the counterterms of the Higgs sector a mixed renormalization scheme employing both on-shell and $\overline{\text{DR}}$ conditions was used. The counterterms from the top and stop sector were either fixed via on-shell or $\overline{\text{DR}}$ conditions. The comparison of these two schemes proves that the inclusion of the $\alpha_s\alpha_t$ corrections reduces the theoretical error due to missing higher order corrections drastically and is therefore essential to allow for a meaningful phenomenological analysis. The computed corrections were implemented in the program package `NMSSMCALC`, which is publicly available.

The numerical analysis of one example scenario revealed that the presented corrections mainly affect the masses of the light Higgs bosons, and especially that of the h_u-dominated state. In addition to the effects on the masses also the effects on the couplings to SM particles are sizeable, which has a large phenomenological impact. We found that the CP-violating phases, which enter at loop level, have a visible influence on the higher order NMSSM Higgs masses, but the effect is not very pronounced. Moreover, the NMSSM specific contributions of the order $\alpha_s\alpha_t$ turn out to be rather small – at least for λ values that respect the perturbativity limit.

The calculation of the correction up to the order $\alpha_s\alpha_t$ was only one step in improving the accuracy of the theoretical prediction for the Higgs masses in the NMSSM. Eventually, we aim at including further two-loop contributions, such as $\mathcal{O}(\alpha_s\alpha_b)$ and later also $\mathcal{O}(\alpha_t^2)$.

Part III investigated the implications of the experimental analysis provided by ATLAS and CMS based on the $\sqrt{s} = 7$ TeV and 8 TeV run of the LHC for the general NMSSM. We per-

formed scans over the NMSSM parameter space searching for parameters points compatible with the experimental observations. We found that in the NMSSM both, the lightest and the next-to-lightest Higgs boson, can take on the role of the 125 GeV Higgs boson. However, these different types of scenarios are realized in different subspaces of the NMSSM parameter space. Furthermore, the presented signal strength values prove that the superposition of the signals of two Higgs bosons, which are close in mass, can play an important role, especially for search channels with a low mass resolution.

The investigations of the predictions for the LHC run at 13 TeV, which is currently in progress, on the one hand showed that if the NMSSM is realized in nature, the prospects of discovering at least one of the additional Higgs bosons are good. On the other hand, the discovery of the heavy Higgs states is challenging and there are also scenarios that might not be accessible at all. Still, even if no further Higgs states are discovered, it is unlikely that the NMSSM will be completely ruled out, as the parameter space of the general NMSSM is vast. However, it will be possible to severely constrain important subspaces. But to do so it might be necessary to take into account search channels including non-SM decays. We explicitly discussed decay chains involving Higgs-to-Higgs decays. Such decay chains can lead to exotic final states with sizeable signals. The most interesting one we found was a six photon final state. Moreover, the consideration of Higgs-to-Higgs decays could in the future also give access to the Higgs self-couplings. For now the experiments have already started to search for new scalar resonances that decay into the observed Higgs boson (see e.g. [209–211]). Hence, we have very interesting times ahead of us as the search for new physics continues at the LHC.

APPENDIX A

Loop Functions

The D dimensional one-loop integrals we encounter in our calculation are the vacuum integral A_0, the scalar two-point function B_0 and the coefficient of the two-point tensor integral of rank one B_1. Following the `LoopTools` [108] convention they are defined as

$$A_0(m^2) = 16\pi^2 \mu_R^{4-D} \int \frac{d^D q}{\mathrm{i}(2\pi)^D} \frac{1}{(q^2 - m^2)} \,, \tag{A.1}$$

$$B_0(p^2, m_1^2, m_2^2) = 16\pi^2 \mu_R^{4-D} \int \frac{d^D q}{\mathrm{i}(2\pi)^D} \frac{1}{(q^2 - m_1^2)((q+p)^2 - m_2^2)} \,, \tag{A.2}$$

$$p_\mu B_1(p^2, m_1^2, m_2^2) = 16\pi^2 \mu_R^{4-D} \int \frac{d^D q}{\mathrm{i}(2\pi)^D} \frac{q_\mu}{(q^2 - m_1^2)((q+p)^2 - m_2^2)} \,. \tag{A.3}$$

Here μ_R is the scale, which has to be introduced when the momentum integration is extended from 4 to D dimensions to ensure the correct dimensionality of the integral. The external momentum is denoted by p, while m, m_1 and m_2 are the masses of the loop particles.

Performing the integral yields

$$A_0(m^2) = m^2 \left(\Delta - \ln \frac{m^2}{\mu_R^2} + 1 \right) + \mathcal{O}(D-4) \quad \text{with} \quad \Delta = \frac{2}{4-D} - \gamma_E + \ln 4\pi \,, \tag{A.4}$$

where $\gamma_E \approx 0.5772$ is the Euler-Mascheroni constant. The divergence that occurs in the limit $D \to 4$ is absorbed in Δ together with a finite contribution. All contributions proportional to Δ will cancel in the calculation of a physical observable. For the scalar two-point function one obtains

$$B_0(p^2, m_1^2, m_2^2) = \Delta - \ln \frac{p^2}{\mu_R^2} - f_B(x_+) - f_B(x_-) + \mathcal{O}(D-4) \tag{A.5}$$

$$\text{with} \quad f_B(x) = \ln(1-x) - x \ln(1 - x^{-1}) - 1 \,,$$

$$x_\pm = \frac{s \pm \sqrt{s^2 - 4p^2(m_1^2 - \mathrm{i}\epsilon)}}{2p^2} \quad \text{and} \quad s = p^2 - m_2^2 + m_1^2 \,.$$

Finally, the tensor coefficient can be expressed in terms of A_0 and B_0 according to

$$B_1(p^2, m_1^2, m_2^2) = \frac{1}{2p^2}\Big[A_0(m_1^2) - A_0(m_2^2) - (p^2 - m_2^2 + m_1^2)B_0(p^2, m_1^2, m_2^2)\Big] \,. \tag{A.6}$$

The two-loop vacuum integral in D dimensions is defined as

$$I(m_1^2, m_2^2, m_3^2) = \left(16\pi^2 \mu_R^{4-D}\right)^2 \int \frac{d^D q_1}{\mathrm{i}(2\pi)^D} \frac{d^D q_2}{\mathrm{i}(2\pi)^D} \frac{1}{(q_1^2 - m_1^2)(q_2^2 - m_2^2)((q_1 - q_2)^2 - m_3^2)} \,. \tag{A.7}$$

An analytic form of this two-loop integral exists, both for the finite part as well as for the parts that diverge in the limit $D \to 4$. The respective expressions can be found in the literature [129–135].

APPENDIX B

Running of the Top Mass

For our calculation we require the running $\overline{\text{DR}}$ top mass at the renormalization scale, which we choose to be equal to the SUSY scale M_{SUSY}. First the pole mass is converted to the running $\overline{\text{MS}}$ mass at the scale of the pole mass using the two-loop SM formula [212]

$$m_t^{\overline{\text{MS}}}(M_t) = \left(1 - \frac{4}{3}\left(\frac{\alpha_s(M_t)}{\pi}\right) - 9.1253\left(\frac{\alpha_s(M_t)}{\pi}\right)^2\right) M_t \,, \tag{B.1}$$

where M_t denotes the top pole mass and $m^{\overline{\text{MS}}}$ is the running $\overline{\text{MS}}$ mass.

Then the $\overline{\text{MS}}$ mass is evolved to the SUSY scale via

$$m_t^{\overline{\text{MS}}}(M_{\text{SUSY}}) = U_6(M_{\text{SUSY}}, M_t) m_t^{\overline{\text{MS}}}(M_t) \quad \text{for } M_{\text{SUSY}} > M_t \,, \tag{B.2}$$

where the factor U_n is evaluated for six flavors (i.e. $n = 6$) and is given by [213]

$$U_n(Q_2, Q_1) = \left(\frac{\alpha_s(Q_2)}{\alpha_s(Q_1)}\right)^{d_n} \left[1 + \frac{\alpha_s(Q_1) - \alpha_s(Q_2)}{4\pi} J_n\right] \,, \qquad Q_2 > Q_1 \tag{B.3}$$

$$\text{with} \quad d_n = \frac{12}{33 - 2n} \quad \text{and} \qquad J_n = -\frac{8982 - 504n + 40n^2}{3(33 - 2n)^2} \,.$$

The thus obtained $\overline{\text{MS}}$ mass is converted to the corresponding $\overline{\text{DR}}$ mass according to the two-loop formula[1] [216]

$$m_t^{\overline{\text{DR}},\text{SM}}(M_{\text{SUSY}}) = m_t^{\overline{\text{MS}}}(M_{\text{SUSY}}) \left[1 - \frac{\alpha_s(M_{\text{SUSY}})}{3\pi} - \frac{\alpha_s^2(M_{\text{SUSY}})}{144\pi^2}(73 - 3n)\right] \,. \tag{B.4}$$

Finally, the SUSY corrections are included at the SUSY scale which yields the running $\overline{\text{DR}}$ mass in the supersymmetric theory

$$m_t^{\overline{\text{DR}},\text{NMSSM}} = m_t^{\overline{\text{DR}},\text{SM}}(M_{\text{SUSY}}) + dm_t \,. \tag{B.5}$$

[1] The relation is applied at the SUSY scale, where the full supersymmetric theory holds and the evanescent coupling α_e can be identified with the $\overline{\text{DR}}$ coupling $\alpha_s^{\overline{\text{DR}}}$ [214, 215].

The SUSY corrections involve stops and gluinos in the loop and are given by

$$\begin{aligned} dm_t =& \frac{\alpha_s(M_{\text{SUSY}})}{6\pi}\Big[-2m_t \text{Re}\Big(B_1(m_t^2, m_{\tilde{g}}^2, m_{\tilde{t}_1}^2) + B_1(m_t^2, m_{\tilde{g}}^2, m_{\tilde{t}_2}^2)\Big) \\ &+ 2m_{\tilde{g}} \text{Re}\left(B_0(m_t^2, m_{\tilde{g}}^2, m_{\tilde{t}_1}^2) - B_0(m_t^2, m_{\tilde{g}}^2, m_{\tilde{t}_2}^2)\right) \\ &\times (e^{i(\varphi_{M_3}+\varphi_u)} \mathcal{U}_{\tilde{t}_{22}} \mathcal{U}^*_{\tilde{t}_{21}} + e^{-i(\varphi_{M_3}+\varphi_u)} \mathcal{U}_{\tilde{t}_{21}} \mathcal{U}^*_{\tilde{t}_{22}})\Big] . \end{aligned} \tag{B.6}$$

Here B_0 and B_1 are the loop functions as defined in App. A, $m_{\tilde{t}_1}$ and $m_{\tilde{t}_2}$ are the stop masses and $m_{\tilde{g}}$ is the gluino mass, which is given by the absolute value of the soft SUSY breaking parameter M_3. Furthermore, the phase of M_3, the phase φ_u and the mixing matrix of the stop sector as defined in Eq. (9.10) enter the SUSY corrections.

APPENDIX C

Higgs Counterterm Mass Matrix at Two-Loop Level

Here we give the finite contributions of the counterterm mass matrix at the order $\alpha_s\alpha_t$. We explicitly dropped counterterms that only include a divergent part. In any case the only non-vanishing $\overline{\text{DR}}$ counterterms of the order $\alpha_s\alpha_t$ are those of $|\lambda|$ and $\tan\beta$. And as we argued earlier in Sec. 9.4, it can be shown analytically that the divergent contributions from the counterterms, which are related to the wavefunction renormalization constant $\delta^{(2)}Z_{H_u}$, cancel against the contributions of the wavefunction renormalization terms in the renormalized Higgs self-energy in most of the components anyway – only one contribution in the $h_d h_s$ component is left. Therefore, we restrict ourselves to the two-loop counterterms $\delta^{(2)}M^2_{H^\pm}$, $\delta^{(2)}v$, $\delta^{(2)}t_{h_u}$, $\delta^{(2)}t_{h_d}$, $\delta^{(2)}t_{h_s}$, $\delta^{(2)}t_{a_d}$ and $\delta^{(2)}t_{a_s}$, which yield finite contributions. The symmetric counterterm mass matrix is given in the basis of the interaction eigenstates.

$$\begin{aligned}\delta^{(2)}\mathcal{M}_{\text{Higgs}}\big|^{\text{fin}}_{h_d h_d} =&\delta^{(2)}v\, v|\lambda|^2\sin^2\beta + \delta^{(2)}M^2_{H^\pm}\sin^2\beta + \\ &+\frac{\delta^{(2)}t_{h_d}\left(1-\sin^4\beta\right)}{v\cos\beta} - \frac{\delta^{(2)}t_{h_u}\sin\beta\cos^2\beta}{v}\,,\end{aligned} \tag{C.1}$$

$$\delta^{(2)}\mathcal{M}_{\text{Higgs}}\big|^{\text{fin}}_{h_d h_u} =\delta^{(2)}v\, v|\lambda|^2\sin\beta\cos\beta - \delta^{(2)}M^2_{H^\pm}\sin\beta\cos\beta + \frac{\delta^{(2)}t_{h_d}\sin^3\beta}{v} + \frac{\delta^{(2)}t_{h_u}\cos^3\beta}{v}\,, \tag{C.2}$$

$$\begin{aligned}\delta^{(2)}\mathcal{M}_{\text{Higgs}}\big|^{\text{fin}}_{h_d h_s} =&\frac{\delta^{(2)}v\,\left(|\lambda|^2\cos\beta\left(2v_s^2-3v^2\sin^2\beta\right) - \sin\beta\left(v_s^2|\kappa||\lambda|\cos\varphi_y + \sin 2\beta\, M^2_{H^\pm}\right)\right)}{2v_s} + \\ &-\frac{\delta^{(2)}M^2_{H^\pm}v\sin^2\beta\cos\beta}{v_s} + \frac{\delta^{(2)}t_{h_d}\sin^4\beta}{v_s} + \frac{\delta^{(2)}t_{h_u}\sin\beta\cos^3\beta}{v_s}\,,\end{aligned} \tag{C.3}$$

$$\delta^{(2)}\mathcal{M}_{\text{Higgs}}\big|^{\text{fin}}_{h_d a} =\frac{\delta^{(2)}t_{a_d}}{v\tan\beta}\,, \tag{C.4}$$

$$\delta^{(2)}\mathcal{M}_{\text{Higgs}}\big|^{\text{fin}}_{h_d a_s} = \frac{\delta^{(2)} t_{a_d}}{v_s} - \frac{3}{2}\delta^{(2)} v\, v_s |\kappa||\lambda| \sin\beta \sin\varphi_y \,, \tag{C.5}$$

$$\begin{aligned}\delta^{(2)}\mathcal{M}_{\text{Higgs}}\big|^{\text{fin}}_{h_u h_u} =& \delta^{(2)} v\, v|\lambda|^2 \cos^2\beta + \delta^{(2)} M^2_{H^\pm} \cos^2\beta + \\ & - \frac{\delta^{(2)} t_{h_d} \sin^2\beta \cos\beta}{v} + \frac{\delta^{(2)} t_{h_u}(5\sin\beta + \sin 3\beta)}{4v} \,,\end{aligned} \tag{C.6}$$

$$\begin{aligned}\delta^{(2)}\mathcal{M}_{\text{Higgs}}\big|^{\text{fin}}_{h_u h_s} =& \frac{\delta^{(2)} v\, \left(\sin\beta \left(|\lambda|^2 \left(2v_s^2 - 3v^2\cos^2\beta\right) - 2\cos^2\beta M^2_{H^\pm}\right) - v_s^2 |\kappa||\lambda| \cos\beta\cos\varphi_y\right)}{2 v_s} + \\ & - \frac{\delta^{(2)} M^2_{H^\pm} v \sin\beta\cos^2\beta}{v_s} + \frac{\delta^{(2)} t_{h_d} \sin^3\beta\cos\beta}{v_s} + \frac{\delta^{(2)} t_{h_u}\cos^4\beta}{v_s} \,,\end{aligned} \tag{C.7}$$

$$\delta^{(2)}\mathcal{M}_{\text{Higgs}}\big|^{\text{fin}}_{h_u a} = \frac{\delta^{(2)} t_{a_d}}{v} \,, \tag{C.8}$$

$$\delta^{(2)}\mathcal{M}_{\text{Higgs}}\big|^{\text{fin}}_{h_u a_s} = \frac{\delta^{(2)} t_{a_d}}{v_s \tan\beta} - \frac{3}{2}\delta^{(2)} v\, v_s |\kappa||\lambda| \cos\beta \sin\varphi_y \,, \tag{C.9}$$

$$\begin{aligned}\delta^{(2)}\mathcal{M}_{\text{Higgs}}\big|^{\text{fin}}_{h_s h_s} =& \frac{\delta^{(2)} v v}{2 v_s^2}\Big(\sin^2 2\beta \big(v^2|\lambda|^2 + M^2_{H^\pm}\big) + v_s^2 |\kappa||\lambda| \big(3\sin 2\beta \sin\varphi_y \tan\varphi'_z + \\ & - 2\sin\beta\cos\beta\cos\varphi_y\big)\Big) + \frac{\delta^{(2)} M^2_{H^\pm} v^2 \sin^2\beta\cos^2\beta}{v_s^2} + \\ & - \frac{\delta^{(2)} t_{a_d} v\cos\beta\tan\varphi'_z}{v_s^2} + \frac{\delta^{(2)} t_{a_s}\tan\varphi'_z}{v_s} + \\ & - \frac{\delta^{(2)} t_{h_d} v \sin^4\beta\cos\beta}{v_s^2} + \frac{\delta^{(2)} t_{h_s}}{v_s} - \frac{\delta^{(2)} t_{h_u} v \sin\beta\cos^4\beta}{v_s^2} \,,\end{aligned} \tag{C.10}$$

$$\delta^{(2)}\mathcal{M}_{\text{Higgs}}\big|^{\text{fin}}_{h_s a} = \frac{1}{2}\delta^{(2)} v\, v_s |\kappa||\lambda| \sin\varphi_y + \frac{\delta^{(2)} t_{a_d}}{v_s \sin\beta} \,, \tag{C.11}$$

$$\delta^{(2)}\mathcal{M}_{\text{Higgs}}\big|^{\text{fin}}_{h_s a_s} = 2\delta^{(2)} v\, v|\kappa||\lambda| \sin 2\beta \sin\varphi_y - \frac{2\delta^{(2)} t_{a_d} v\cos\beta}{v_s^2} + \frac{2\delta^{(2)} t_{a_s}}{v_s} \,, \tag{C.12}$$

$$\delta^{(2)}\mathcal{M}_{\text{Higgs}}\big|^{\text{fin}}_{a\, a} = \delta^{(2)} v\, v|\lambda|^2 + \delta^{(2)} M^2_{H^\pm} \,, \tag{C.13}$$

$$\begin{aligned}\delta^{(2)}\mathcal{M}_{\text{Higgs}}\big|^{\text{fin}}_{a\, a_s} =& \frac{\delta^{(2)} v\, \left(\sin 2\beta \left(3v^2|\lambda|^2 + 2M^2_{H^\pm}\right) - 6 v_s^2 |\kappa||\lambda| \cos\varphi_y\right)}{4 v_s} + \frac{\delta^{(2)} M^2_{H^\pm} v \sin\beta\cos\beta}{v_s} + \\ & - \frac{\delta^{(2)} t_{h_d}\sin^3\beta}{v_s} - \frac{\delta^{(2)} t_{h_u}\cos^3\beta}{v_s} \,,\end{aligned} \tag{C.14}$$

$$\delta^{(2)}\mathcal{M}_{\text{Higgs}}\Big|^{\text{fin}}_{a_s a_s} = \frac{\delta^{(2)} v v \sin 2\beta}{2 v_s^2}\Big(\sin 2\beta \big(v^2 |\lambda|^2 + M_{H^\pm}^2 \big) + \\ + 3 v_s^2 |\kappa| |\lambda| \big(\cos\varphi_y - 3 \sin\varphi_y \tan\varphi_z' \big) \Big) + \frac{\delta^{(2)} M_{H^\pm}^2 v^2 \sin^2\beta \cos^2\beta}{v_s^2} + \\ + \frac{3\delta^{(2)} t_{a_d} v \cos\beta \tan\varphi_z'}{v_s^2} - \frac{3\delta^{(2)} t_{a_s} \tan\varphi_z'}{v_s} + \\ - \frac{\delta^{(2)} t_{h_d} v \sin^4\beta \cos\beta}{v_s^2} + \frac{\delta^{(2)} t_{h_s}}{v_s} - \frac{\delta^{(2)} t_{h_u} v \sin\beta \cos^4\beta}{v_s^2} \,. \tag{C.15}$$

Acknowledgments

First of all, I would like to thank Prof. Dr. Margarete Mühlleitner for offering me the opportunity to work on this interesting topic. She was always very supportive and also gave me the opportunity to attend interesting conferences and schools. I am especially grateful for her tremendous support when it came to preparing publications.

Thanks go also to Prof. Dr. Matthias Steinhauser for acting as the second reviewer of this thesis.

I am also greatly in debt to my collaborators Julien Baglio, Ramona Gröber, Steve King, Roman Nevzorov, Dao Thi Nhung, Heidi Rzehak and Juraj Streicher. I really enjoyed working with them. Without their help and all the productive discussions this thesis would not exist.

For their careful proofreading of this manuscript I thank Johannes Bellm, Manfred Ender, Hanna Hoffmann, Juraj Streicher, Michael Walz and Alexander Wlotzka.

Furthermore, I would like to express my gratitude to the whole institute for the great atmosphere during the last four years I spent here. Special thanks go to my office mates Johannes Bellm, Bastian Feigel, Christian Hangst and Genessis Perez.

My funding during this PhD thesis was provided by "Graduiertenkolleg KIT, GRK 1694, Elementarteilchenphysik bei höchster Energie und höchster Präzision". I also acknowledge support by "Karlsruhe School of Elementary Particle and Astroparticle Physics: Science and Technology (KSETA)".

Finally, many many thanks to my family for the moral and emotional support they provide.

References

[1] **ATLAS** Collaboration, G. Aad *et al.*, *Observation of a new particle in the search for the Standard Model Higgs boson with the ATLAS detector at the LHC*. Phys.Lett. **B716** (2012) 1–29, arXiv:1207.7214.

[2] **CMS** Collaboration, S. Chatrchyan *et al.*, *Observation of a new boson at a mass of 125 GeV with the CMS experiment at the LHC*. Phys.Lett. **B716** (2012) 30–61, arXiv:1207.7235.

[3] **ATLAS** Collaboration, *Measurements of the Higgs boson production and decay rates and coupling strengths using pp collision data at $\sqrt{s} = 7$ and 8 TeV in the ATLAS experiment*.

[4] **CMS** Collaboration, V. Khachatryan *et al.*, *Precise determination of the mass of the Higgs boson and tests of compatibility of its couplings with the standard model predictions using proton collisions at 7 and 8 TeV*. arXiv:1412.8662.

[5] K. Ender, T. Graf, M. Mühlleitner, and H. Rzehak, *Analysis of the NMSSM Higgs Boson Masses at One-Loop Level*. Phys.Rev. **D85** (2012) 075024, arXiv:1111.4952.

[6] T. Graf, R. Gröber, M. Mühlleitner, H. Rzehak, and K. Walz, *Higgs Boson Masses in the Complex NMSSM at One-Loop Level*. JHEP **1210** (2012) 122, arXiv:1206.6806.

[7] M. Mühlleitner, D. T. Nhung, H. Rzehak, and K. Walz, *Two-loop contributions of the order $\mathcal{O}(\alpha_t \alpha_s)$ to the masses of the Higgs bosons in the CP-violating NMSSM*. JHEP **1505** (2015) 128, arXiv:1412.0918.

[8] J. Baglio, R. Gröber, M. Mühlleitner, D. Nhung, H. Rzehak, *et al.*, *NMSSMCALC: A Program Package for the Calculation of Loop-Corrected Higgs Boson Masses and Decay Widths in the (Complex) NMSSM*. Comput.Phys.Commun. **185** (2014) no. 12, 3372–3391, arXiv:1312.4788.

[9] S. King, M. Mühlleitner, R. Nevzorov, and K. Walz, *Natural NMSSM Higgs Bosons*. Nucl.Phys. **B870** (2013) 323–352, arXiv:1211.5074.

[10] S. King, M. Mühlleitner, R. Nevzorov, and K. Walz, *Discovery Prospects for NMSSM Higgs Bosons at the High-Energy Large Hadron Collider*. Phys.Rev. **D90** (2014) no. 9, 095014, arXiv:1408.1120.

[11] C. Englert, A. Freitas, M. Mühlleitner, T. Plehn, M. Rauch, M. Spira, and K. Walz, *Precision Measurements of Higgs Couplings: Implications for New Physics Scales*. J.Phys. **G41** (2014) 113001, arXiv:1403.7191.

[12] D. T. Nhung, M. Mühlleitner, J. Streicher, and K. Walz, *Higher Order Corrections to the Trilinear Higgs Self-Couplings in the Real NMSSM*. JHEP **1311** (2013) 181, arXiv:1306.3926.

[13] J. Streicher, *NMSSM Higgs boson self-couplings at next-to-leading-order*. Diploma thesis **Karlsruhe Institute of Technology** (2012) .

[14] J. Baglio, C. Krauß, M. Mühlleitner, and K. Walz, *Next-to-Leading Order NMSSM Decays with CP-odd Higgs Bosons and Stops*. submitted to JHEP (2015) , arXiv:1505.07125.

[15] C.-O. Krauß, *Zerfall des pseudoskalaren Higgs-Bosons in Stops im reellen NMSSM*. Diploma thesis **Karlsruhe Institute of Technology** (2014) .

[16] S. Glashow, *Partial Symmetries of Weak Interactions*. Nucl.Phys. **22** (1961) 579–588.

[17] S. Weinberg, *A Model of Leptons*. Phys.Rev.Lett. **19** (1967) 1264–1266.

[18] A. Salam, *Weak and Electromagnetic Interactions*. Conf.Proc. **C680519** (1968) 367–377.

[19] S. Glashow, J. Iliopoulos, and L. Maiani, *Weak Interactions with Lepton-Hadron Symmetry*. Phys.Rev. **D2** (1970) 1285–1292.

[20] N. Cabibbo, *Unitary Symmetry and Leptonic Decays*. Phys.Rev.Lett. **10** (1963) 531–533.

[21] M. Kobayashi and T. Maskawa, *CP Violation in the Renormalizable Theory of Weak Interaction*. Prog.Theor.Phys. **49** (1973) 652–657.

[22] P. W. Higgs, *Broken symmetries, massless particles and gauge fields*. Phys.Lett. **12** (1964) 132–133.

[23] P. W. Higgs, *Broken Symmetries and the Masses of Gauge Bosons*. Phys.Rev.Lett. **13** (1964) 508–509.

[24] P. W. Higgs, *Spontaneous Symmetry Breakdown without Massless Bosons*. Phys.Rev. **145** (1966) 1156–1163.

[25] F. Englert and R. Brout, *Broken Symmetry and the Mass of Gauge Vector Mesons*. Phys.Rev.Lett. **13** (1964) 321–322.

[26] T. Kibble, *Symmetry breaking in nonAbelian gauge theories*. Phys.Rev. **155** (1967) 1554–1561.

[27] **Planck** Collaboration, P. Ade *et al.*, *Planck 2013 results. I. Overview of products and scientific results*. Astron.Astrophys. **571** (2014) A1, arXiv:1303.5062.

[28] **Particle Data Group** Collaboration, K. Olive *et al.*, *Review of Particle Physics*. Chin.Phys. **C38** (2014) 090001.

[29] E. Witten, *Mass Hierarchies in Supersymmetric Theories*. Phys.Lett. **B105** (1981) 267.

[30] J. Polchinski and L. Susskind, *Breaking of Supersymmetry at Intermediate-Energy.* Phys.Rev. **D26** (1982) 3661.

[31] S. Dimopoulos and H. Georgi, *Softly Broken Supersymmetry and SU(5).* Nucl.Phys. **B193** (1981) 150.

[32] N. Sakai, *Naturalness in Supersymmetric Guts.* Z.Phys. **C11** (1981) 153.

[33] D. Volkov and V. Akulov, *Is the Neutrino a Goldstone Particle?* Phys.Lett. **B46** (1973) 109–110.

[34] J. Wess and B. Zumino, *Supergauge Transformations in Four-Dimensions.* Nucl.Phys. **B70** (1974) 39–50.

[35] P. Fayet, *Supersymmetry and Weak, Electromagnetic and Strong Interactions.* Phys.Lett. **B64** (1976) 159.

[36] P. Fayet, *Spontaneously Broken Supersymmetric Theories of Weak, Electromagnetic and Strong Interactions.* Phys.Lett. **B69** (1977) 489.

[37] P. Fayet, *Relations Between the Masses of the Superpartners of Leptons and Quarks, the Goldstino Couplings and the Neutral Currents.* Phys.Lett. **B84** (1979) 416.

[38] G. R. Farrar and P. Fayet, *Phenomenology of the Production, Decay, and Detection of New Hadronic States Associated with Supersymmetry.* Phys.Lett. **B76** (1978) 575–579.

[39] E. Witten, *Dynamical Breaking of Supersymmetry.* Nucl.Phys. **B188** (1981) 513.

[40] H. P. Nilles, *Supersymmetry, Supergravity and Particle Physics.* Phys.Rept. **110** (1984) 1–162.

[41] H. E. Haber and G. L. Kane, *The Search for Supersymmetry: Probing Physics Beyond the Standard Model.* Phys.Rept. **117** (1985) 75–263.

[42] M. Sohnius, *Introducing Supersymmetry.* Phys.Rept. **128** (1985) 39–204.

[43] J. Gunion and H. E. Haber, *Higgs Bosons in Supersymmetric Models. 1.* Nucl.Phys. **B272** (1986) 1.

[44] J. Gunion and H. E. Haber, *Higgs Bosons in Supersymmetric Models. 2. Implications for Phenomenology.* Nucl.Phys. **B278** (1986) 449.

[45] A. Lahanas and D. V. Nanopoulos, *The Road to No Scale Supergravity.* Phys.Rept. **145** (1987) 1.

[46] S. R. Coleman and J. Mandula, *All Possible Symmetries of the S Matrix.* Phys.Rev. **159** (1967) 1251–1256.

[47] R. Haag, J. T. Lopuszanski, and M. Sohnius, *All Possible Generators of Supersymmetries of the s Matrix.* Nucl.Phys. **B88** (1975) 257.

[48] J. R. Ellis, S. Kelley, and D. V. Nanopoulos, *Probing the desert using gauge coupling unification.* Phys.Lett. **B260** (1991) 131–137.

[49] C. Giunti, C. Kim, and U. Lee, *Running coupling constants and grand unification models.* Mod.Phys.Lett. **A6** (1991) 1745–1755.

[50] P. Fayet, *Supergauge Invariant Extension of the Higgs Mechanism and a Model for the electron and Its Neutrino.* Nucl.Phys. **B90** (1975) 104–124.

[51] R. Barbieri, S. Ferrara, and C. A. Savoy, *Gauge Models with Spontaneously Broken Local Supersymmetry*. Phys.Lett. **B119** (1982) 343.

[52] M. Dine, W. Fischler, and M. Srednicki, *A Simple Solution to the Strong CP Problem with a Harmless Axion*. Phys.Lett. **B104** (1981) 199.

[53] H. P. Nilles, M. Srednicki, and D. Wyler, *Weak Interaction Breakdown Induced by Supergravity*. Phys.Lett. **B120** (1983) 346.

[54] J. Frere, D. Jones, and S. Raby, *Fermion Masses and Induction of the Weak Scale by Supergravity*. Nucl.Phys. **B222** (1983) 11.

[55] J. Derendinger and C. A. Savoy, *Quantum Effects and SU(2) x U(1) Breaking in Supergravity Gauge Theories*. Nucl.Phys. **B237** (1984) 307.

[56] J. R. Ellis, J. Gunion, H. E. Haber, L. Roszkowski, and F. Zwirner, *Higgs Bosons in a Nonminimal Supersymmetric Model*. Phys.Rev. **D39** (1989) 844.

[57] M. Drees, *Supersymmetric Models with Extended Higgs Sector*. Int.J.Mod.Phys. **A4** (1989) 3635.

[58] U. Ellwanger, M. Rausch de Traubenberg, and C. A. Savoy, *Particle spectrum in supersymmetric models with a gauge singlet*. Phys.Lett. **B315** (1993) 331–337, arXiv:hep-ph/9307322.

[59] U. Ellwanger, M. Rausch de Traubenberg, and C. A. Savoy, *Higgs phenomenology of the supersymmetric model with a gauge singlet*. Z.Phys. **C67** (1995) 665–670, arXiv:hep-ph/9502206.

[60] U. Ellwanger, M. Rausch de Traubenberg, and C. A. Savoy, *Phenomenology of supersymmetric models with a singlet*. Nucl.Phys. **B492** (1997) 21–50, arXiv:hep-ph/9611251.

[61] T. Elliott, S. King, and P. White, *Unification constraints in the next-to-minimal supersymmetric standard model*. Phys.Lett. **B351** (1995) 213–219, arXiv:hep-ph/9406303.

[62] S. King and P. White, *Resolving the constrained minimal and next-to-minimal supersymmetric standard models*. Phys.Rev. **D52** (1995) 4183–4216, arXiv:hep-ph/9505326.

[63] F. Franke and H. Fraas, *Neutralinos and Higgs bosons in the next-to-minimal supersymmetric standard model*. Int.J.Mod.Phys. **A12** (1997) 479–534, arXiv:hep-ph/9512366.

[64] M. Maniatis, *The Next-to-Minimal Supersymmetric extension of the Standard Model reviewed*. Int.J.Mod.Phys. **A25** (2010) 3505–3602, arXiv:0906.0777.

[65] U. Ellwanger, C. Hugonie, and A. M. Teixeira, *The Next-to-Minimal Supersymmetric Standard Model*. Phys.Rept. **496** (2010) 1–77, arXiv:0910.1785.

[66] J. E. Kim and H. P. Nilles, *The mu Problem and the Strong CP Problem*. Phys.Lett. **B138** (1984) 150.

[67] S. Weinberg, *A New Light Boson?* Phys.Rev.Lett. **40** (1978) 223–226.

[68] D. Miller, R. Nevzorov, and P. Zerwas, *The Higgs sector of the next-to-minimal supersymmetric standard model*. Nucl.Phys. **B681** (2004) 3–30, arXiv:hep-ph/0304049.

[69] P. Z. Skands, B. Allanach, H. Baer, C. Balazs, G. Belanger, *et al.*, *SUSY Les Houches accord: Interfacing SUSY spectrum calculators, decay packages, and event generators.* JHEP **0407** (2004) 036, arXiv:hep-ph/0311123.

[70] B. Allanach, C. Balazs, G. Belanger, M. Bernhardt, F. Boudjema, *et al.*, *SUSY Les Houches Accord 2.* Comput.Phys.Commun. **180** (2009) 8–25, arXiv:0801.0045.

[71] M. Spira, *HIGLU: A program for the calculation of the total Higgs production cross-section at hadron colliders via gluon fusion including QCD corrections.* arXiv:hep-ph/9510347.

[72] M. Spira, *HIGLU and HDECAY: Programs for Higgs boson production at the LHC and Higgs boson decay widths.* Nucl.Instrum.Meth. **A389** (1997) 357–360, arXiv:hep-ph/9610350.

[73] U. Ellwanger, J. F. Gunion, and C. Hugonie, *NMHDECAY: A Fortran code for the Higgs masses, couplings and decay widths in the NMSSM.* JHEP **0502** (2005) 066, arXiv:hep-ph/0406215.

[74] U. Ellwanger and C. Hugonie, *NMHDECAY 2.0: An Updated program for sparticle masses, Higgs masses, couplings and decay widths in the NMSSM.* Comput.Phys.Commun. **175** (2006) 290–303, arXiv:hep-ph/0508022.

[75] U. Ellwanger and C. Hugonie, *NMSPEC: A Fortran code for the sparticle and Higgs masses in the NMSSM with GUT scale boundary conditions.* Comput.Phys.Commun. **177** (2007) 399–407, arXiv:hep-ph/0612134.

[76] **ATLAS** Collaboration, G. Aad *et al.*, *Search for Scalar Diphoton Resonances in the Mass Range* $65 - 600$ *GeV with the ATLAS Detector in pp Collision Data at* $\sqrt{s} = 8$ *TeV*. Phys.Rev.Lett. **113** (2014) no. 17, 171801, arXiv:1407.6583.

[77] R. Harlander, P. Kant, L. Mihaila, and M. Steinhauser, *Higgs boson mass in supersymmetry to three loops.* Phys.Rev.Lett. **100** (2008) 191602, arXiv:0803.0672.

[78] S. Borowka, T. Hahn, S. Heinemeyer, G. Heinrich, and W. Hollik, *Momentum-dependent two-loop QCD corrections to the neutral Higgs-boson masses in the MSSM.* Eur.Phys.J. **C74** (2014) no. 8, 2994, arXiv:1404.7074.

[79] U. Ellwanger, *Radiative corrections to the neutral Higgs spectrum in supersymmetry with a gauge singlet.* Phys.Lett. **B303** (1993) 271–276, arXiv:hep-ph/9302224.

[80] T. Elliott, S. King, and P. White, *Supersymmetric Higgs bosons at the limit.* Phys.Lett. **B305** (1993) 71–77, arXiv:hep-ph/9302202.

[81] T. Elliott, S. King, and P. White, *Squark contributions to Higgs boson masses in the next-to-minimal supersymmetric standard model.* Phys.Lett. **B314** (1993) 56–63, arXiv:hep-ph/9305282.

[82] P. Pandita, *Radiative corrections to the scalar Higgs masses in a nonminimal supersymmetric Standard Model.* Z.Phys. **C59** (1993) 575–584.

[83] T. Elliott, S. King, and P. White, *Radiative corrections to Higgs boson masses in the next-to-minimal supersymmetric Standard Model.* Phys.Rev. **D49** (1994) 2435–2456, arXiv:hep-ph/9308309.

[84] U. Ellwanger and C. Hugonie, *Yukawa induced radiative corrections to the lightest Higgs boson mass in the NMSSM.* Phys.Lett. **B623** (2005) 93–103, arXiv:hep-ph/0504269.

[85] G. Degrassi and P. Slavich, *On the radiative corrections to the neutral Higgs boson masses in the NMSSM*. Nucl.Phys. **B825** (2010) 119–150, arXiv:0907.4682.

[86] F. Staub, W. Porod, and B. Herrmann, *The Electroweak sector of the NMSSM at the one-loop level*. JHEP **1010** (2010) 040, arXiv:1007.4049.

[87] M. D. Goodsell, K. Nickel, and F. Staub, *On the two-loop corrections to the Higgs masses in the NMSSM*. arXiv:1411.4665.

[88] S. Ham, J. Kim, S. Oh, and D. Son, *The Charged Higgs boson in the next-to-minimal supersymmetric standard model with explicit CP violation*. Phys.Rev. **D64** (2001) 035007, arXiv:hep-ph/0104144.

[89] S. Ham, S. Oh, and D. Son, *Neutral Higgs sector of the next-to-minimal supersymmetric standard model with explicit CP violation*. Phys.Rev. **D65** (2002) 075004, arXiv:hep-ph/0110052.

[90] S. Ham, Y. Jeong, and S. Oh, *Radiative CP violation in the Higgs sector of the next-to-minimal supersymmetric model*. arXiv:hep-ph/0308264.

[91] K. Funakubo and S. Tao, *The Higgs sector in the next-to-MSSM*. Prog.Theor.Phys. **113** (2005) 821–842, arXiv:hep-ph/0409294.

[92] S. Ham, S. Kim, S. OH, and D. Son, *Higgs bosons of the NMSSM with explicit CP violation at the ILC*. Phys.Rev. **D76** (2007) 115013, arXiv:0708.2755.

[93] K. Cheung, T.-J. Hou, J. S. Lee, and E. Senaha, *The Higgs Boson Sector of the Next-to-MSSM with CP Violation*. Phys.Rev. **D82** (2010) 075007, arXiv:1006.1458.

[94] B. Allanach, *SOFTSUSY: a program for calculating supersymmetric spectra*. Comput.Phys.Commun. **143** (2002) 305–331, arXiv:hep-ph/0104145.

[95] B. Allanach, P. Athron, L. C. Tunstall, A. Voigt, and A. Williams, *Next-to-Minimal SOFTSUSY*. Comput.Phys.Commun. **185** (2014) 2322–2339, arXiv:1311.7659.

[96] F. Staub, *From Superpotential to Model Files for FeynArts and CalcHep/CompHep*. Comput.Phys.Commun. **181** (2010) 1077–1086, arXiv:0909.2863.

[97] F. Staub, *Automatic Calculation of supersymmetric Renormalization Group Equations and Self Energies*. Comput.Phys.Commun. **182** (2011) 808–833, arXiv:1002.0840.

[98] F. Staub, *SARAH 3.2: Dirac Gauginos, UFO output, and more*. Comput.Phys.Commun. **184** (2013) pp. 1792–1809, arXiv:1207.0906.

[99] F. Staub, *SARAH 4: A tool for (not only SUSY) model builders*. Comput.Phys.Commun. **185** (2014) 1773–1790, arXiv:1309.7223.

[100] W. Porod, *SPheno, a program for calculating supersymmetric spectra, SUSY particle decays and SUSY particle production at e+ e- colliders*. Comput.Phys.Commun. **153** (2003) 275–315, arXiv:hep-ph/0301101.

[101] W. Porod and F. Staub, *SPheno 3.1: Extensions including flavour, CP-phases and models beyond the MSSM*. Comput.Phys.Commun. **183** (2012) 2458–2469, arXiv:1104.1573.

[102] P. Athron, J.-h. Park, D. Stöckinger, and A. Voigt, *FlexibleSUSY – A spectrum generator generator for supersymmetric models*. arXiv:1406.2319.

[103] F. Domingo, *A New Tool for the study of the CP-violating NMSSM*. arXiv:1503.07087.

[104] M. Frank, T. Hahn, S. Heinemeyer, W. Hollik, H. Rzehak, *et al.*, *The Higgs Boson Masses and Mixings of the Complex MSSM in the Feynman-Diagrammatic Approach*. JHEP **0702** (2007) 047, arXiv:hep-ph/0611326.

[105] K. Williams and G. Weiglein, *Precise predictions for $h_a \to h_b h_c$ decays in the complex MSSM*. Phys.Lett. **B660** (2008) 217–227, arXiv:0710.5320.

[106] A.-K. Ender, *Analysis of the Higgs Boson Masses at One-Loop Level in the Complex NMSSM*. Diploma thesis **Karlsruhe Institute of Technology** (2011) .

[107] T. Hahn, *Generating Feynman diagrams and amplitudes with FeynArts 3*. Comput.Phys.Commun. **140** (2001) 418–431, arXiv:hep-ph/0012260.

[108] T. Hahn and M. Perez-Victoria, *Automatized one loop calculations in four-dimensions and D-dimensions*. Comput.Phys.Commun. **118** (1999) 153–165, arXiv:hep-ph/9807565.

[109] A. Denner, *Techniques for calculation of electroweak radiative corrections at the one loop level and results for W physics at LEP-200*. Fortsch.Phys. **41** (1993) 307–420, arXiv:0709.1075.

[110] K. E. Williams, H. Rzehak, and G. Weiglein, *Higher order corrections to Higgs boson decays in the MSSM with complex parameters*. Eur.Phys.J. **C71** (2011) 1669, arXiv:1103.1335.

[111] M. Steinhauser, *Leptonic contribution to the effective electromagnetic coupling constant up to three loops*. Phys.Lett. **B429** (1998) 158–161, arXiv:hep-ph/9803313.

[112] K. Hagiwara, A. Martin, D. Nomura, and T. Teubner, *Predictions for g-2 of the muon and alpha(QED) (M**2(Z))*. Phys.Rev. **D69** (2004) 093003, arXiv:hep-ph/0312250.

[113] A. Brignole, *Radiative corrections to the supersymmetric neutral Higgs boson masses*. Phys.Lett. **B281** (1992) 284–294.

[114] P. H. Chankowski, S. Pokorski, and J. Rosiek, *One loop corrections to the supersymmetric Higgs boson couplings and LEP phenomenology*. Phys.Lett. **B286** (1992) 307–314.

[115] P. H. Chankowski, S. Pokorski, and J. Rosiek, *Complete on-shell renormalization scheme for the minimal supersymmetric Higgs sector*. Nucl.Phys. **B423** (1994) 437–496, arXiv:hep-ph/9303309.

[116] A. Dabelstein, *The One loop renormalization of the MSSM Higgs sector and its application to the neutral scalar Higgs masses*. Z.Phys. **C67** (1995) 495–512, arXiv:hep-ph/9409375.

[117] A. Dabelstein, *Fermionic decays of neutral MSSM Higgs bosons at the one loop level*. Nucl.Phys. **B456** (1995) 25–56, arXiv:hep-ph/9503443.

[118] A. Freitas and D. Stockinger, *Gauge dependence and renormalization of tan beta in the MSSM*. Phys.Rev. **D66** (2002) 095014, arXiv:hep-ph/0205281.

[119] R. Mertig, M. Bohm, and A. Denner, *FEYN CALC: Computer algebraic calculation of Feynman amplitudes*. Comput.Phys.Commun. **64** (1991) 345–359.

[120] R. Mertig and R. Scharf, *TARCER: A Mathematica program for the reduction of two loop propagator integrals*. Comput.Phys.Commun. **111** (1998) 265–273, arXiv:hep-ph/9801383.

[121] O. Tarasov, *Connection between Feynman integrals having different values of the space-time dimension*. Phys.Rev. **D54** (1996) 6479–6490, arXiv:hep-th/9606018.

[122] O. Tarasov, *Generalized recurrence relations for two loop propagator integrals with arbitrary masses*. Nucl.Phys. **B502** (1997) 455–482, arXiv:hep-ph/9703319.

[123] D. Capper, D. Jones, and P. van Nieuwenhuizen, *Regularization by Dimensional Reduction of Supersymmetric and Nonsupersymmetric Gauge Theories*. Nucl.Phys. **B167** (1980) 479.

[124] W. Beenakker, R. Hopker, and P. Zerwas, *SUSY QCD decays of squarks and gluinos*. Phys.Lett. **B378** (1996) 159–166, arXiv:hep-ph/9602378.

[125] W. Hollik, E. Kraus, and D. Stockinger, *Renormalization and symmetry conditions in supersymmetric QED*. Eur.Phys.J. **C11** (1999) 365–381, arXiv:hep-ph/9907393.

[126] W. Hollik and D. Stockinger, *Regularization and supersymmetry restoring counterterms in supersymmetric QCD*. Eur.Phys.J. **C20** (2001) 105–119, arXiv:hep-ph/0103009.

[127] I. Fischer, W. Hollik, M. Roth, and D. Stockinger, *Restoration of supersymmetric Slavnov-Taylor and Ward identities in presence of soft and spontaneous symmetry breaking*. Phys.Rev. **D69** (2004) 015004, arXiv:hep-ph/0310191.

[128] W. Hollik and D. Stockinger, *MSSM Higgs-boson mass predictions and two-loop non-supersymmetric counterterms*. Phys.Lett. **B634** (2006) 63–68, arXiv:hep-ph/0509298.

[129] A. I. Davydychev and J. Tausk, *Two loop selfenergy diagrams with different masses and the momentum expansion*. Nucl.Phys. **B397** (1993) 123–142.

[130] C. Ford, I. Jack, and D. Jones, *The Standard model effective potential at two loops*. Nucl.Phys. **B387** (1992) 373–390, arXiv:hep-ph/0111190.

[131] R. Scharf and J. Tausk, *Scalar two loop integrals for gauge boson selfenergy diagrams with a massless fermion loop*. Nucl.Phys. **B412** (1994) 523–552.

[132] G. Weiglein, R. Scharf, and M. Bohm, *Reduction of general two loop selfenergies to standard scalar integrals*. Nucl.Phys. **B416** (1994) 606–644, arXiv:hep-ph/9310358.

[133] F. A. Berends and J. Tausk, *On the numerical evaluation of scalar two loop selfenergy diagrams*. Nucl.Phys. **B421** (1994) 456–470.

[134] S. P. Martin, *Two loop effective potential for a general renormalizable theory and softly broken supersymmetry*. Phys.Rev. **D65** (2002) 116003, arXiv:hep-ph/0111209.

[135] S. P. Martin and D. G. Robertson, *TSIL: A Program for the calculation of two-loop self-energy integrals*. Comput.Phys.Commun. **174** (2006) 133–151, arXiv:hep-ph/0501132.

[136] G. 't Hooft and M. Veltman, *Scalar One Loop Integrals*. Nucl.Phys. **B153** (1979) 365–401.

[137] S. Heinemeyer, W. Hollik, H. Rzehak, and G. Weiglein, *The Higgs sector of the complex MSSM at two-loop order: QCD contributions*. Phys.Lett. **B652** (2007) 300–309, arXiv:0705.0746.

[138] S. Heinemeyer, H. Rzehak, and C. Schappacher, *Proposals for Bottom Quark/Squark Renormalization in the Complex MSSM*. Phys.Rev. **D82** (2010) 075010, arXiv:1007.0689.

[139] U. Nierste, D. Muller, and M. Bohm, *Two loop relevant parts of D-dimensional massive scalar one loop integrals*. Z.Phys. **C57** (1993) 605–614.

[140] G. Degrassi, S. Di Vita, and P. Slavich, *Two-loop QCD corrections to the MSSM Higgs masses beyond the effective-potential approximation*. Eur.Phys.J. **C75** (2015) no. 2, 61, arXiv:1410.3432.

[141] M. Sperling, D. Stöckinger, and A. Voigt, *Renormalization of vacuum expectation values in spontaneously broken gauge theories*. JHEP **1307** (2013) 132, arXiv:1305.1548.

[142] M. Sperling, D. Stöckinger, and A. Voigt, *Renormalization of vacuum expectation values in spontaneously broken gauge theories: Two-loop results*. JHEP **1401** (2014) 068, arXiv:1310.7629.

[143] G. Weiglein, R. Mertig, R. Scharf, and M. Bohm, *Computer algebraic calculation of two loop selfenergies in the electroweak standard model*.

[144] A. Djouadi, J. Kalinowski, and M. Spira, *HDECAY: A Program for Higgs boson decays in the standard model and its supersymmetric extension*. Comput.Phys.Commun. **108** (1998) 56–74, arXiv:hep-ph/9704448.

[145] J. Butterworth, A. Arbey, L. Basso, S. Belov, A. Bharucha, *et al.*, *The Tools and Monte Carlo working group Summary Report*. arXiv:1003.1643.

[146] P. Bechtle, O. Brein, S. Heinemeyer, G. Weiglein, and K. E. Williams, *HiggsBounds: Confronting Arbitrary Higgs Sectors with Exclusion Bounds from LEP and the Tevatron*. Comput.Phys.Commun. **181** (2010) 138–167, arXiv:0811.4169.

[147] P. Bechtle, O. Brein, S. Heinemeyer, G. Weiglein, and K. E. Williams, *HiggsBounds 2.0.0: Confronting Neutral and Charged Higgs Sector Predictions with Exclusion Bounds from LEP and the Tevatron*. Comput.Phys.Commun. **182** (2011) 2605–2631, arXiv:1102.1898.

[148] P. Bechtle, O. Brein, S. Heinemeyer, O. Stål, T. Stefaniak, *et al.*, HiggsBounds – 4*: Improved Tests of Extended Higgs Sectors against Exclusion Bounds from LEP, the Tevatron and the LHC*. Eur.Phys.J. **C74** (2014) no. 3, 2693, arXiv:1311.0055.

[149] P. Bechtle, S. Heinemeyer, O. Stål, T. Stefaniak, and G. Weiglein, *HiggsSignals: Confronting arbitrary Higgs sectors with measurements at the Tevatron and the LHC*. Eur.Phys.J. **C74** (2014) no. 2, 2711, arXiv:1305.1933.

[150] **ATLAS** Collaboration, G. Aad *et al.*, *Search for top squark pair production in final states with one isolated lepton, jets, and missing transverse momentum in* $\sqrt{s}$ *=8 TeV pp collisions with the ATLAS detector*. JHEP **1411** (2014) 118, arXiv:1407.0583.

[151] **ATLAS** Collaboration, G. Aad *et al.*, *Search for light scalar top quark pair production in final states with two leptons with the ATLAS detector in* $\sqrt{s} = 7$ *TeV proton-proton collisions*. Eur.Phys.J. **C72** (2012) 2237, arXiv:1208.4305.

[152] **ATLAS** Collaboration, G. Aad *et al.*, *Search for light top squark pair production in final states with leptons and b^- jets with the ATLAS detector in $\sqrt{s} = 7$ TeV proton-proton collisions*. Phys.Lett. **B720** (2013) 13–31, arXiv:1209.2102.

[153] **ATLAS** Collaboration, G. Aad *et al.*, *Search for direct third-generation squark pair production in final states with missing transverse momentum and two b-jets in $\sqrt{s} = 8$ TeV pp collisions with the ATLAS detector*. JHEP **1310** (2013) 189, arXiv:1308.2631.

[154] **ATLAS** Collaboration, G. Aad *et al.*, *Search for direct top-squark pair production in final states with two leptons in pp collisions at $\sqrt{s} = 8$TeV with the ATLAS detector*. JHEP **1406** (2014) 124, arXiv:1403.4853.

[155] **ATLAS** Collaboration, G. Aad *et al.*, *Search for squarks and gluinos with the ATLAS detector in final states with jets and missing transverse momentum using $\sqrt{s} = 8$ TeV proton–proton collision data*. JHEP **1409** (2014) 176, arXiv:1405.7875.

[156] **ATLAS** Collaboration, G. Aad *et al.*, *Search for direct pair production of the top squark in all-hadronic final states in proton-proton collisions at $\sqrt{s} = 8$ TeV with the ATLAS detector*. JHEP **1409** (2014) 015, arXiv:1406.1122.

[157] **CMS** Collaboration, S. Chatrchyan *et al.*, *Search for top-squark pair production in the single-lepton final state in pp collisions at $\sqrt{s} = 8$ TeV*. Eur.Phys.J. **C73** (2013) no. 12, 2677, arXiv:1308.1586.

[158] **CMS** Collaboration, *Search for supersymmetry in pp collisions at sqrt(s) = 8 TeV in events with three leptons and at least one b-tagged jet.*

[159] **CMS** Collaboration, S. Chatrchyan *et al.*, *Search for new physics in events with same-sign dileptons and jets in pp collisions at $\sqrt{s} = 8$ TeV*. JHEP **1401** (2014) 163, arXiv:1311.6736.

[160] **CMS** Collaboration, S. Chatrchyan *et al.*, *Search for top squark and higgsino production using diphoton Higgs boson decays*. Phys.Rev.Lett. **112** (2014) 161802, arXiv:1312.3310.

[161] F. Jegerlehner, *Electroweak effective couplings for future precision experiments*. Nuovo Cim. **C034S1** (2011) 31–40, arXiv:1107.4683.

[162] K. Chetyrkin, J. H. Kuhn, and M. Steinhauser, *RunDec: A Mathematica package for running and decoupling of the strong coupling and quark masses*. Comput.Phys.Commun. **133** (2000) 43–65, arXiv:hep-ph/0004189.

[163] H. Baer, J. Ferrandis, K. Melnikov, and X. Tata, *Relating bottom quark mass in DR-BAR and MS-BAR regularization schemes*. Phys.Rev. **D66** (2002) 074007, arXiv:hep-ph/0207126.

[164] S. King, M. Mühlleitner, and R. Nevzorov, *NMSSM Higgs Benchmarks Near 125 GeV*. Nucl.Phys. **B860** (2012) 207–244, arXiv:1201.2671.

[165] **ATLAS** Collaboration, G. Aad *et al.*, *Measurement of the Higgs boson mass from the $H \to \gamma\gamma$ and $H \to ZZ^* \to 4\ell$ channels with the ATLAS detector using 25 fb^{-1} of pp collision data*. Phys.Rev. **D90** (2014) no. 5, 052004, arXiv:1406.3827.

[166] **ATLAS, CMS** Collaboration, G. Aad *et al.*, *Combined Measurement of the Higgs Boson Mass in pp Collisions at $\sqrt{s} = 7$ and 8 TeV with the ATLAS and CMS Experiments*. arXiv:1503.07589.

[167] G. Belanger, F. Boudjema, A. Pukhov, and A. Semenov, *Dark matter direct detection rate in a generic model with micrOMEGAs 2.2.* Comput.Phys.Commun. **180** (2009) 747–767, arXiv:0803.2360.

[168] **ATLAS** Collaboration, *Observation of an excess of events in the search for the Standard Model Higgs boson in the gamma-gamma channel with the ATLAS detector.*

[169] **ATLAS** Collaboration, *Update of the $H \to WW^{(*)} \to e\nu\mu\nu$ Analysis with 13 fb^{-1} of $\sqrt{s} = 8$ TeV Data Collected with the ATLAS Detector.*

[170] **ATLAS** Collaboration, *Observation of an excess of events in the search for the Standard Model Higgs boson in the $H \to ZZ^{(*)} \to 4\ell$ channel with the ATLAS detector.*

[171] **ATLAS** Collaboration, *Search for the Standard Model Higgs boson in produced in association with a vector boson and decaying to bottom quarks with the ATLAS detector.*

[172] **ATLAS** Collaboration, *Search for the Standard Model Higgs boson in H-> tau tau decays in proton-proton collisions with the ATLAS detector.*

[173] **CMS** Collaboration, *Evidence for a new state decaying into two photons in the search for the standard model Higgs boson in pp collisions.*

[174] **CMS** Collaboration, *Evidence for a particle decaying to W+W- in the fully leptonic final state in a standard model Higgs boson search in pp collisions at the LHC.*

[175] **CMS** Collaboration, *Updated results on the new boson discovered in the search for the standard model Higgs boson in the ZZ to 4 leptons channel in pp collisions at sqrt(s) = 7 and 8 TeV.*

[176] **CMS** Collaboration, *Search for the standard model Higgs boson produced in association with W or Z bosons, and decaying to bottom quarks for HCP 2012.*

[177] **CMS** Collaboration, *Search for the standard model Higgs boson decaying to tau pairs.*

[178] **ATLAS** Collaboration, *Search for supersymmetry at $\sqrt{s} = 8$ TeV in final states with jets, missing transverse momentum and one isolated lepton.*

[179] **ATLAS** Collaboration, *Search for squarks and gluinos with the ATLAS detector using final states with jets and missing transverse momentum and 5.8 fb^{-1} of $\sqrt{s}$=8 TeV proton-proton collision data.*

[180] **CMS** Collaboration, *Interpretation of Searches for Supersymmetry.*

[181] **ATLAS** Collaboration, G. Aad *et al.*, *Search for a supersymmetric partner to the top quark in final states with jets and missing transverse momentum at $\sqrt{s} = 7$ TeV with the ATLAS detector.* Phys.Rev.Lett. **109** (2012) 211802, arXiv:1208.1447.

[182] **ATLAS** Collaboration, G. Aad *et al.*, *Search for direct top squark pair production in final states with one isolated lepton, jets, and missing transverse momentum in $\sqrt{s} = 7$ TeV pp collisions using 4.7 fb^{-1} of ATLAS data.* Phys.Rev.Lett. **109** (2012) 211803, arXiv:1208.2590.

[183] **ATLAS** Collaboration, G. Aad *et al.*, *Search for a heavy top-quark partner in final states with two leptons with the ATLAS detector at the LHC.* JHEP **1211** (2012) 094, arXiv:1209.4186.

[184] **CMS** Collaboration, S. Chatrchyan *et al.*, *Search for new physics in events with same-sign dileptons and b-tagged jets in pp collisions at $\sqrt{s} = 7$ TeV*. JHEP **1208** (2012) 110, arXiv:1205.3933.

[185] **CMS** Collaboration, *Search for supersymmetry in events with same-sign dileptons*.

[186] **ATLAS** Collaboration, *Combined coupling measurements of the Higgs-like boson with the ATLAS detector using up to 25 fb^{-1} of proton-proton collision data*.

[187] **CMS** Collaboration, *Combination of standard model Higgs boson searches and measurements of the properties of the new boson with a mass near 125 GeV*.

[188] J. R. Espinosa, M. Mühlleitner, C. Grojean, and M. Trott, *Probing for Invisible Higgs Decays with Global Fits*. JHEP **1209** (2012) 126, arXiv:1205.6790.

[189] **ATLAS** Collaboration, *Observation and study of the Higgs boson candidate in the two photon decay channel with the ATLAS detector at the LHC*.

[190] **ATLAS** Collaboration, *Search for the Standard Model Higgs boson in the $H \to Z\gamma$ decay mode with pp collisions at $\sqrt{s} = 7$ and 8 TeV*.

[191] **ATLAS** Collaboration, *Search for a Standard Model Higgs boson in $H \to \mu\mu$ decays with the ATLAS detector*.

[192] **ATLAS** Collaboration, *Measurements of the properties of the Higgs-like boson in the four lepton decay channel with the ATLAS detector using 25 fb-1 of proton-proton collision data*.

[193] **ATLAS** Collaboration, *Measurements of the properties of the Higgs-like boson in the $WW^{(*)} \to \ell\nu\ell\nu$ decay channel with the ATLAS detector using 25 fb^{-1} of proton-proton collision data*.

[194] **CMS** Collaboration, *Updated measurements of the Higgs boson at 125 GeV in the two photon decay channel*.

[195] **CMS** Collaboration, *Properties of the Higgs-like boson in the decay H to ZZ to 4l in pp collisions at sqrt s =7 and 8 TeV*.

[196] **CMS** Collaboration, *Update on the search for the standard model Higgs boson in pp collisions at the LHC decaying to W + W in the fully leptonic final state*.

[197] **CMS** Collaboration, *Search for the Standard-Model Higgs boson decaying to tau pairs in proton-proton collisions at sqrt(s) = 7 and 8 TeV*.

[198] **CMS** Collaboration, *Search for the standard model Higgs boson in the Z boson plus a photon channel in pp collisions at sqrt-s = 7 and 8 TeV*.

[199] M. Carena, S. Gori, N. R. Shah, and C. E. Wagner, *A 125 GeV SM-like Higgs in the MSSM and the $\gamma\gamma$ rate*. JHEP **1203** (2012) 014, arXiv:1112.3336.

[200] K. Schmidt-Hoberg and F. Staub, *Enhanced $h \to \gamma\gamma$ rate in MSSM singlet extensions*. JHEP **1210** (2012) 195, arXiv:1208.1683.

[201] N. Desai, B. Mukhopadhyaya, and S. Niyogi, *Constraints on Invisible Higgs Decay in MSSM in the Light of Diphoton Rates from the LHC*. arXiv:1202.5190.

[202] H. An, T. Liu, and L.-T. Wang, *125 GeV Higgs Boson, Enhanced Di-photon Rate, and Gauged $U(1)_P Q$-Extended MSSM*. Phys.Rev. **D86** (2012) 075030, arXiv:1207.2473.

[203] R. Benbrik, M. Gomez Bock, S. Heinemeyer, O. Stal, G. Weiglein, *et al.*, *Confronting the MSSM and the NMSSM with the Discovery of a Signal in the two Photon Channel at the LHC*. Eur.Phys.J. **C72** (2012) 2171, arXiv:1207.1096.

[204] K. Choi, S. H. Im, K. S. Jeong, and M. Yamaguchi, *Higgs mixing and diphoton rate enhancement in NMSSM models*. JHEP **1302** (2013) 090, arXiv:1211.0875.

[205] U. Ellwanger, *A Higgs boson near 125 GeV with enhanced di-photon signal in the NMSSM*. JHEP **1203** (2012) 044, arXiv:1112.3548.

[206] U. Ellwanger, *Enhanced di-photon Higgs signal in the Next-to-Minimal Supersymmetric Standard Model*. Phys.Lett. **B698** (2011) 293–296, arXiv:1012.1201.

[207] J. Cao, Z. Heng, T. Liu, and J. M. Yang, *Di-photon Higgs signal at the LHC: A Comparative study for different supersymmetric models*. Phys.Lett. **B703** (2011) 462–468, arXiv:1103.0631.

[208] R. V. Harlander, S. Liebler, and H. Mantler, *SusHi: A program for the calculation of Higgs production in gluon fusion and bottom-quark annihilation in the Standard Model and the MSSM*. Comput.Phys.Commun. **184** (2013) 1605–1617, arXiv:1212.3249.

[209] **CMS** Collaboration, *Search for the resonant production of two Higgs bosons in the final state with two photons and two bottom quarks*.

[210] **ATLAS** Collaboration, G. Aad *et al.*, *Search For Higgs Boson Pair Production in the $\gamma\gamma b\bar{b}$ Final State using pp Collision Data at $\sqrt{s} = 8$ TeV from the ATLAS Detector*. Phys.Rev.Lett. **114** (2015) no. 8, 081802, arXiv:1406.5053.

[211] **ATLAS** Collaboration, *A search for resonant Higgs-pair production in the $b\bar{b}b\bar{b}$ final state in pp collisions at $\sqrt{s} = 8$ TeV*.

[212] K. Melnikov and T. v. Ritbergen, *The Three loop relation between the MS-bar and the pole quark masses*. Phys.Lett. **B482** (2000) 99–108, arXiv:hep-ph/9912391.

[213] M. S. Carena, D. Garcia, U. Nierste, and C. E. Wagner, *Effective Lagrangian for the $\bar{t}bH^+$ interaction in the MSSM and charged Higgs phenomenology*. Nucl.Phys. **B577** (2000) 88–120, arXiv:hep-ph/9912516.

[214] R. Harlander, P. Kant, L. Mihaila, and M. Steinhauser, *Dimensional Reduction applied to QCD at three loops*. JHEP **0609** (2006) 053, arXiv:hep-ph/0607240.

[215] R. Harlander, L. Mihaila, and M. Steinhauser, *Running of alpha(s) and m(b) in the MSSM*. Phys.Rev. **D76** (2007) 055002, arXiv:0706.2953.

[216] L. Avdeev and M. Y. Kalmykov, *Pole masses of quarks in dimensional reduction*. Nucl.Phys. **B502** (1997) 419–435, arXiv:hep-ph/9701308.